Marine Ecosystems

Aquaculture Environmental Monitoring Program: 2019-2023

Jason E. Tanner, Mark Doubell and Charles James

SARDI Publication No. F2019/000334-2
SARDI Research Report Series No. 1231

SARDI Aquatic and Livestock Sciences
PO Box 120 Henley Beach SA 5022

October 2024

Report prepared for PIRSA Fisheries and Aquaculture

Government of South Australia
Department of Primary Industries and Regions

SARDI
SOUTH AUSTRALIAN RESEARCH AND DEVELOPMENT INSTITUTE

Aquaculture Environmental Monitoring Program: 2019-2023

Report prepared for PIRSA Fisheries and Aquaculture

Jason E. Tanner, Mark Doubell and Charles James

SARDI Publication No. F2019/000334-2
SARDI Research Report Series No. 1231

October 2024

The South Australian Research and Development Institute respects Aboriginal people as the state's first people and nations. We recognise Aboriginal people as traditional owners and occupants of South Australian land and waters. We pay our respects to Aboriginal cultures and to Elders past, present and emerging.

This publication may be cited as:
Tanner, J.E., Doubell, M. and James, C. (2024). Aquaculture Environmental Monitoring Program: 2019-2023. Report prepared for PIRSA Fisheries and Aquaculture. South Australian Research and Development Institute (Aquatic and Livestock Sciences), Adelaide. SARDI Publication No. F2019/000334-2. SARDI Research Report Series No. 1231. 59pp.

DISCLAIMER

The authors warrant that they have taken all reasonable care in producing this report. The report has been through the SARDI internal review process, and has been formally approved for release by the Research Director, Aquatic and Livestock Sciences. Although all reasonable efforts have been made to ensure quality, SARDI does not warrant that the information in this report is free from errors or omissions. SARDI and its employees do not warrant or make any representation regarding the use, or results of the use, of the information contained herein as regards to its correctness, accuracy, reliability and currency or otherwise. SARDI and its employees expressly disclaim all liability or responsibility to any person using the information or advice. Use of the information and data contained in this report is at the user's sole risk. If users rely on the information they are responsible for ensuring by independent verification its accuracy, currency or completeness. The SARDI Report Series is an Administrative Report Series which has not been reviewed outside the department and is not considered peer-reviewed literature. Material presented in these Administrative Reports may later be published in formal peer-reviewed scientific literature.

Author(s):	Jason E. Tanner, Mark Doubell and Charles James
Reviewer(s):	Sarah Catalano and Adrian Linnane (SARDI)
Approved by:	Prof. Simon Goldsworthy Program Leader – Marine Ecosystems
Signed:	
Date:	24 October 2024
Distribution:	PIRSA Fisheries and Aquaculture, EPA, SARDI Aquatic and Livestock Sciences, Parliamentary Library, State Library and National Library
Circulation:	OFFICIAL

ALL ENQUIRIES

South Australian Research and Development Institute - Aquatic and Livestock Sciences
2 Hamra Avenue West Beach SA 5024
PO Box 120 Henley Beach SA 5022
P: (08) 8207 5400 **F:** (08) 8207 5415
E: pirsa.sardiaquatics@sa.gov.au **W:** http://www.pir.sa.gov.au/research

TABLE OF CONTENTS

LIST OF FIGURES

LIST OF TABLES

ACKNOWLEDGEMENTS

The authors acknowledge the support of PIRSA Fisheries and Aquaculture, Australian Southern Bluefin Tuna Industry Association Inc. and Clean Seas Aquaculture Growout Pty Ltd. We thank Tian Shi, Hugo Bastos de Oliveira, Paul Malthouse, Ian Moody, Ben Stobart, David Delaine, Doug Graske and the crew of the *RV Ngerin* for assistance with the field work component of this project. Ian Moody counted and identified the zooplankton. Paul Malthouse and Ian Moody prepared and led the pelagic field surveys. Tian Shi analysed the phytoplankton pigment data and performed the CHEMTAX analysis. Hugo Bastos de Oliveira quality assured the collected oceanographic CTD and ADCP data. Mandee Theil and Sharon Drabsch processed seagrass samples. Samantha Chown provided access to Clean Seas seagrass monitoring data, while Sam Gaylard and Matt Nelson provided EPA data. Thank you also to Simon Goldsworthy, Adrian Linnane and Sarah Catalano (SARDI) and Sam Gaylard and Tara Ingerson (EPA) for providing constructive comments on the manuscript.

EXECUTIVE SUMMARY

An independent review of the environmental monitoring program for aquaculture in South Australia recommended the development of regional and zone-scale environmental monitoring, as well as site-scale auditing of industry practices. Consequently, SARDI conducted a 4-year environmental monitoring program from 2015/16 to 2018/19 for the tuna and other finfish sectors, which included regional and zone scale measurements and monitoring of benthic and pelagic ecosystems. As 'Tuna' and 'Other Finfish' aquaculture primarily occurred in the Boston Bay aquaculture zone and the Lincoln aquaculture zone, the environmental monitoring program focused on this region. In this report, we describe the second phase of this program, which runs from 2019/20 to 2022/23.

This Aquaculture Environmental Monitoring Program (AEMP) is divided into two components: 1) a pelagic and oceanographic monitoring: which includes updating the coupled hydrodynamic-biogeochemical model to investigate the status and trends of water quality and the structure of the lower pelagic ecosystem in the region; and 2) benthic monitoring: which focuses on assessing the regional effects of aquaculture derived nutrients on seagrasses.

The pelagic monitoring program identified significant levels of spatial and temporal variation in the physical, chemical, and biological parameters investigated. Trends for several plankton-based indicators of eutrophication suggest that the trophic status of the inshore waters of Louth Bay and Boston Bay are different from offshore waters and may be changing from mesotrophic to slightly eutrophic. The environmental drivers responsible for the changes observed in the plankton and phytoplankton communities at the inshore sites included temperature, flushing timescales and, to a reduced extent, nutrients. Multivariate analysis of the plankton and phytoplankton community structure suggests the region's inshore waters are sensitive to a range of different nutrient types, including aquaculture derived nutrients in the form of ammonium. Collectively, these findings are consistent with nutrient observations and oceanographic modelling results and suggest the enrichment of inshore waters with nutrients sourced from aquaculture is likely to be in part responsible for the observed changes in the trophic state, particularly during cooler autumn periods. It is not clear to what extent variability in the supply of nutrients from other sources in the region may also contribute to the differences in water quality and the composition of the plankton community observed at the inshore sites.

Overall, although there was extensive spatial and temporal variation in the seagrass parameters investigated, the only significant impact of aquaculture was on the amino acid composition of epiphytes. Sampling looked at cover and composition using video transects, seagrass biomass and morphology using core samples, and the biochemical composition of both seagrasses and epiphytes. However, it should be noted that seagrass sampling only began several decades after the commencement of aquaculture and that it is not possible to detect historical impacts with the methods utilised. Another concern is that one of the control sites, Tumby Bay, experienced a substantial decline in seagrass cover. If this was caused by local factors, or the site is actually within the aquaculture nutrient plume, then this decline would obscure impacts from aquaculture. To help resolve this, future monitoring should include extra control sites, and directly assess any links between modelled nutrient loadings at a site and changes in seagrass cover at that site.

Keywords: oceanography, nutrients, phytoplankton, hydrodynamic modelling, biogeochemical modelling, seagrass, biomarkers, aquaculture impacts.

1. INTRODUCTION

1.1. Background

Aquaculture is an important economic activity in Australia, with a gross production value of $1.94 billion in 2021/22 (Tuynman et al. 2023). Key marine species include Pacific oyster *Crassostrea gigas*, Atlantic salmon *Salmo salar*, southern bluefin tuna (SBT) *Thunnus maccoyii*, ocean rainbow trout *Oncorhynchus mykiss* and yellowtail kingfish (YTK) *Seriola lalandi* (Tuynman et al. 2023). In 2021/22, the aquaculture industry in South Australia had a total production value of $237.9 million, of which $110 million was for SBT and $42 million for other marine finfish (BDO EconSearch 2023). Total aquaculture production increased by 13% by weight and 19% by value in the previous year.

The management of the finfish aquaculture industry, which includes SBT and YTK, is based on the principles of ecologically sustainable development (ESD) enshrined in the South Australian *Aquaculture Act 2001*. An aspect of ESD is to ensure that aquaculture operations do not deleteriously and irreversibly change the marine environment. To assess compliance with this requirement, aquaculture licensees are legally required under the South Australian *Aquaculture Act 2001* and the *Aquaculture Regulations 2016* to undertake an Environmental Monitoring Program.

The Tuna Environmental Monitoring Program (TEMP) and Finfish Aquaculture Environmental Monitoring Program (FEMP) were both farm-site compliance-based monitoring programs using a system developed by South Australian Research and Development Institute (SARDI), comprising DNA-based assays using quantitative real-time PCR (qPCR) for selected benthic marine organisms in sediment, and an Environmental Compliance Scorecard system for analysing and presenting the results from the assays (Loo et al. 2006, 2010). This system was implemented for the TEMP in 2005 (e.g. Loo and Giblot-Ducray 2015) and the FEMP in 2009 (e.g. Loo and Giblot-Ducray 2014), and continued to 2014 and 2013, respectively.

An independent review of the environmental monitoring program for aquaculture in South Australia recommended the development of regional and zone-scale environmental monitoring, as well as site-scale auditing of industry practices. These recommendations were based on the recognition that a significant portion of finfish aquaculture waste products ultimately occur as dissolved nutrients whose cumulative impacts are likely to be realised at some distance from their source. Consequently, SARDI conducted a 4-year environmental monitoring program from

2015/16 to 2018/19 that included regional and zone-scale measurements and monitoring of benthic and pelagic ecosystems (Tanner et al. 2020). The benthic component of this program found that, while there was significant spatial and temporal variation in the infaunal assemblages, there was no indication that aquaculture had a significant impact on the infauna. Additionally, a combined analysis of all previous tuna and finfish environmental monitoring data collected between 2005 and 2014 failed to detect any aquaculture impacts on infauna. As a consequence, it was recommended that the focus on infauna for benthic monitoring be reduced and that other potentially vulnerable components of the ecosystem be examined instead.

The pelagic environment and oceanography monitoring detected significant spatial and temporal variations in the physical environment, circulation, water quality and planktonic ecosystem composition. Compared to previous studies, several indicators based on water quality and phytoplankton showed that inshore sites within Boston and Louth Bay differed significantly from offshore sites. The trends for several indicators collectively indicated that the differences observed at the inshore sites were consistent with the impacts expected from anthropogenic nutrient enrichment. These indicators were nutrients, chlorophyll *a*, phytoplankton abundance and community composition, harmful algal bloom species and frequency, and lower structure and composition of the lower planktonic ecosystem.

'Tuna' and 'Other Finfish' aquaculture is currently most active in two zones within the Lower Eyre Peninsula Aquaculture Zone (LEPZ), the Boston Bay aquaculture zone and the Lincoln aquaculture zone. The Lincoln aquaculture zone comprises the Lincoln (inner) sector, located east of Boston Island, and the Lincoln (outer) sector, located south-east of Sir Joseph Banks group of islands (Figure 1-1). Most active leases for 'Tuna' (SBT) are currently operating in the southern part of the Lincoln (inner) sector, while active leases for 'Other Finfish' (YTK) are operating in the Boston Bay aquaculture zone. As only one SBT lease was operating in the Lincoln (outer) sector at the beginning of this project, the scope of this study did not include this region.

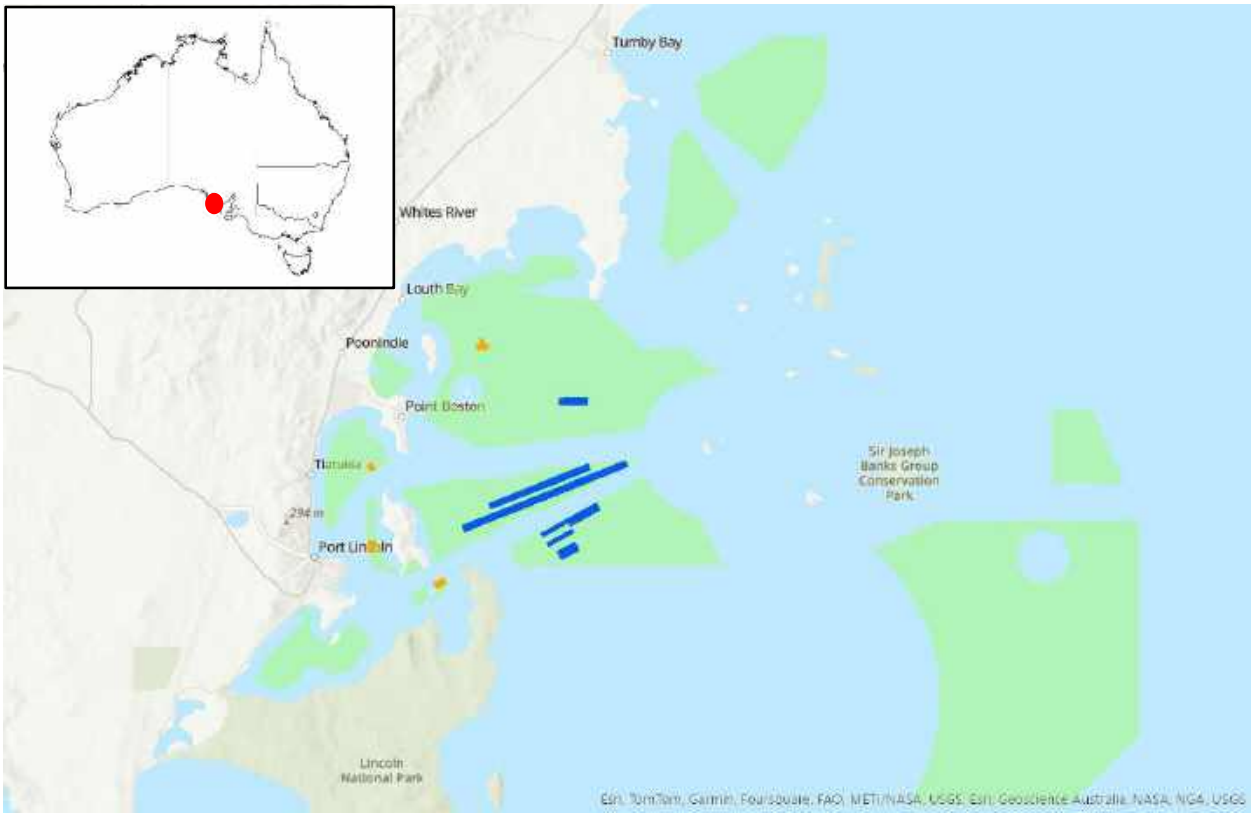

Figure 1-1: Map of the Boston Bay region showing the location of aquaculture zones (green) and active finfish (orange) and tuna (blue) aquaculture leases in 2024. Inset shows the location of the Boston Bay region (red dot).

The monitoring program described here was designed to assess key ecosystem groups to better understand the localised and cumulative impacts of finfish aquaculture in the Lincoln aquaculture zone (inner sector) and the Boston Bay aquaculture zone. It is divided into two components:

1) A pelagic and oceanographic monitoring component that also includes an update of the coupled hydrodynamic-biogeochemical model (Middleton et al. 2013) used by PIRSA Fisheries and Aquaculture for aquaculture planning and management, and which largely follows what was undertaken in the previous 4-year program; and

2) A benthic ecosystem component that looks at regional effects on seagrasses.

Seagrasses have been identified as an important ecosystem component that have shown worrying signs of decline in some areas around Port Lincoln, and around Spencer Gulf more broadly, and that are vulnerable to anthropogenic nutrient enrichment, particularly through epiphyte overgrowth.

This program is in line with the recommendations of the independent review and covers the minimum requirements to ensure baseline scientific rigour in the results. The combined monitoring and modelling program (as well as outcomes from other research projects, e.g. seagrass condition) will assist in the refinement of any future monitoring programs.

1.2. Objectives

The objectives of the pelagic and oceanography component of the program are to:

- Assess status of water quality and the trophic structure of the lower pelagic ecosystem at key sites within and outside aquaculture zones in the Port Lincoln region.
- Update and validate a coupled hydrodynamic-biogeochemical model for the region to (i) better understand regional dispersal and connectivity of nutrients sourced from the shelf and supplementary fed aquaculture, (ii) help optimise the location of the aquaculture lease and estimates of carrying capacity, and (iii) inform the future design of the monitoring program.

The objectives of the benthic component of the program reported here are to:

- Assess the status of seagrasses at key sites within and outside aquaculture nutrient plumes in the Port Lincoln region.
- Assess the contribution of aquaculture-derived nutrients to seagrass nutrient budgets at these sites and the potential contribution of these nutrients to any seagrass decline.

2. PELAGIC AND OCEANOGRAPHY COMPONENT

2.1. Introduction

The water quality and health of coastal marine systems are vulnerable to nutrient over enrichment, which can lead to an increase in organic matter (i.e., carbon) production (Nixon 1995). Natural drivers that influence the supply of nutrients in Spencer Gulf include climate and weather drivers that determine the circulation and exchange of waters between the shelf and the gulf (Middleton et al. 2013) and processes that affect the remineralisation and resuspension of nutrient-rich sediment particulate matter (Tanner and Volkman 2009). The sources of anthropogenic nutrients into Spencer Gulf are dominated by those originating from finfish aquaculture (i.e., SBT and YTK), with smaller contributions sourced from other industries, including wastewater treatment plants (Gaylard 2014).

Nutrients from supplementary fed aquaculture enter the marine environment as feed waste, faeces and urine, with approximately 85% released as dissolved nitrogen (Fernandes et al. 2007, Fernandes and Tanner 2008) readily available to autotrophs (e.g., phytoplankton and seagrass). The remainder consists of particulates which settle on the seabed, where sediment processes act to slowly return these nutrients in dissolved form to the water column. Since nitrogen is typically considered to limit phytoplankton growth by nutrient in coastal marine systems (Howarth and Marino 2006), the availability of additional nitrogen has the potential to lead to eutrophication. Globally, the impacts of eutrophication are well documented, with common symptoms including increases in phytoplankton biomass, changes in plankton community composition and food-web structure, increased harmful algal bloom frequency, habitat degradation and a loss of biodiversity (Howarth 2008, Glibert 2017).

Since plankton form the base of the marine food web, their biomass and composition are useful indicators to manage coastal waterways (Cloern 2001, Paerl et al. 2003, Suthers et al. 2019). This is because plankton contains most of the pelagic biomass and is responsible for the bulk of primary production and nutrient cycling. Hence, the size structure and composition of plankton assemblages is a key characteristic which influences lower trophic ecosystem productivity, dynamics and stability (Glibert 2017, Suthers et al. 2019, Van Meerssche and Pinckney 2019). For example, phytoplankton form the base of marine food webs and are responsible for primary production. The size of phytoplankton cells spans several orders of magnitude (picophytoplankton 0.2-2 µm, nanophytoplankton 2-20 µm, microphytoplankton 20-200 µm) and strongly influence the uptake of dissolved nutrients from the environment. Bacteria and zooplankton are important

heterotrophic organisms that play key roles in food web dynamics. Bacteria are the main organisms involved in nutrient recycling via the microbial loop (Azam and Malfatti 2007). Zooplankton grazers provide the main pathway from plankton to fish (Suthers et al. 2019).

This chapter provides baseline measurements of key water quality variables and the basic structural properties of plankton assemblages, including their temporal and spatial variability and their relation to environmental forcing, for several sites in and around the Boston Bay and Lincoln aquaculture zones. The measurements extend upon the previous 4-year program and are used to assess changes in the trophic state of coastal waters surrounding these two aquaculture zones. An update of the coupled hydrodynamic-biogeochemical model for Spencer Gulf (Middleton et al. 2013) is carried out to better understand the influence of the physical environment on nutrient supply and the response of the planktonic ecosystem, as well as the connectivity and cumulative impact of anthropogenic nutrient loads at local and regional scales.

2.2. Methods

Field Surveys

This report combines observations taken in the second phase of the Pelagic Monitoring program in 2020, 2021 and 2022 with those made during the initial program in 2016, 2017 and 2018 (Tanner et al. 2020) to develop a baseline for understanding the natural variability in the system and for assessing temporal changes in water quality and pelagic ecosystem structure.

Monitoring focused on two seasons, summer and autumn. During each season, sampling was undertaken at five sites (Figure 2-1); one within the zone where tuna farming exists (LFZ; 136.0441°E, 34.6761°S), one just outside the Boston Bay aquaculture zone (BXZ; 135.9034°E, 34.6793°S), one to the south of the tuna farming zone used as a control site (LRS; 136.1432°E, 34.7859°S), and sites in Louth Bay (BRN; 136.0005°E, 34.5323°S) and to the north of the tuna farming aquaculture zone (LRN; 136.2062°E, 34.4911°S). Site selection was chosen based on an understanding of variations in the timescales of the flushing of aquaculture leases throughout the region (Middleton et al. 2013, 2014) and where circulation models predict the cumulative transport of nutrients sourced from SBT and YTK aquaculture (Middleton et al. 2013, Doubell et al. 2015).

Summer sampling was undertaken in late January as the annual cycle of nutrient loads from aquaculture begins to ramp up (see Figure 2-12) and connectivity with the shelf and summertime upwelling is generally restricted by the establishment of a temperature front across the entrance

to the gulf (Petrusevics 1993). Autumn sampling was undertaken in May, when the collective nitrogen loads from supplementary fed aquaculture are greatest. At this time, the annual flushing of the gulf draws an inflow of water from the shelf into and along the western side of the gulf (Lennon et al. 1987, Nunes Vaz et al. 1990) which is accompanied by a peak in phytoplankton productivity and biomass in the LEPZ region (Tanner and Volkman 2009, Middleton et al. 2013).

An oceanographic mooring was deployed at the LRS site in January and collected in May each year. The mooring contained an acoustic doppler current profiler (either an RDI Sentinel II 300 kHz or a Nortek Signature 500 ADCP) and provided hourly measurements of currents throughout the water column. A Seabird16+ CTD provided near bottom measures of temperature, salinity and pressure (i.e., sea surface height). The mooring was placed in a relatively flat area south of the Lincoln aquaculture zone to support the validation of hydrodynamic models developed for the region.

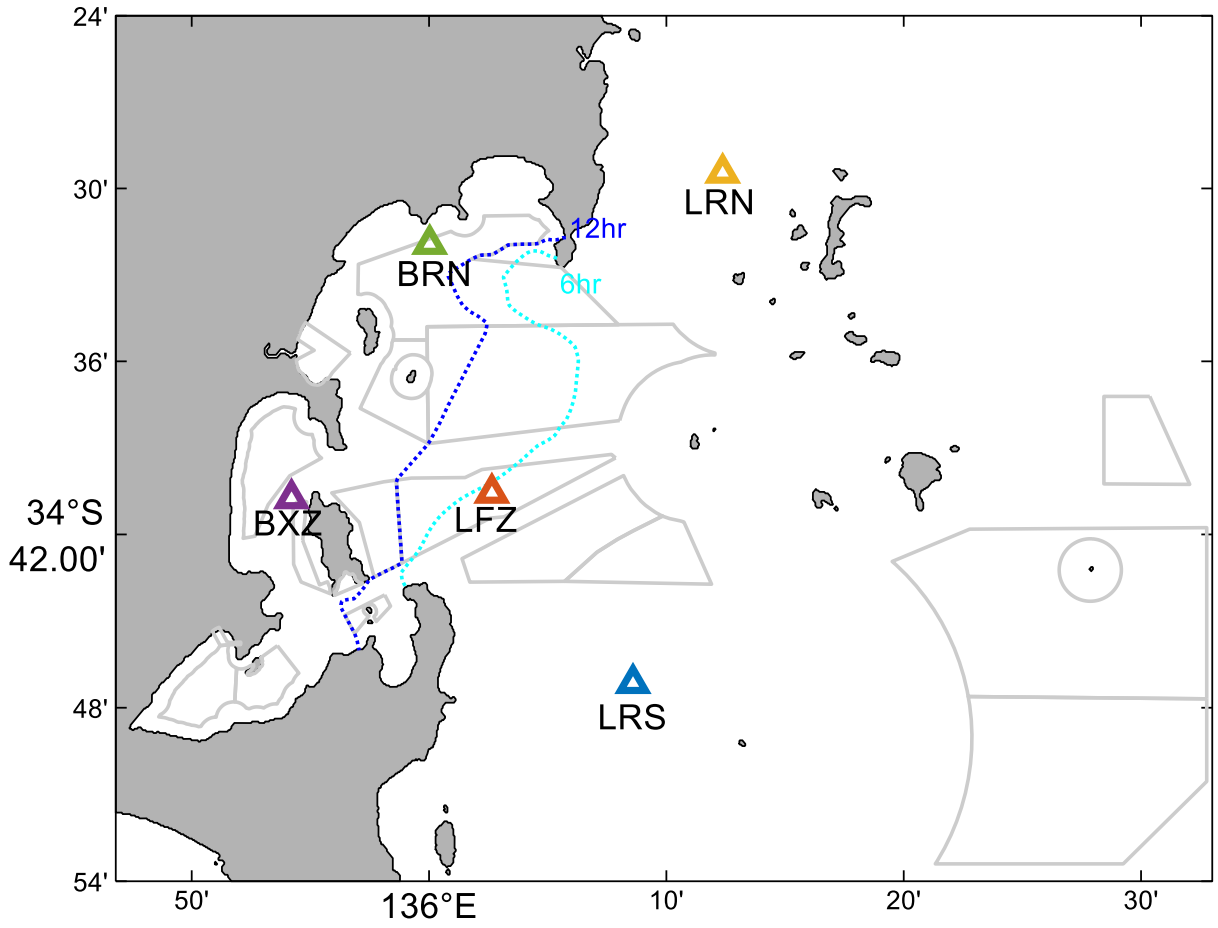

Figure 2-1: Map of the Boston Bay region showing the location of the pelagic monitoring sites (coloured triangles) relative to the aquaculture zones (grey polygons) and the 6- and 12-hour aquaculture lease-scale flushing timescale contours (blue dotted lines) adapted from Middleton et al. (2014).

At each pelagic sampling site, vertical measurements of temperature and salinity across the water column were collected using a Seabird19+CTD. Vertical net tows with a dual bongo net (64 and 150 µm mesh sizes) were used to collect zooplankton samples. Water samples were collected approximately 1 m above (below) the bottom (surface) using a Niskin bottle and combined to form a water column composite sample. From this the following sub-samples were taken:

- triplicate samples for macro-nutrient analysis including oxides of nitrogen (NO_x), ammonium (NH_4^+), phosphorus (PO_4^{3-}) and silicate (SiO_2)
- triplicate samples for total suspended solid (TSS) concentration
- triplicate samples for the flow cytometric determination of bacteria and picophytoplankton abundances
- a single sample for phytoplankton pigment composition using High Pressure Liquid Chromatography (HPLC)
- a single sample for microphytoplankton identification and abundance via light microscopy.

A more detailed description of the analytical methods for each of the above-mentioned environmental variables is provided in the Appendix.

Trophic Status Indicator

Following Claustre (1994), the biomass ratio of new to total production, referred to as the F_p ratio, was determined from the HPLC-derived phytoplankton pigment composition. The F_p ratio provides a simple indicator of trophic status and ranges between 0 and 1. Increasing values indicate a change from oligotrophic (~0-0.3) through mesotrophic (~0.3-0.6) to eutrophic (>~0.6) conditions.

Phytoplankton Community Structure

To determine the biomass contribution of different phytoplankton taxonomic groups to the total chl-*a* biomass, measured HPLC pigment concentrations were analysed with the CHEMTAX program (V1.95) (Mackey et al. 1996, Wright et al. 2009). Light microscopy and flow cytometry data were first used to guide the selection of the most dominant phytoplankton groups and their associated marker pigments (Table 2-1). Initial pigment ratios for the ten dominant phytoplankton groups (Table 2-2) were then selected from the literature (Hallegraeff 1981, Wright et al. 2009, 2010, Thompson et al. 2011, Armbrecht et al. 2015). Pigments used in the CHEMTAX analysis included chlorophyll *a* (chl-*a*), fucoxanthin (Fuco), chlorophyll b (Chlb), chlorophyll c2 (Chlc2), 19-hex-fucoxanthin (Hex-fuco), zeaxanthin (Zea), prasinoxanthin (Pras), peridinin (Peri), 19-but-

fucoxanthin (But-fuco), alloxanthin (Allo), neoxanthin (Neo), lutein (Lut) and divinyl chlorophyll a (DVChla).

CHEMTAX uses a steepest descent algorithm to optimise the biomass estimates returned for each phytoplankton group. To achieve this, a series of 60 pigment ratio matrixes were generated by multiplying the initial pigment ratio matrix by a random function. Each of the 60 pigment ratio tables was used as a starting point for CHEMTAX optimisation, with the best 10% (n=6) of the generated ratios with the lowest root mean square error averaged to determine the contribution of each taxonomic group to the total chl-*a* biomass (Wright et al. 2009). The optimised output matrix of pigment ratios is shown in Table 2-3.

Table 2-1: Identified dominant phytoplankton taxonomic groups and associated marker pigments included in the CHEMTAX analysis.

Algal class	Size class	Example dominant species	Marker pigment
Diatoms	micro/nanoplankton	*Chaetoceros, Leptocylindrus, Pseudo-nitzschia, Rhizosolenia setigera, Nitzschia*	Fuco, Chlc2
Dinoflagellates	micro/nanoplankton	*Amphidinium, Gonyaulax, Protoperidinium*	Peri, Chlc2
Chrysophytes	nanoplankton	*Aureococcus, Dictyocha*	Fuco, But-fuco
Cryptophytes	nanoplankton	*Cryptomonas salino*	Allo, Chlc2
Prymnesiophytes	nanoplankton	*Emiliania huxleyi, Gephyrocapsa oceanica*	Hex-fuco, Chlc2, Fuco, But-fuco
Euglenophytes	nanoplankton	*Eutreptiella*	Chlb, Neo, Zea, Lut
Prasinophytes	nanoplankton	*Micromonas, Tetraselmis*	Pras, Chlb, Neo, Zea, Lut
Cyanobacteria-1	nano/picoplankton	*Trichodesmium*	Zea
Cyanobacteria-2	picoplankton	*Synechococcus*	Zea
Cyanobacteria-4	picoplankton	*Prochlorococcus marinus, Oscillatoria* sp.*, Gloecapsa* sp.	Zea, DVChla

Table 2-2: Initial pigment ratios to chlorophyll-*a* for each phytoplankton group used in CHEMTAX.

Group / Pigment	$Chlc_2$	Peri	But-fuco	Fuco	Neo	Pras	Hex-fuco	Allo	Zea	Lut	DVChla	Chlb	chl_*a*
Diatoms	0.12	0	0	0.73	0	0	0	0	0	0	0	0	1
Dinoflagellates	0.23	0.54	0	0	0	0	0	0	0	0	0	0	1
Chrysophytes	0	0	0.37	0.98	0	0	0	0	0	0	0	0	1
Cryptophytes	0.17	0	0	0	0	0	0	0.36	0	0	0	0	1
Prymnesiophytes	0.18	0	0.06	0.01	0	0	0.42	0	0	0	0	0	1
Euglenophytes	0	0	0	0	0.08	0	0	0	0.01	0.01	0	0.39	1
Prasinophytes	0	0	0	0	0.05	0.15	0	0	0.08	0.01	0	0.37	1
Cyanobacteria-1	0	0	0	0	0	0	0	0	0.06	0	0	0	1
Cyanobacteria-2	0	0	0	0	0	0	0	0	0.36	0	0	0	1
Cyanobacteria-4	0	0	0	0	0	0	0	0	0.22	0	0.41	0	1

Table 2-3: Final optimised pigment ratios to chlorophyll-a for each phytoplankton group output from CHEMTAX.

Group / Pigment	$Chlc_2$	Peri	But-fuco	Fuco	Neo	Pras	Hex-fuco	Allo	Zea	Lut	DVChl a	Chlb	chla
Diatoms	0.12	0	0	0.62	0	0	0	0	0	0	0	0	1
Dinoflagellates	0.24	0.48	0	0	0	0	0	0	0	0	0	0	1
Chrysophytes	0	0	0.45	0.96	0	0	0	0	0	0	0	0	1
Cryptophytes	0.17	0	0	0	0	0	0	0.37	0	0	0	0	1
Prymnesiophytes	0.34	0	0.10	0.15	0	0	0.70	0	0	0	0	0	1
Euglenophytes	0	0	0	0	0.06	0	0	0	0.07	0.01	0	0.44	1
Prasinophytes	0	0	0	0	0.16	0.52	0	0	0.23	0.04	0	0.44	1
Cyanobacteria-1	0	0	0	0	0	0	0	0	0.06	0	0	0	1
Cyanobacteria-2	0	0	0	0	0	0	0	0	1.76	0	0	0	1
Cyanobacteria-4	0	0	0	0	0	0	0	0	0.24	0	0.40	0	1

Lower Trophic Ecosystem Community Structure

The carbon biomass for key autotrophic and heterotrophic groups of the planktonic ecosystem was estimated based on published empirical relationships (Fukuda et al. 1998, Menden-Deuer and Lessard 2000, Marquis et al. 2011). Carbon conversion factors of 0.020, 0.034, 0.076 and 1.0 pg C per cell were applied to the abundances of bacteria, *Prochlorococcus*, *Synechococcus* (picophytoplankton) and picoeukaryotes (nanophytoplankton) (Fukuda et al. 1998) abundances determined by flow cytometry. Carbon conversions of 531 pg C per cell were applied to dinoflagellate and 'other' flagellates abundances, and 249 pg C per cell to diatom abundances obtained from microscopy (Menden-Deuer and Lessard 2000, Marquis et al. 2011). Zooplankton biomass was estimated from settling and displacement volumes as described in the Appendix.

Statistical Analysis

Results for each environmental (dependent) variable sampled with replication are expressed as mean ± standard error (se). Factorial Analysis of Variance (ANOVA) was conducted to compare the main effects of site, season, and year and interactions on individual environmental variables. Prior to ANOVA, environmental variables were $\log_{(x+1)}$ transformed to improve the normality and homoscedasticity of the data. Q-Q plots and the Shapiro-Wilk test were used to assess the normality of the residuals. Assumptions implicit in ANOVA were generally met. The Tukey-Kramer test was used to conduct pairwise tests using the Matlab™ 'multcompare' function.

Differences in phytoplankton community composition (in units of µg chl-*a*/L) and lower trophic ecosystem structure (in units of µg C/L) between years, seasons and sites were assessed using the PERMANOVA (Anderson 2001) add-on for Primer (v7) (Clarke and Gorley 2015). Relationships with the measured environmental variables were analysed using a stepwise

distance-based linear model (DistLM), distance-based redundancy analysis (dbRDA), and principal coordinates analysis (PCO). Longitude was excluded from the analysis due to a high correlation with flushing time (r=0.92) and particulate inorganic matter was excluded due to its correlation with total suspended solids (r=0.95). Resemblance matrices were calculated using the Bray-Curtis index to eliminate the influence of the joint absences of groups. 9999 permutations were performed under a reduced model to calculate significance levels. *P* values <0.05 were considered statistically significant for all analyses.

Coupled Hydrodynamic-Biogeochemical Model

The coupled hydrodynamic-biogeochemical model is based on the Regional Ocean Modelling System (ROMS) and corresponds to the nested high-resolution hydrodynamic model (300 m horizontal grid spacing) for Boston Bay (HRBBM) (Doubell and James 2023) which was embedded within a 1.5 km resolution hydrodynamic model of Spencer Gulf and Gulf St Vincent (Two Gulfs Model; TGM). The hydrodynamic model is coupled to the Fennel et al. (2006) biogeochemical model previously developed for Spencer Gulf (Middleton et al. 2013).

The hydrodynamic model was configured to use the bulk-fluxes formulation to compute atmospheric forcing (Fairall et al. 1996) using air pressure, temperature, wind, humidity, heat-fluxes, and precipitation from the NCEP Climate Forecast System Reanalysis v.2 (CFSv2; Saha et al. 2014). Tidal forcing was provided by the global TPXO8 model (Fedoseeva and Egbert 2014). Lateral oceanic boundary conditions and initial fields for temperature, salinity, currents, and sea level were provided by the 10 km resolution CSIRO's Blue Link Reanalysis 2020 (BRAN2020; Oke et al. 2013). The Smagorinsky scheme (Smagorinsky 1963) was used to calculate the horizontal eddy viscosity and a constant horizontal tracer diffusion of 2 m^2/s was used for temperature and salt. The LMD turbulence closure scheme was used for vertical mixing. A quadratic bottom stress formulation was assumed with a bottom roughness length of 2 cm. Validation of the hydrodynamic model is presented in Doubell and James (2022).

The biogeochemical model was initialised with low concentrations of 2 µg/L for all state variables (i.e., ammonium, phytoplankton, zooplankton and detritus) except nitrate (NO_3), which was derived from the CSIRO Atlas of Regional Seas climatology (CARS). Interpolated seasonal values of the CARS nitrate climatology are used as forcing on the ocean boundaries. Anthropogenic nitrogen loads were estimated from monthly SBT and YTK feed data reported to PIRSA Fisheries and Aquaculture following Fernandes et al. (2007) and Fernandes and Tanner (2008), and are entered into the model as NH_4^+. Other anthropogenic nutrient inputs into the Gulf, including

wastewater treatment plants (WWTP), were downloaded from the National Pollution Inventory (http://www.npi.gov.au/) and are input into the model as both NO_x and NH_4^+, consistent with previous modelling studies for Spencer Gulf (Middleton et al. 2013, Doubell et al. 2015). The coupled model was run from January 1, 2016, to January 1, 2023. Model results were stored at hourly intervals.

2.3. Results

Physical Environment

Temperature and salinity measurements made at the LRS site between January and May 2016-2018 and 2020-2022 showed strong inter-annual variability with variations of up to 3 ^oC and 1.5 psu observed from year to year (Figure 2-2). Decreases in temperature from mid to late March each year characterise the seasonal cooling of the waters. For salinity, the onset of sharp decreases in salinity observed between mid-March and mid-April is indicative of relatively lower salinity shelf water being transported into southern Spencer Gulf along the western side of the gulf. This transport is associated with the clockwise inverse estuarine circulation of the gulf and the corresponding outflow of water on the eastern side of the gulf (Nunes and Lennon 1987, Nunes Vaz et al. 1990, Middleton et al. 2013).

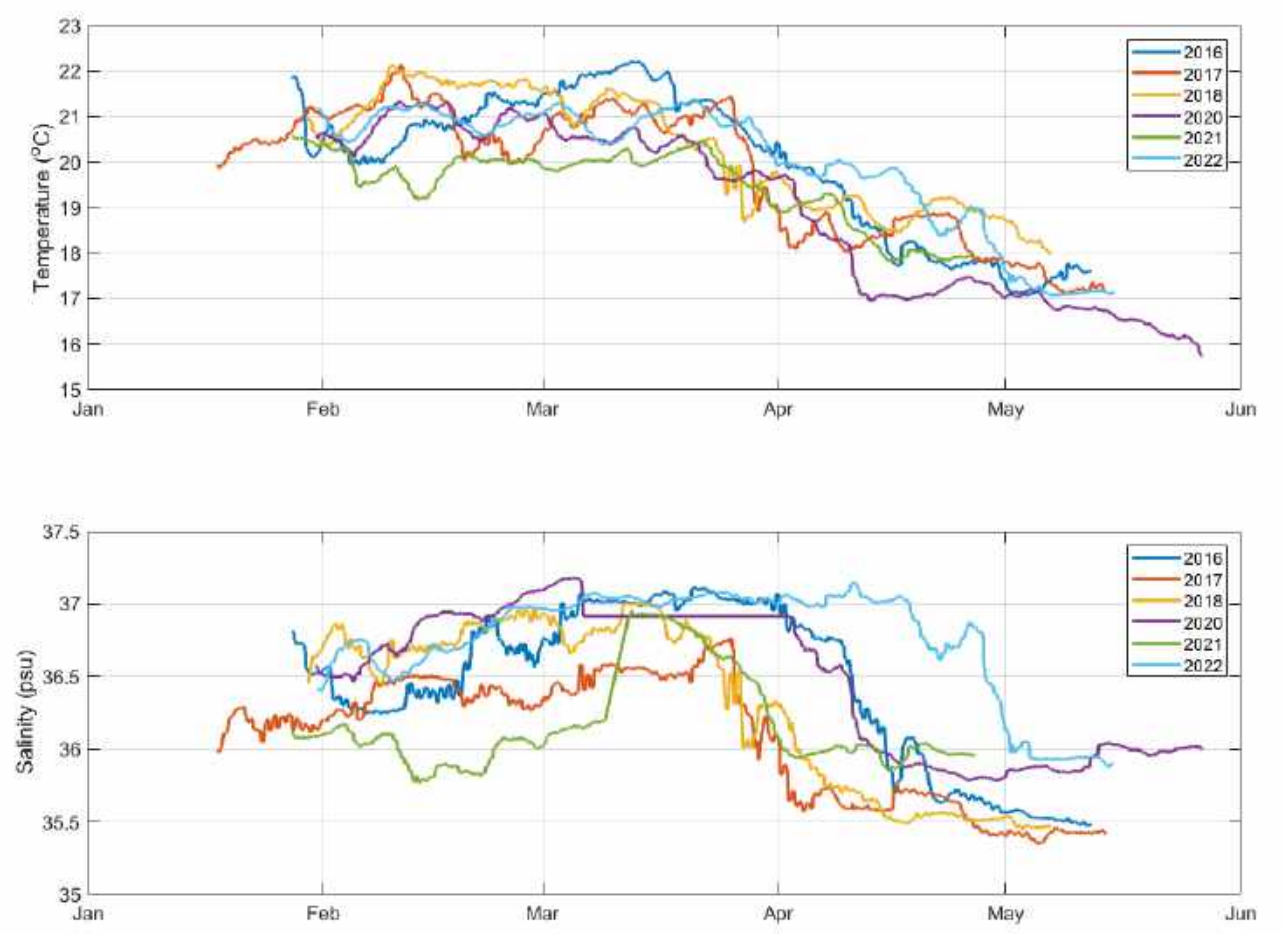

Figure 2-2: Time series of (top) near-bottom temperature and (bottom) salinity measured at LRS.

Vertical profiles of temperature, salinity, and density taken at the sampling sites show that the water column was generally well mixed (Figure 2-3). Evidence of stratification was demonstrated at times by decreases in temperature of ~1 °C and increases in salinity of ~0.5 psu over the water column. Depth averaged summer temperature and salinity values ranged between 19.9 °C at LRS in 2017 and 23.5 °C at BRN in 2018, and 36.1 psu at LRS and LFZ in 2017 and 36.8 psu at BRN and BXZ in 2016 and BRN in 2018. The average depth values of autumn temperature and salinity ranged between 14.8 °C at BXZ and BRN in 2020 and 18.5 °C at BRN in 2021, and 35.8 psu at LRN 2020 and 36.6 psu at BXZ in 2021. In general, warmer (colder) water is found at nearshore sites (e.g., BXZ, BRN) during summer (autumn) and is likely the result of summer heating (autumn cooling) acting on the shallower embayment where these sites are located. Similarly, salinity levels at the nearshore sites were generally higher than those at the offshore sites, as local evaporation will have a greater effect in shallower waters.

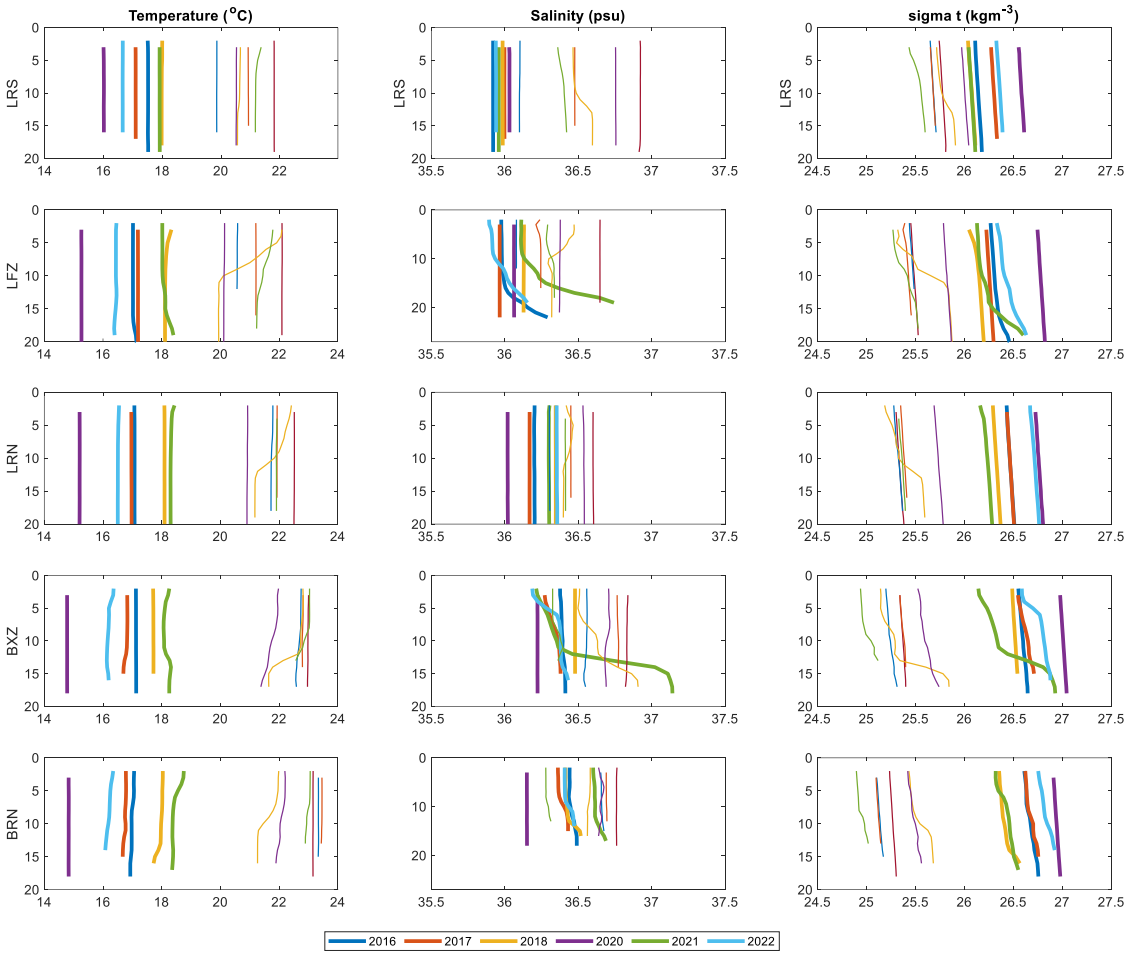

Figure 2-3: Vertical profiles of temperature, salinity and density (sigma t = density-1000) measured at each site in summer (thin lines) and in autumn (thick lines). The line colours correspond to the measurement year shown in the legend.

Aquaculture Derived Nitrogen Inputs

Between 2016 and 2022, 95% of the dissolved inorganic nitrogen (DIN) loads sourced from supplementary fed aquaculture were released into the Lower Eyre Peninsula Aquaculture Zone (LEPZ) region. The estimated annual DIN loads in the LEPZ ranged from 1,429 tonnes in 2021 to 1,625 tonnes in 2018 (Table 2-4). On average, 83% of the DIN released into the LEPZ over this period was from tuna and 17% from finfish aquaculture. Monthly DIN loads peaked around April-May and coincided with the peak input of SBT and YTK feed (Figure 2-4), with a maximum of 360.6 tonnes (343.1 t SBT and 17.5 t YTK) estimated to be released in March 2022. The maximum annual and monthly loads into the LEPZ are approximately 16% and 12% less than those estimated in 2006 for SBT alone (Tanner and Volkman 2009).

Table 2-4: Estimated annual dissolved inorganic nitrogen (DIN) loads (tonnes) emitted into the Lower Eyre Peninsula Zone from the supplementary feeding of southern bluefin tuna (SBT) and yellowtail kingfish (YTK).

Year	SBT DIN	YTK DIN	Total DIN
2016	1,237	232	1,469
2017	1,215	270	1,485
2018	1,359	266	1,625
2019	1,352	206	1,558
2020	1,305	240	1,545
2021	1,143	287	1,430
2022	1,281	290	1,571

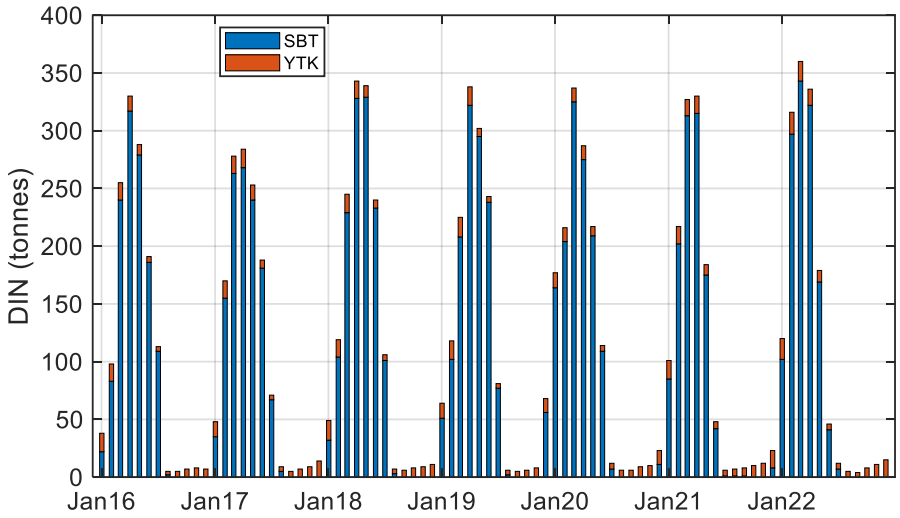

Figure 2-4: Estimated monthly dissolved inorganic nitrogen (DIN) loads (tonnes) emitted into the Lower Eyre Peninsula Zone. Blue and orange colours indicate the nitrogen component for the two main feed types; baitfish and manufactured associated with the supplementary feeding of southern bluefin tuna (SBT) and yellowtail kingfish (YTK), respectively.

Coupled Hydrodynamic-Biogeochemical Model Validation

Comparison of the hydrodynamic model results with the observations taken at LRS is shown in Figure 2-5. For validation, the predictive skill and performance of the model were assessed using three metrics: bias, root-mean-square error (RMS), and coefficient of determination (r^2). Bias is the difference between the mean value predicted by the model and the measured mean, RMS error is the sum of the root-mean-square of the differences between the model and the measurement, and r^2 is a measure of the fraction of variability (i.e., variance) explained by the model.

In general, the performance of the hydrodynamic model was very good. The model can reproduce the observed magnitude and variability associated with high (i.e., tidal) and low frequency (i.e., weather band to seasonal changes) variations across each of the parameters. The model shows excellent predictive ability (i.e., small bias and RMS values and high r^2 values) for tidal currents (r^2=0.94, bias=0 m/s and RMS=0.05 m/s) and temperature (r^2=0.90, bias= 0.47 ^oC and RMS=0.7 ^oC). Salinity was the most sensitive parameter to validate (r^2=0.32, bias= -0.08 psu and RMS=0.45 psu). This is in part due to the limitations in the global atmospheric forcing (e.g., precipitation and evaporation rates, spatial and temporal resolution) and its interactions with shallow gulf waters, which influence the prediction of salinity, and the difficulty of calibrating sensors and measuring salinity with high accuracy due to sensor drift and bio-fouling.

The comparison of the daily average of modelled and measured dissolved inorganic nitrogen (NH_4^+ and NO_x) and chl-*a* concentration taken at the monitoring sites over the period 2016-2022 is shown in Figure 2-6. The model considerably underestimated NO_x and chl-*a* concentrations. This is likely due to the underestimation of nitrate supplied into Spencer Gulf from the CARS climatology applied on the model's shelf boundary. The model provided reasonable predictions for NH_4^+ (r^2= 0.28) and at times reproduced elevated concentrations (> 5 µg/L) associated with aquaculture emissions. Comparison of mean NH_4^+ concentrations averaged at the five monitoring sites between 2016 and 2022 showed that the model (4.3±3.9 µg/L) slightly overestimated the observed concentrations (2.7±3.6 µg/L). Given the good validation of hydrodynamic models for ocean currents, the model is useful to inform on the transport and connectivity of NH_4^+ sourced from aquaculture and other anthropogenic sources, but it has limited capacity to predict concentrations of nitrate or chl-*a*.

Figure *2-7* demonstrates the seasonally averaged distribution of surface NH_4^+ concentrations predicted by the model for the 2022 calendar year. During autumn (and winter) NH_4^+ sourced from SBT aquaculture in the Lincoln inner sector zone dominates the system in the offshore waters east of Boston Island. Due to the increased flushing capacity of offshore waters, NH4 + emissions are generally rapidly dispersed and diluted below 35 µg/L within the boundaries of the Lincoln inner sector zone. These nutrients are transported into Boston Bay and Louth Bay, where they undergo further dilution and mixing with nutrients emitted from YTK aquaculture located in the Boston Bay aquaculture zone. For all other seasons, NH_4^+ emissions sourced from SBT and YTK aquaculture are smaller with highly localised footprints. The maximum predicted concentrations at leases of ~10 µg/L are quickly diluted to background levels (< 5 µg/L) within a few hundred metres of the lease sites. Figure 2-8 shows the mean surface ammonium (NH4+, µg/L)

concentrations averaged during the period 2019 to 2022 and provides an example of the average long-term nutrient exposure of the regions bays to aquaculture-derived nutrient emissions.

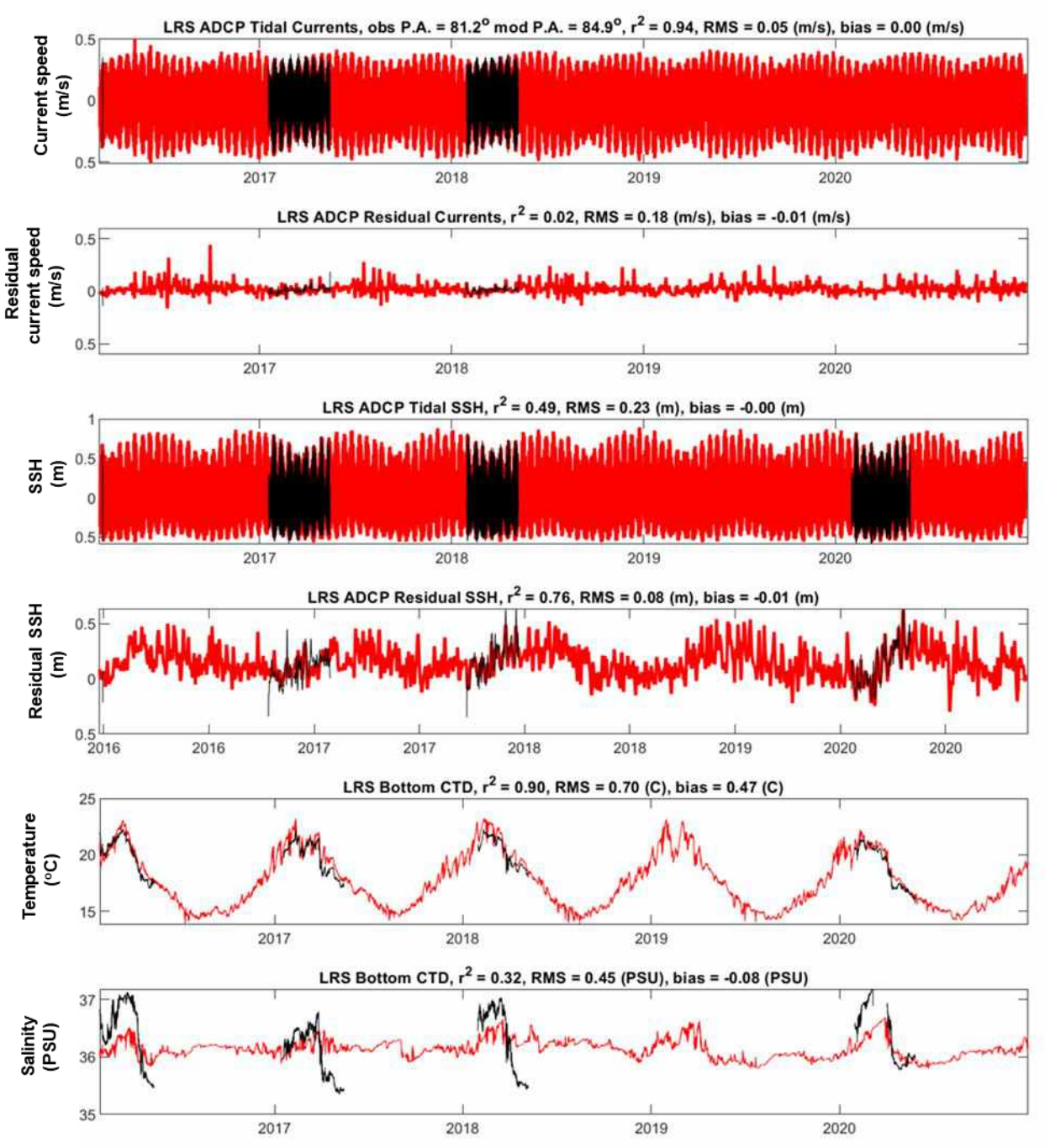

Figure 2-5: Example of the validation results for currents (tidal and residual) (m/s), sea-surface height (SSH; tidal and residual (m)), temperature (°C), and salinity (PSU) at LRS. Black lines show measured observations and red lines model predictions. Comparison statistics are shown above each plot.

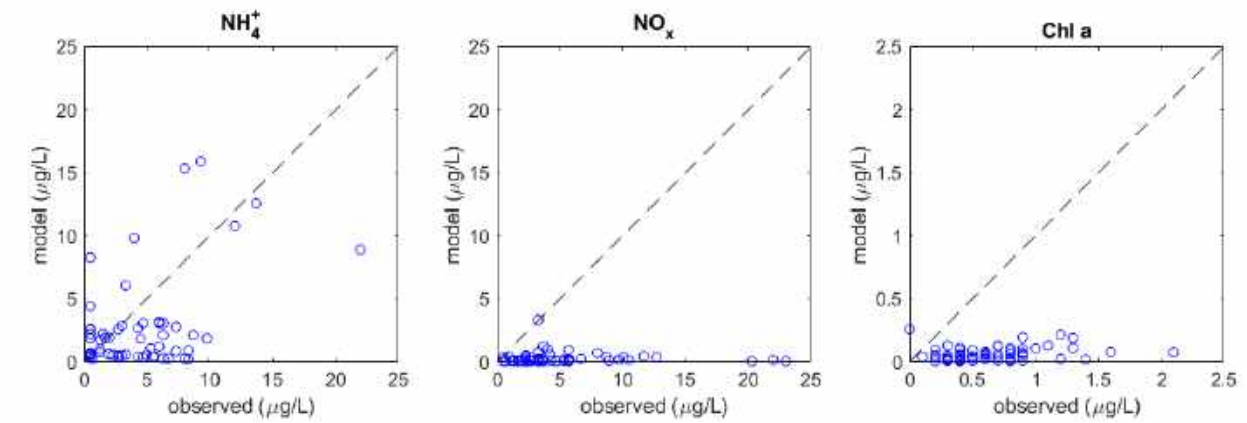

Figure 2-6: Comparison of observed concentrations versus the predictions of the corresponding daily averaged model for oxides of nitrogen (NO_x) ammonium (NH_4^+) and chlorophyll *a* (chl-*a*).

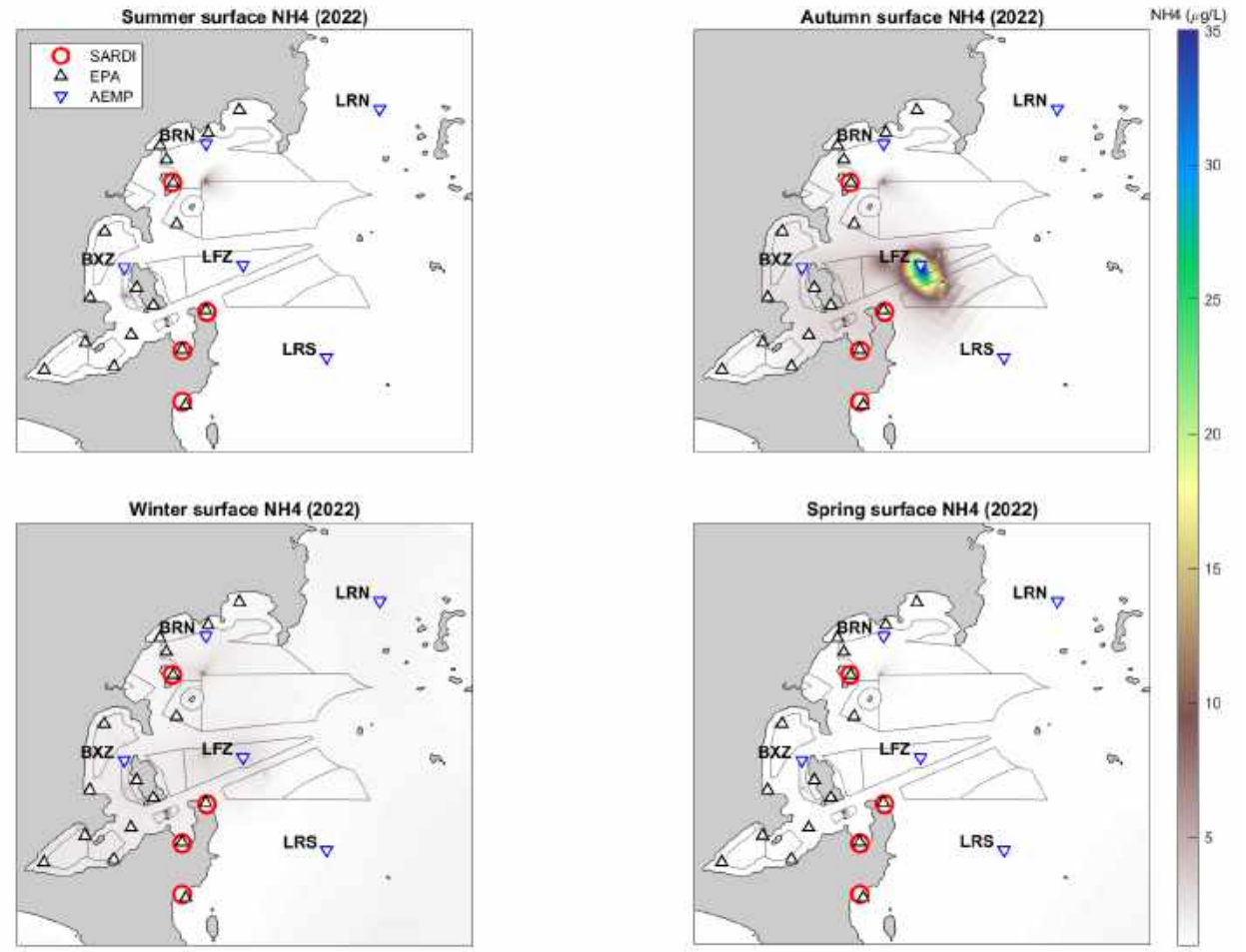

Figure 2-7: Modelled predictions of the seasonally averaged distribution of surface NH_4^+ concentrations (µg/L) in the Port Lincoln region for the 2022 calendar year. The location of the SARDI and EPA seagrass sites (red circles) and the boundaries of the aquaculture zone (grey polygons) are shown for reference.

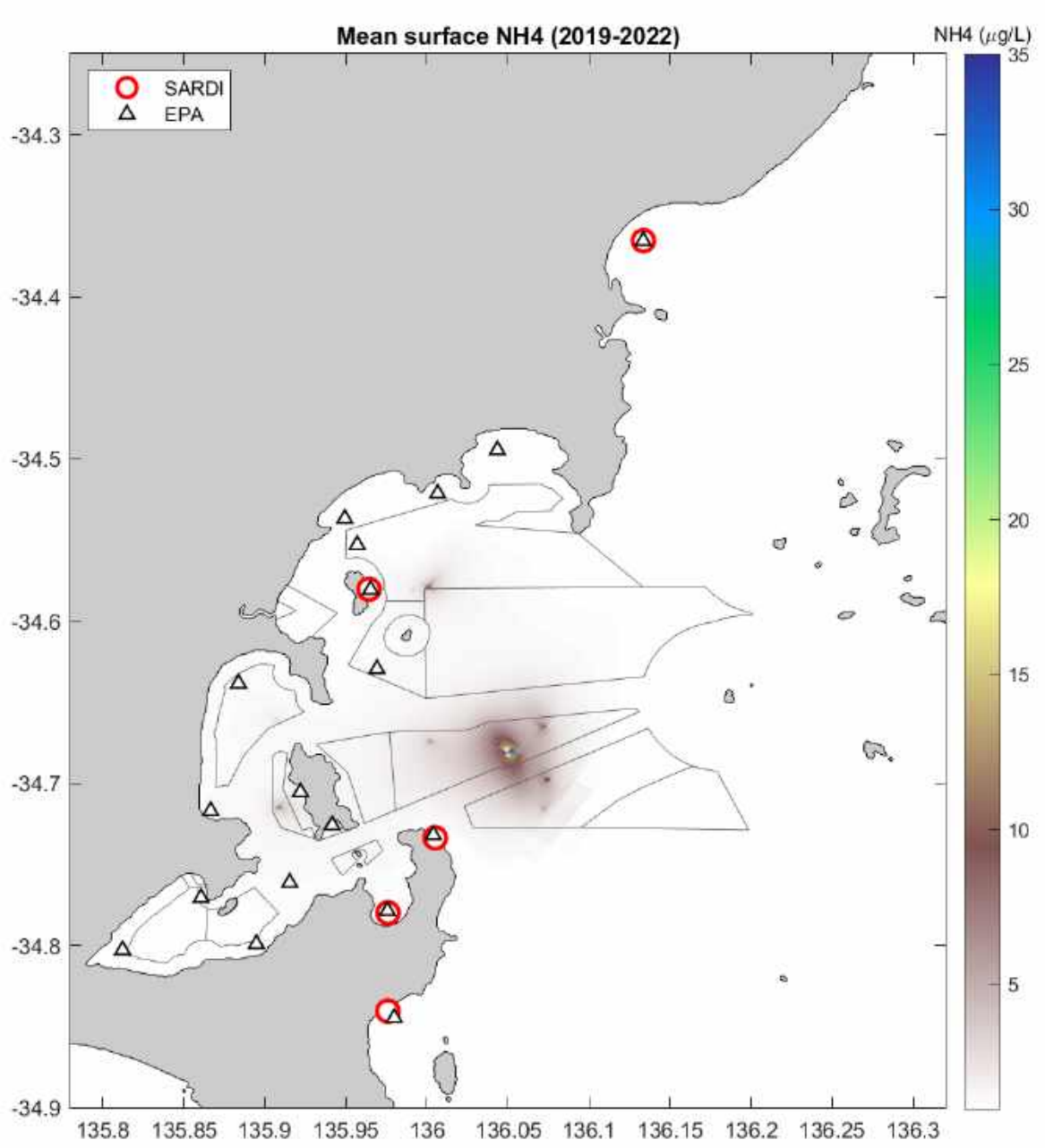

Figure 2-8: The modelled mean surface ammonium (NH4+, µg/L) concentrations were averaged over the period 2019 to 2022. The location of the SARDI and EPA seagrass sites and the boundaries of the aquaculture zone are shown for reference.

Water Quality: Dissolved Inorganic Nutrients, Chlorophyll *a* Biomass and F_p Ratio

Dissolved inorganic nutrient concentrations measured at each site during the summer and autumn surveys are shown in Figure 2-9 and Figure 2-10. NO_x concentrations ranged from the detectable limits to 35±7.2 µg/L and were below the historical south-central regional ANZECC/ARMCANZ (2000) water quality trigger value of 50 µg/L. Mean NO_x concentrations were significantly different

between years (ANOVA: $F_{5,20}$ = 11.5, *P*<0.001) and seasons ($F_{1,20}$ = 4.4, *P*<0.05). A significant interaction between year and season ($F_{5,20}$ = 15.5, *P*<0.001) indicated that the seasonal changes are different between years. Pairwise comparisons showed that this interaction was driven by the large concentrations of NO_x observed at all sites in summer 2020. A possible explanation for the high concentrations measured in 2020 is an influx of nutrient rich upwelled water from the adjacent shelf region. This is supported by the low bottom temperatures <13 ^oC observed at the IMOS Kangaroo Island National Reference Station during January and February 2020 (data not shown) which are associated with increased NO_x concentrations (Shute et al. 2022), and the coincident cooler temperatures (Figure 2-3) and offshore to inshore NO_x gradient observed across the AEMP monitoring sites (Figure 2-9).

Excluding the anomalously high summer 2020 observations, mean seasonal NO_x concentrations ranged between 2.4±0.4 µg/L (BXZ) to 3.2±0.3 µg/L (LRS) in summer, and 3.7±0.3 µg/L (BXZ and BRN) to 7.8±0.5 µg/L (LFZ) in autumn. Mean seasonal concentrations exceeded the 2018 revised 80th percentile Integrated Marine and Coastal Regionalisation of Australia (IMCRA) default guideline value (DGV) (Table 2-5) for slightly to moderately disturbed systems recommended for the Spencer Gulf bioregion (ANZG 2018).

Table 2-5: Updated ANZG 2018 default guideline values (DGVs) (µg/L) recommended for the Spencer Gulf bioregion based on the finer-scale Integrated Marine and Coastal Regionalisation of Australia (IMCRA) 80th percentile values for slightly to moderately disturbed systems.

Variable	Summer	Autumn	Winter	Spring
NO_3-N (µg/L)	1.8	2.5	3.9	1.1
PO_4^{3-}-P (µg/L)	3.1	2.8	6.7	8.6
SiO_4-Si (µg/L)	35.5	39.9	35.9	49.8
Chl-*a* (µg/L)	0.8	1.2	1.0	0.6

NH_4^+ concentrations ranged from below detectable limits to 22±1.2 µg/L, with the maximum recorded at LFZ in 2018 (Figure 2-9). The mean concentrations of NH_4^+ were significantly different between years (ANOVA: $F_{5,20}$ = 31.1, *P*<0.001) and seasons ($F_{1,20}$ = 6.6, *P*<0.05). Significant interactions between year and season ($F_{5,20}$ = 4.1, *P*<0.05) and season and site ($F_{4,20}$ = 5.5, *P*<0.05), indicate that seasonal changes are different between years and sites. Pairwise comparisons showed significantly higher mean concentrations in 2016, 2020 and 2022 compared to other years. The mean concentrations in summer averaged at all sites (3.6 ±0.09 µg/L) were

significantly lower than those measured in autumn (5.0 ±0.16 µg/L). The mean concentrations at LFZ during the autumn were significantly higher than those measured at other sites. The observed NH_4^+ concentrations were below the historical ANZECC/ARMCANZ (2000) water quality trigger level of 50 µg/L previously recommended for the south-central region. While there are no updated DGVs for NH_4^+recommended by IMCRA at the resolution of Spencer Gulf, the 2018 revision of water quality guideline values significantly changed the broader regional scale DGV for NH_4^+ down to a concentration of 5 µg/L for marine waters in the south-west Australia mesoscale bioregion (ANZG 2018). This lower DGV level was regularly exceeded, especially within the aquaculture zone at LFZ in autumn, however it is also exceeded outside of the zone and the main aquaculture plume at LRS in both summer and autumn, suggesting that it is likely to be too stringent for this region of Spencer Gulf.

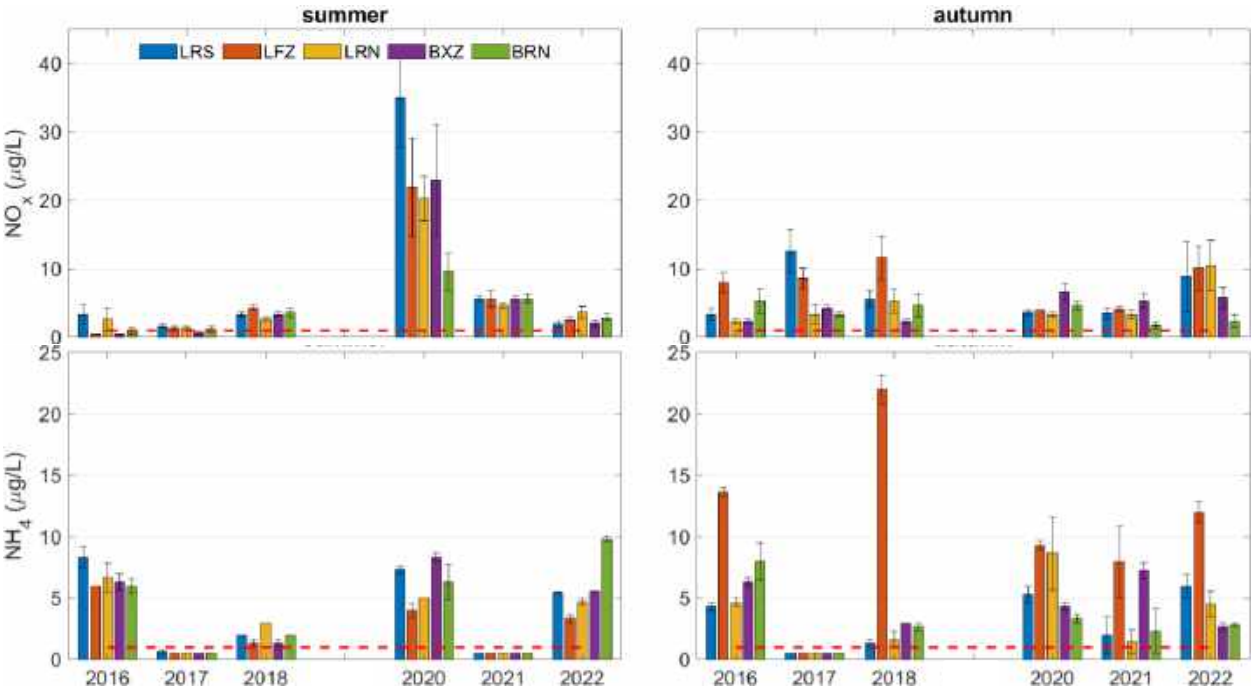

Figure 2-9: Mean dissolved inorganic nutrient concentrations for NO_x and NH_4^+ (µg/L) measured in (left panels) summer and (right panels) autumn at each site. Error bars are ± 1 standard error. Red dashed line shows the detection limit. No data were available for 2019.

PO_4^+ concentrations ranged between below detectable limits to 8.7±0.3µg/L, with the maximum recorded at LRN in 2020 (Figure 2-10). The mean concentrations of PO_4^+ were significantly different between years (ANOVA: $F_{5,20} = 21.1$, $P<0.001$), seasons ($F_{1,20} = 8.7$, $P<0.001$) and sites ($F_{4,20} = 7.6$, $P<0.001$) with no significant interactions. PO_4^+ concentrations were commonly very low or below detectable limits, except in 2020 when they were significantly higher than in other years. The mean concentrations measured at LFZ in the autumn were significantly higher than

those measured at other sites. Except for 2020 or during autumn at LFZ, PO_4^+ concentrations remained below the recommended IMCRA DGV values.

Si concentrations ranged between below detectable limits to 130±0.0µg/L, with maximums recorded at BXZ in summer and autumn 2018 (Figure 2-10). Mean Si concentrations were significantly different between years ($F_{5,20}$ = 4.9, P<0.001), seasons ($F_{1,20}$ = 6.3, P<0.05) and sites ($F_{4,20}$ = 6.3, P<0.05) with no significant interactions. Si concentrations exceeded the IMCRA DGV's and were significantly higher in 2016, 2018, 2021 and 2022 compared to 2017 and 2020, and during autumn (62.9±1.1 µg/L) compared to summer (52.8±1.0 µg/L). The mean concentrations at BXZ were significantly higher than those measured at LRS, LFZ and LRN. There was no significant difference between the BXZ and BRN inshore sites.

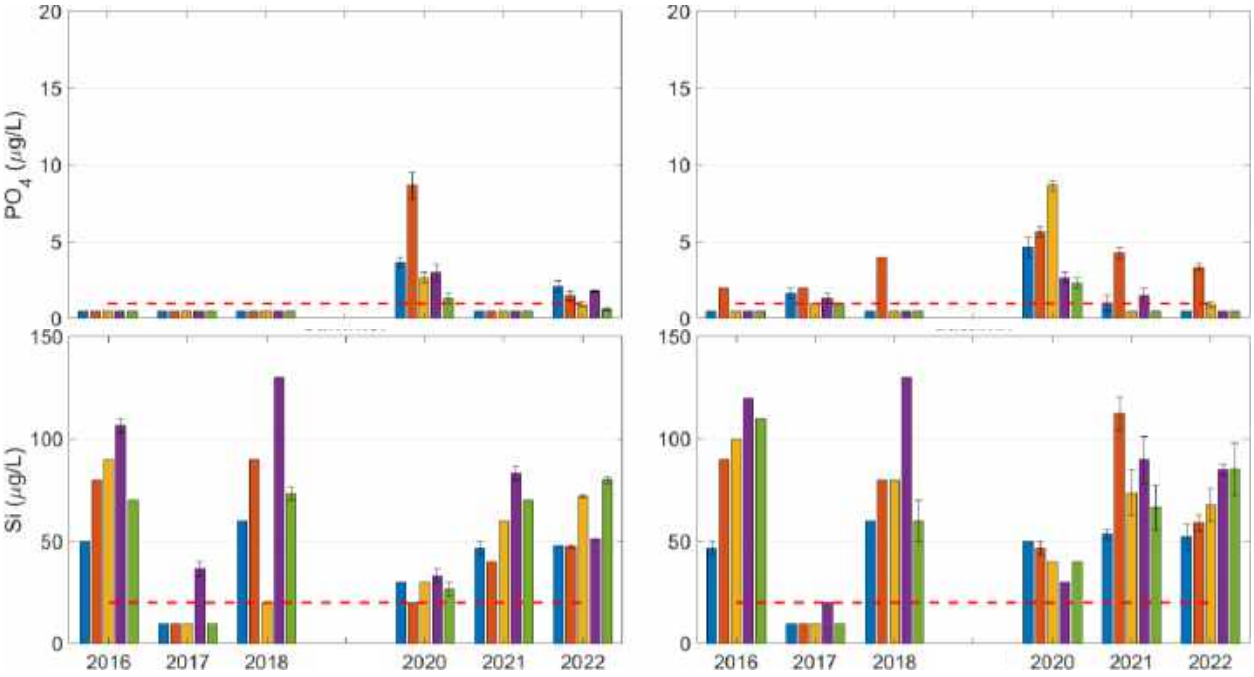

Figure 2-10: Mean dissolved inorganic nutrient concentrations for PO_4^+ and Si (µg/L) measured in (left) summer and (right) autumn at each site. Error bars are ± 1 standard error. Red dashed line shows the detection limit. No data were available for 2019.

Following Redfield (1963), examination of the nutrient ratios (N:Si:P = 16:15:1) required to support phytoplankton growth showed that phosphorus was the most likely limiting nutrient; however, periods of potential limitation of nitrogen and silicate also occurred (

Figure **2-11**).

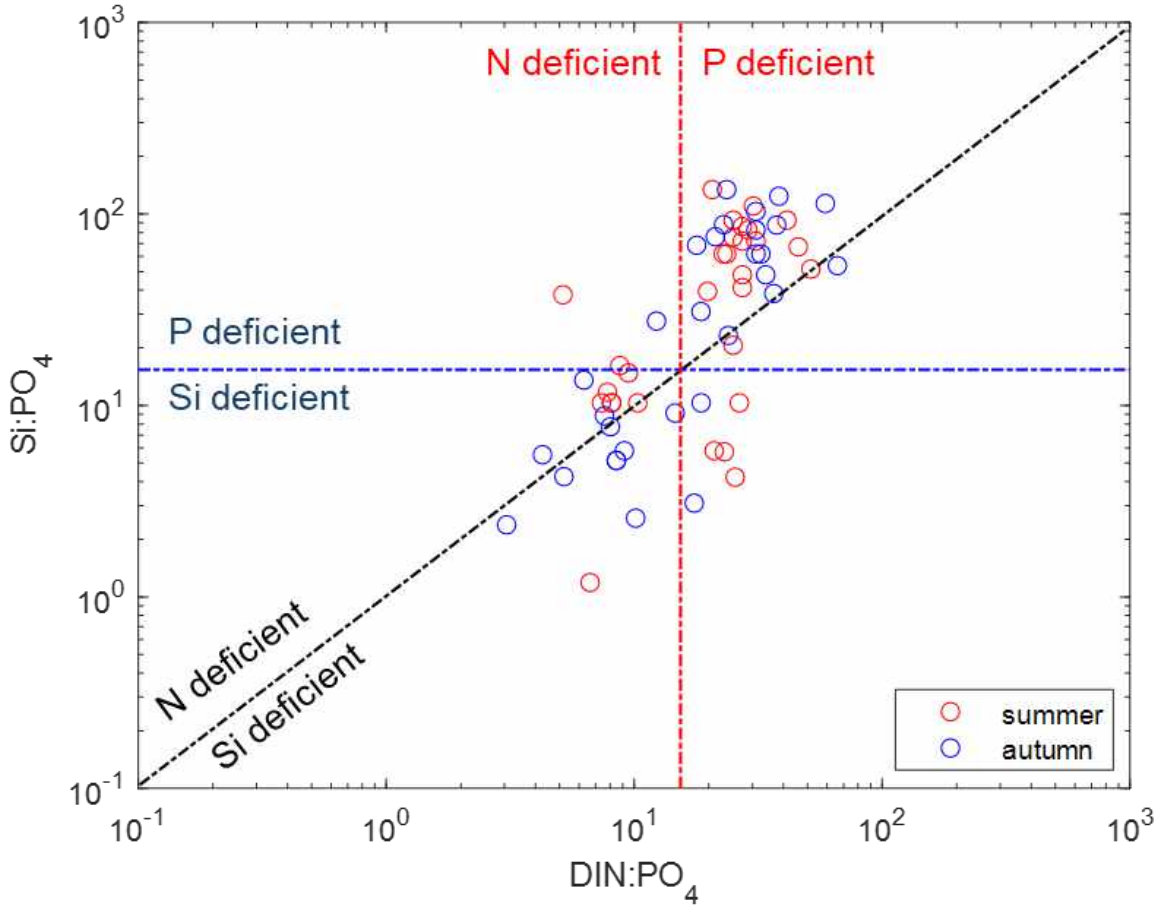

Figure 2-11: Nutrient ratio-ratio plot. The dashed red, blue and black lines represent standard Redfield stoichiometric ratios (16N: 15Si: 1P). The number of points in each sector indicates the potential for limitation by a particular nutrient.

Chl-*a* concentrations ranged from 0.04 µg/L at LFZ in autumn 2017 to 2.12 µg/L at BXZ in 2022 (Figure 2-12). Mean chl-*a* concentrations were significantly different between seasons (ANOVA: $F_{1,20}$ = 25.9, *P*<0.001) and sites ($F_{4,20}$ = 12.3, *P*<0.001). A significant interaction between year and season ($F_{5,20}$ = 3.1, *P*<0.05) indicated that seasonal changes are different between years. The mean summer concentration (0.48 µg/L) across all sites was significantly lower than the autumn concentration (0.83 µg/L). Pairwise comparisons showed that mean autumn 2020 and 2022 concentrations were significantly higher compared to those measured in the corresponding summers. Mean concentrations at LFZ, BRN, and BXZ were significantly higher than those at LRS. The mean concentrations at BXZ were significantly higher than those measured at all other sites, except BRN. Although the mean seasonal concentrations were below the historical

ANZECC/ARMCANZ (2000) trigger value of 1 µg/L and the IMCRA DGV's, observed concentrations at LFZ, BXZ, and BRN at times exceeded the revised 2018 DGV's in autumn.

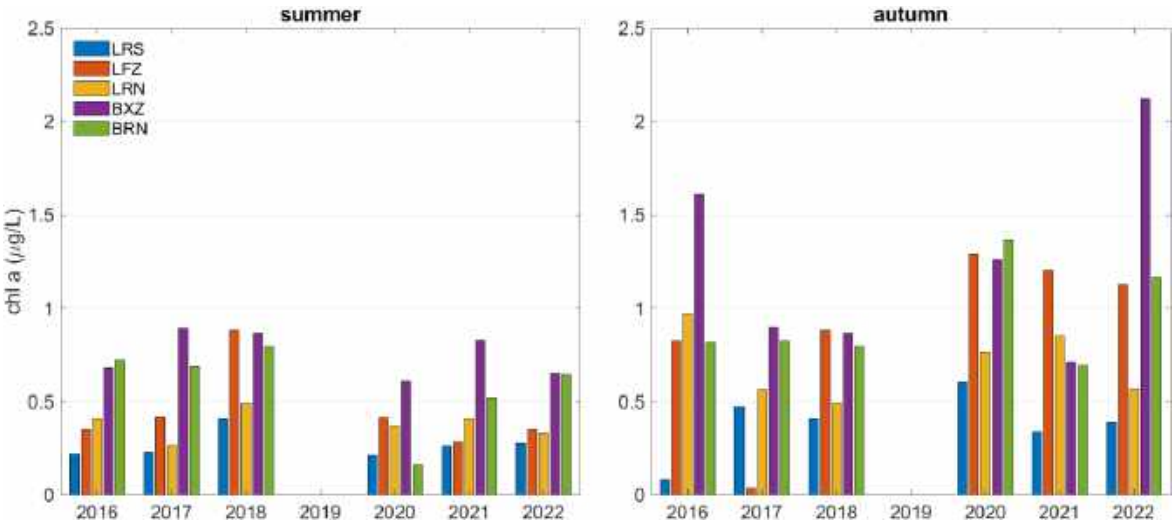

Figure 2-12: Chlorophyll-*a* concentrations (µg/L) measured in (left panels) summer and (right panels) autumn at each site. No data were available for 2019.

The F_p ratio (Figure 2-13) was significantly different between years (ANOVA: $F_{5,20}$ = 27.5, P<0.001), seasons ($F_{1,20}$ = 32.8, P<0.001) and sites ($F_{4,20}$ = 44.6, P<0.001), with significant interactions between year and season and ($F_{5,20}$ = 5.1, P<0.05) and year and site ($F_{20,20}$ = 3.4, P<0.05). These results indicate that the F_p ratio changes between sites and seasons each year. Pairwise tests showed that mean F_p ratios between sites were greater in autumn 2016, summer and autumn 2020, and autumn 2021 compared to other times. The F_p ratios at BRN and LFZ were higher than those estimated for LRS and LRN in 2020. BXZ had significantly higher values than those estimated for offshore sites LRS, LRN and LFZ in most years.

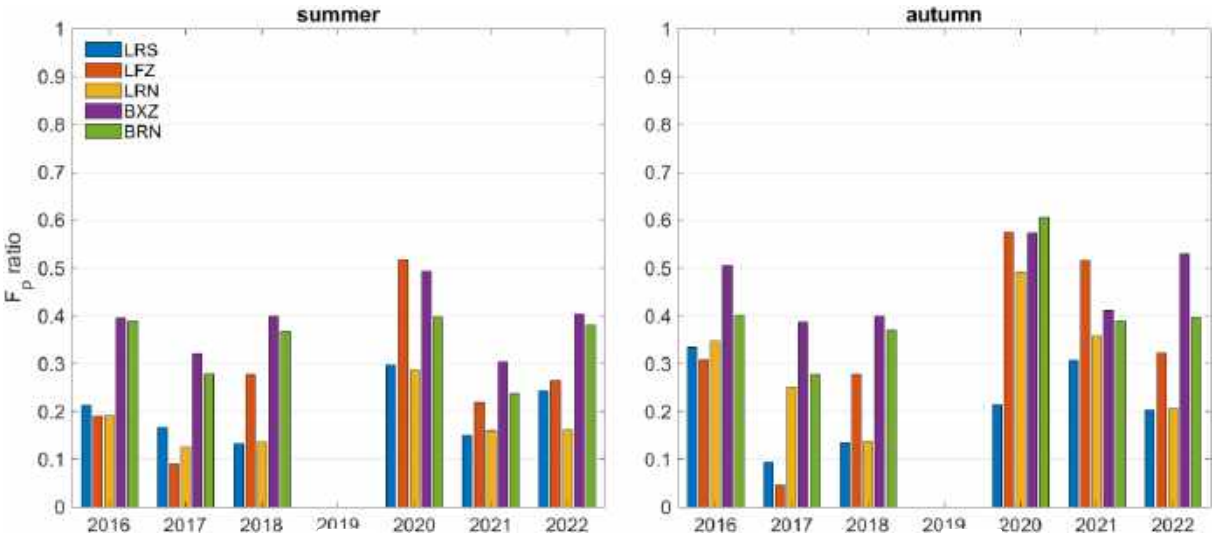

Figure 2-13: Estimated F_p ratios in (left) summer and (right) autumn at each site. No data were available for 2019.

Particulate Matter

TSS concentrations were generally low and below 5.0 mg/L with a minimum concentration of 1.6 mg/L (Figure 2-14). Distinct spikes were observed with maximum concentrations of 71.5 mg/L in summer 2016 at BXZ and 67.5 mg/L in autumn 2017 at LRN. Factorial ANOVA detected no significant differences between year, season or site.

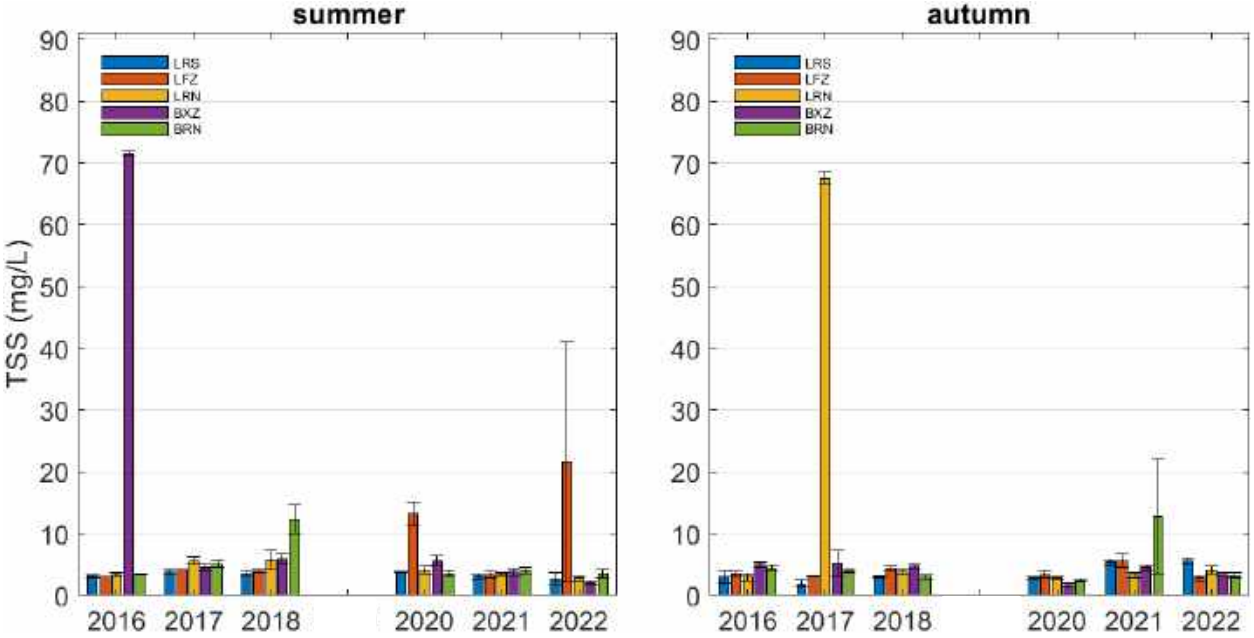

Figure 2-14: Total suspended solid concentrations (mg/L) measured in (left) summer and (right) autumn at each site. No data were available for 2019.

Bacteria and Zooplankton Abundance

Bacterial concentrations ranged from 172,620 ± 4007 cells/mL at LRS in summer 2016 to 15,246,364 ± 139,012 cells/mL at BXZ in autumn 2020 (Figure 2-15). Bacterial concentrations were significantly different between years (ANOVA: $F_{5,20}$ = 10.4, P<0.001) and seasons ($F_{1,20}$ = 19.1, P<0.001). A significant interaction between year and season ($F_{5,20}$ = 2.34, P<0.05) indicated that seasonal changes are different between years. Pairwise comparisons showed this interaction was largely driven by the elevated concentrations of bacteria observed in autumn 2020.

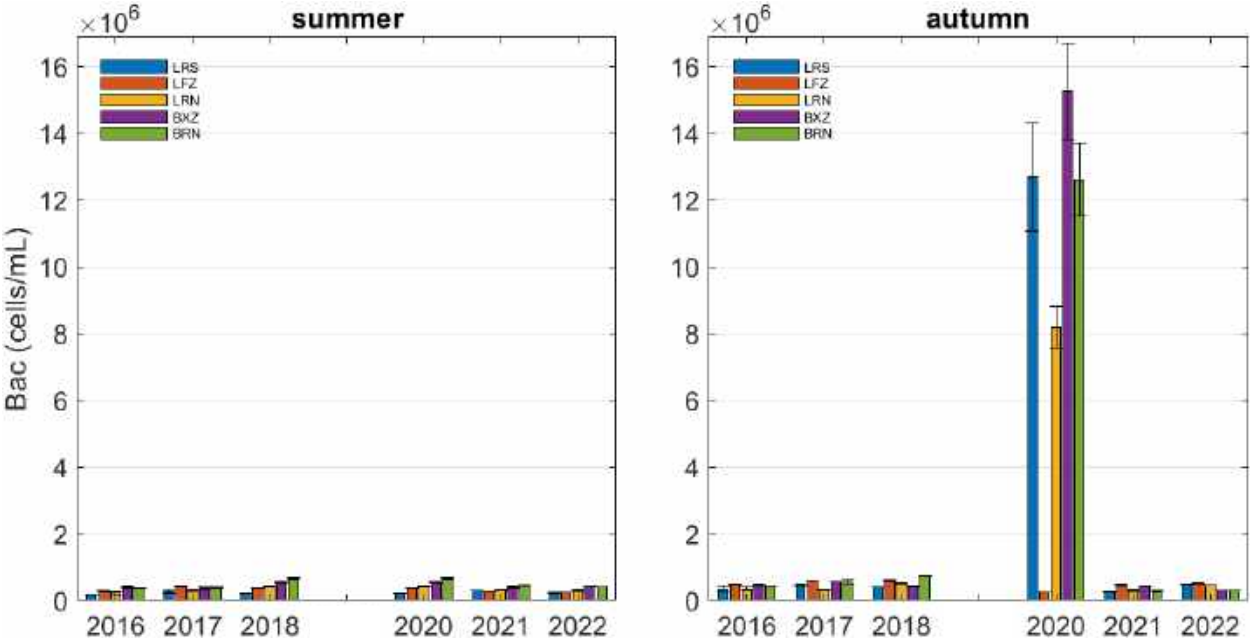

Figure 2-15: Bacterial abundances (cells/mL) measured in (left) summer and (right) autumn at each site. No data were available for 2019.

Zooplankton abundances in the small size fraction were generally greater than those observed in the large size fraction (Figure 2-16). Small zooplankton were significantly different between sites ($F_{4,20}$ = 7.6, P<0.001). Pairwise comparisons showed that mean abundances at BXZ and BRN were significantly greater than those observed at other sites. The abundances of large zooplankton were significantly different between years ($F_{5,20}$ = 9.9, P<0.001). Pairwise comparisons showed that mean abundances in 2020, 2021 and 2022 were significantly higher than observed in 2016, 2017 and 2018.

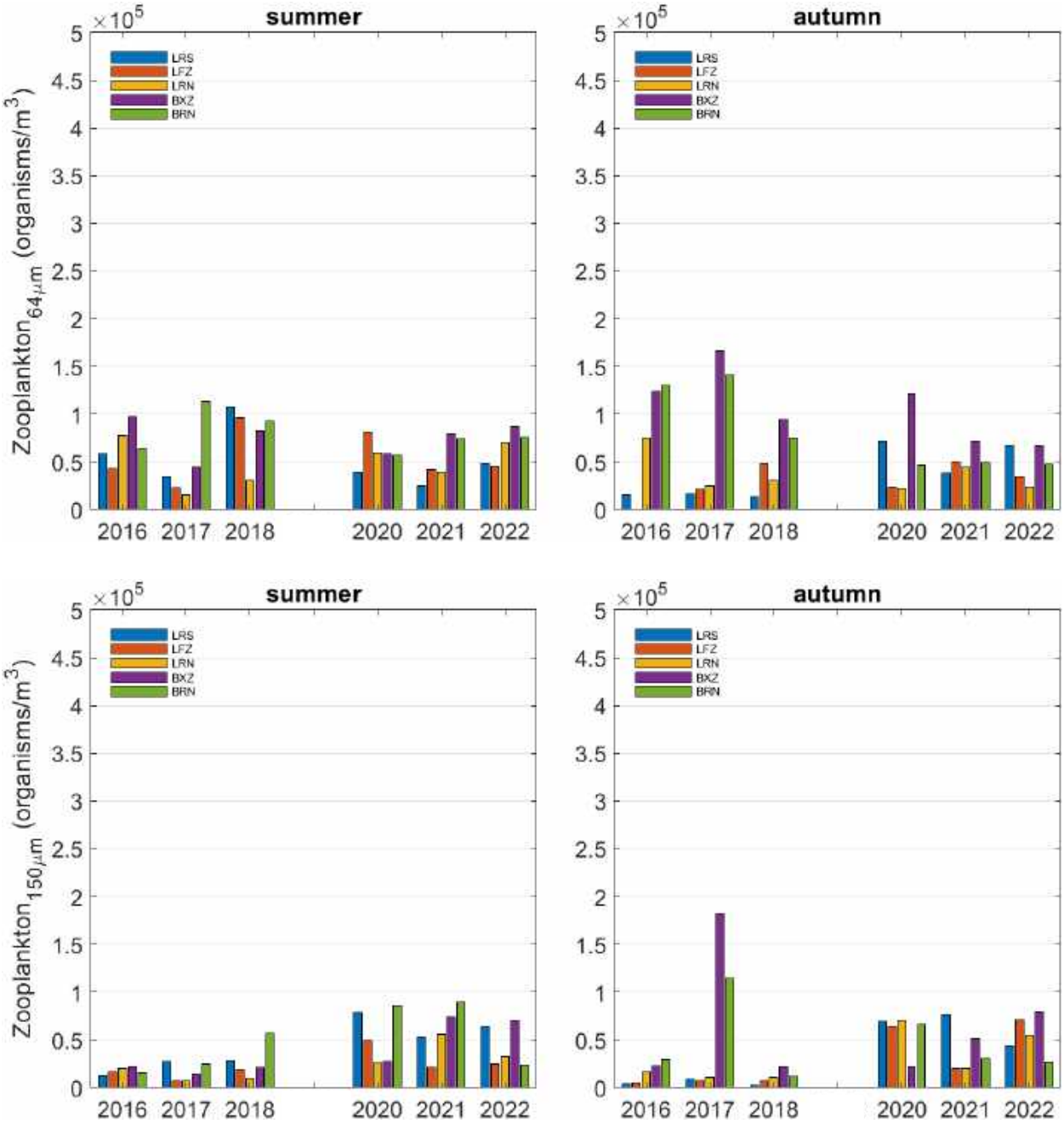

Figure 2-16: Zooplankton abundance (organisms m^{-3}) collected from the (top) 64 µm and (bottom) 150 µm mesh net in (left panels) summer and (right panels) autumn at each site. No data were available for 2019.

Phytoplankton Community Composition

Microscopy identified 193 species of phytoplankton belonging to 8 genera, including 65 species of diatoms, 74 species of dinoflagellates, 3 species of chrysophytes, 10 species of cryptophytes, 8 species of prymnesiophytes, 7 species of prasinophytes, 1 species of euglenophyta, 5 species of cyanoprokaryota and 20 species belonging to other genera. Total phytoplankton abundances ranged between 15,450 cells/L at LRS in autumn 2022 and 1,582,700 cells/L at BXZ in summer 2016 (Figure 2-17).

Mean abundances were significantly different between years (ANOVA: $F_{5,20} = 4.4$, $P<0.05$) and sites ($F_{4,20} = 13.4$, $P<0.001$) with no interaction effects. Pairwise comparisons showed that mean abundances in 2020 were significantly greater than in 2022, with no other differences between years. Between sites, mean abundances at BXZ were significantly higher than those observed at LFZ, LRN, and LRS, and mean abundances at BRN were significantly higher than those observed at LRS.

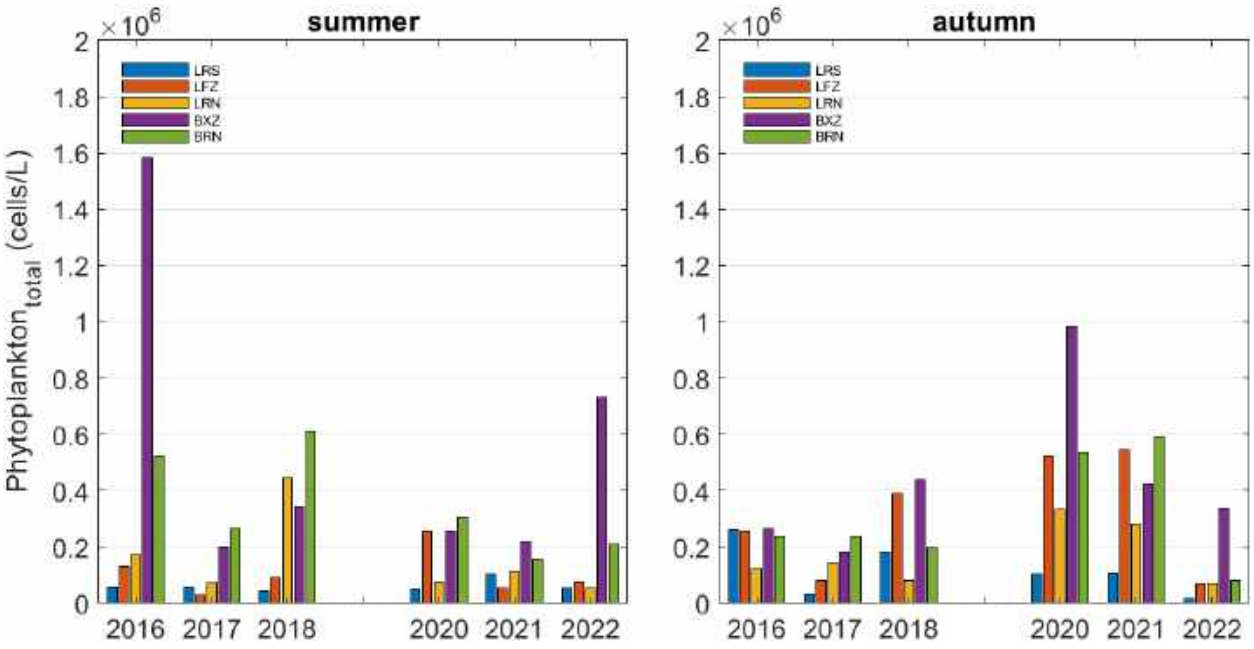

Figure 2-17: Total phytoplankton abundances (cells/L) identified by light microscopy in (left) summer and (right) autumn at each site. No data were available for 2019.

Figure 2-18 shows a breakdown of the total phytoplankton cell abundances identified by microscopy by diatoms, dinoflagellates and other flagellates. Maximum diatom abundances peaked at 488,500 cells/L (BXZ 2022) and 373,000 cells/L (BXZ 2020), in summer and autumn,

respectively. The most abundant species were *Cylindrotheca closterium, Cyclotella* spp*., Chaetoceros* spp*., Leptocylindrus danicus* and *L. minimus*. The abundances of diatoms were significantly different between years (ANOVA: $F_{5,20}$ = 2.9, *P*<0.05) and sites ($F_{4,20}$ = 7.9, *P*<0.001). A significant interaction between year and season ($F_{5,20}$ = 2.8, *P*<0.05) indicated that seasonal changes are different between years. Pairwise comparisons showed that mean abundances at BRN were greater than those at LRS. The mean abundances of BXZ were greater than those of LRS and LFZ.

Maximum dinoflagellate abundances peaked at 221,700 (BXZ 2016) and 177,150 (BXZ 2022) cells/L, in summer and autumn, respectively. The most abundant species were *Amphidinium* spp*., Gonyaulaxs* spp*.* and *Protoperidinium* spp*.* The abundance of dinoflagellates was significantly different between years (ANOVA: $F_{5,20}$ = 8.0, *P*<0.001) and sites ($F_{4,20}$ = 34.7, *P*<0.001). A significant interaction between season and site ($F_{4,20}$ = 2.9, *P*<0.05) indicated sites changes are different between seasons. Pairwise tests showed that mean abundances in 2017 were less than those measured in 2018, 2020 and 2021. Mean abundances at BXZ and BRN were significantly greater than LRS and LFZ and LRN in most years and mean abundances at LFZ were at times significantly greater than LRS and LRN.

The maximum abundances of ‘other’ flagellated genera in summer and autumn peaked at 1,120,600 (BXZ, 2016) and 492,600 (BXZ, 2020) cells/L, respectively. Examples of the most abundant species are shown in Table 2-1. Abundances showed a significant difference between years (ANOVA: $F_{5,20}$ = 2.2, *P*<0.05) and sites ($F_{4,20}$ = 12.8, *P*<0.001), with no significant interactions. Pairwise tests showed that the mean abundance of other flagellates in 2016 was greater than in 2017 and 2022, and greater in 2020 than in 2022. Mean abundances at BXZ and BRN were significantly higher than those at LRS and LRN, and mean abundances at BXZ were significantly higher than LFZ.

No significant changes were detected in the ratio of diatom to dinoflagellate or dinoflagellate to other flagellate over years, seasons or sites.

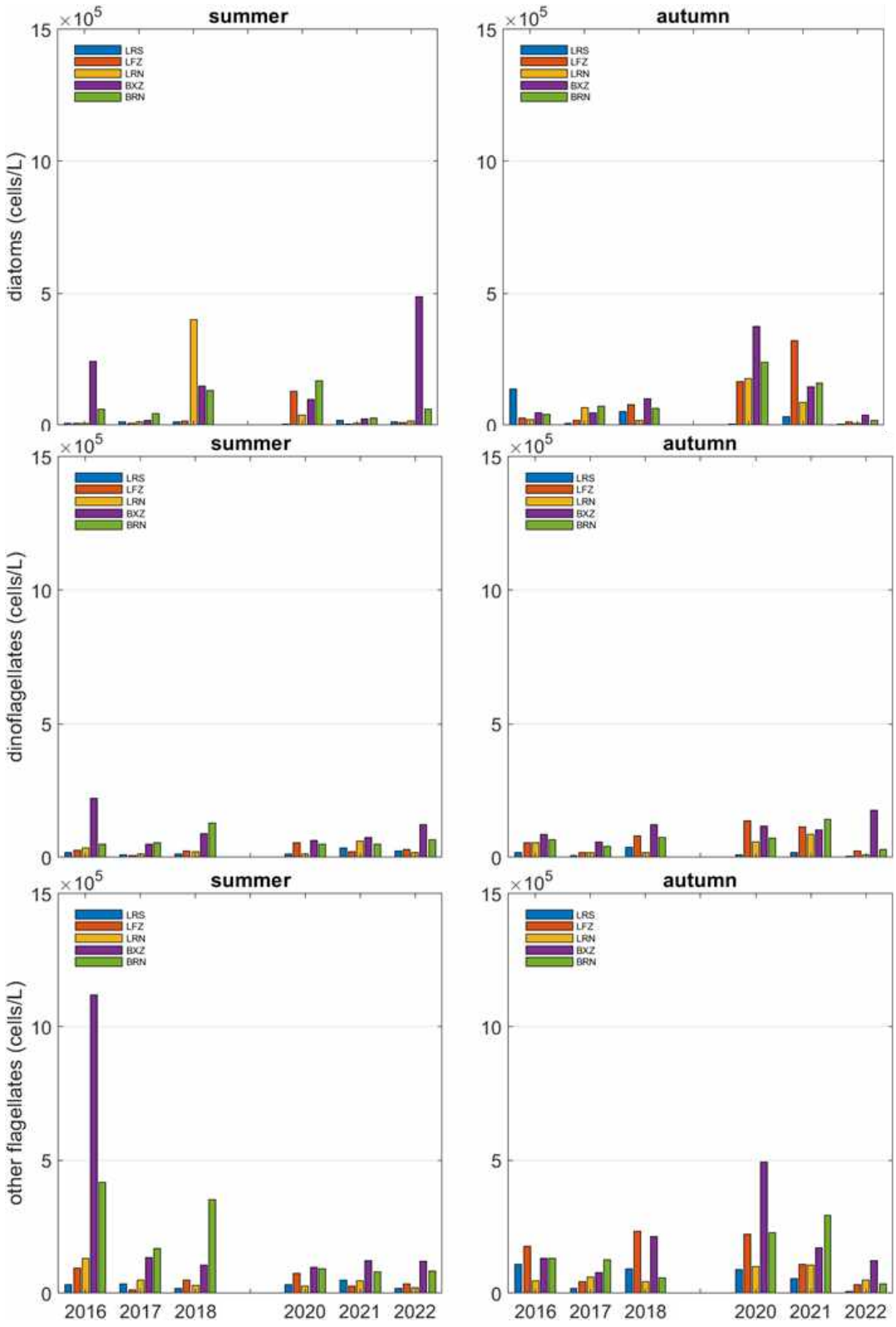

Figure 2-18: Total cell abundances (cells/L) identified by light microscopy in (left) summer and (right) autumn at each site for (top) diatoms, (middle) dinoflagellates, and (bottom) other flagellates. No data were available for 2019.

Total picophytoplankton abundances ranged between 26,497 ± 319 cells/mL at LRS in summer 2017 and 270,497 ± 4,303 cells/mL at LFZ in autumn 2017 (Figure 2-19). Within the detection capacity of flow cytometry, *Synechococcus* contributed to 80% and 62%, and *Prochlorococcus* to 18% and 28%, of the total abundances of picophytoplankton in summer and autumn, respectively. Total picophytoplankton abundances differed significantly different between years (ANOVA: $F_{5,20}$ = 3.9, P<0.05), seasons ($F_{1,20}$ = 5.2, P<0.05) and sites ($F_{4,20}$ = 3.5, P<0.05). A significant interaction between year and season ($F_{5,20}$ = 2.9, P<0.05) indicated that seasonal changes are different between years. Pairwise comparisons showed that mean abundances in 2020 and 2022 were significantly greater than in 2017 and 2018, with no other differences between years. Between seasons mean abundances were significantly greater in summer than autumn. The mean abundances at LRN and BXZ and BRN were greater than observed at LRS.

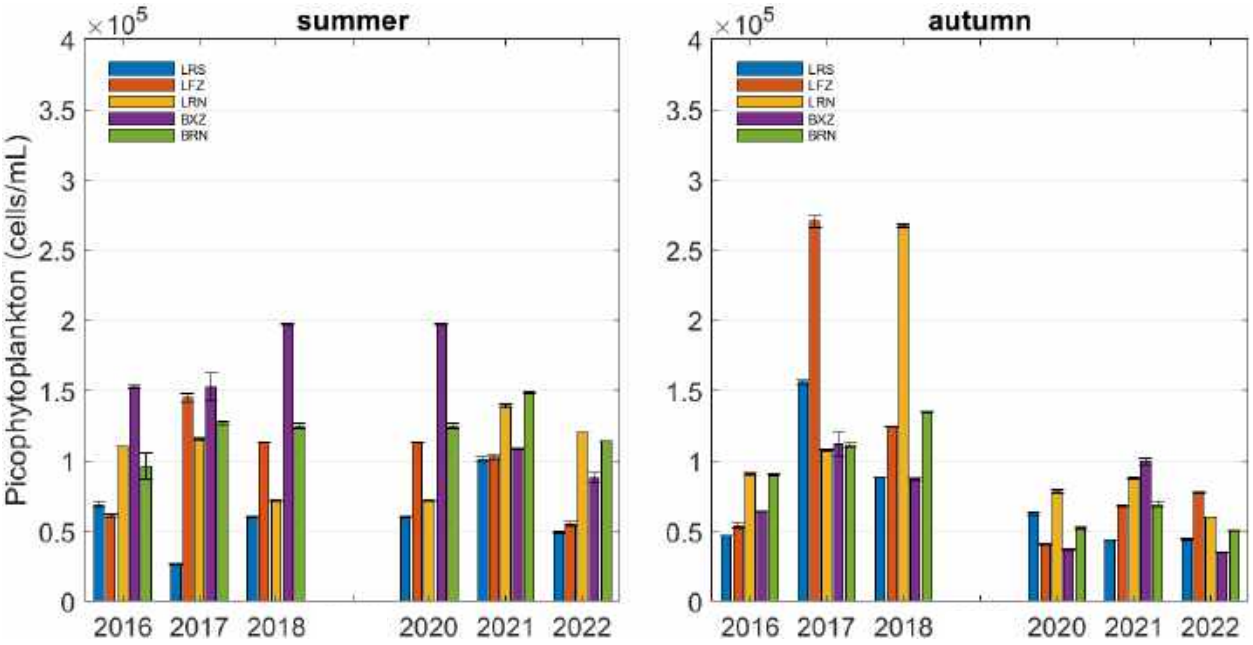

Figure 2-19: Picophytoplankton abundances (cells/mL) identified by light microscopy in (left) summer and (right) autumn at each site. No data were available for 2019.

Harmful Algal Bloom Species

A total of 37 potentially harmful algal bloom species (HAB), including both toxic and non-toxic species were identified. The dominant HAB species included diatoms of the genus *Pseudo-nitschia*, dinoflagellates of the genus *Dinophysis, Cochlodinium* and *Karenia,* and prymnesiophytes of the genus *Phaeocystis* and *Prymnesium.* Table 2-6 lists the occurrence of

the dominant HAB events identified by abundances over 20,000 cells/L. The occurrences of HAB occurrences were most prevalent in autumn in BXZ and BRN followed by LFZ. Within the limitation of the sampling frequency (i.e., 2 sampling events per year) the occurrence of HAB events (>10,000 cells/L) decreased over the course of the combined monitoring periods (Figure 2-20).

Table 2-6: Ranked list of HAB species abundances (cells/L) by site, year and season.

Site	Year	Season	Abundance	Group	Species
BRN	2016	Summer	160,000	Prymnesiophytes	*Prymnesium patellifera*
LFZ	2018	Autumn	50,000	Dinoflagellates	*Cochlodinium* spp.
LFZ	2016	Summer	50,000	Prymnesiophytes	*Prymnesium patellifera*
BRN	2021	Autumn	48,000	Prymnesiophytes	*Phaeocystis pouchetii*
BXZ	2018	Autumn	42,000	Dinoflagellates	*Cochlodinium* spp.
BRN	2018	Autumn	40,000	Dinoflagellates	*Cochlodinium* spp.
BRN	2016	Autumn	37,000	Dinoflagellates	*Dinophysis acuminata*
LRN	2021	Autumn	28,000	Prymnesiophytes	*Phaeocystis pouchetii*
BXZ	2017	Autumn	27,000	Dinoflagellates	*Dinophysis acuminata*
BXZ	2016	Autumn	26,000	Dinoflagellates	*Dinophysis acuminata*

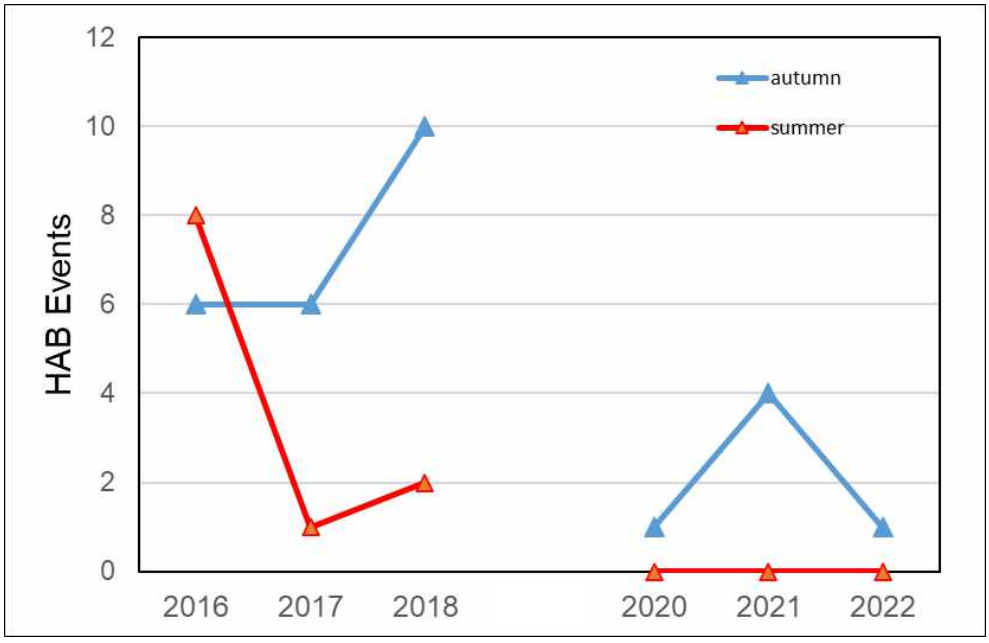

Figure 2-20: Frequency of HAB events identified by cell concentrations >10,000 cells/L across all sites during summer and autumn sampling events. No data were available for 2019.

Environmental Drivers of the Phytoplankton Community Composition

Figure 2-21 shows the contribution of the different phytoplankton groups identified by CHEMTAX analysis to the total biomass of chl-*a* (Tchl-*a*) biomass. On average, across seasons Cyanobacteria 1 (*Trichodesmium*) made the greatest contribution (25-29%) to Tchl-*a*, followed by diatoms (18-23%) and prymnesiophytes (15-16%) (Figure 2-22). Smaller contributions ranging between 3-8% were associated with euglenophytes, prasinophytes, cryptophytes, dinoflagellates, and chrysophytes, followed by cyanobacteria-2 (*Synechococcus*) and cyanobacteria-4 (*Prochlorococcus*) (1-4%).

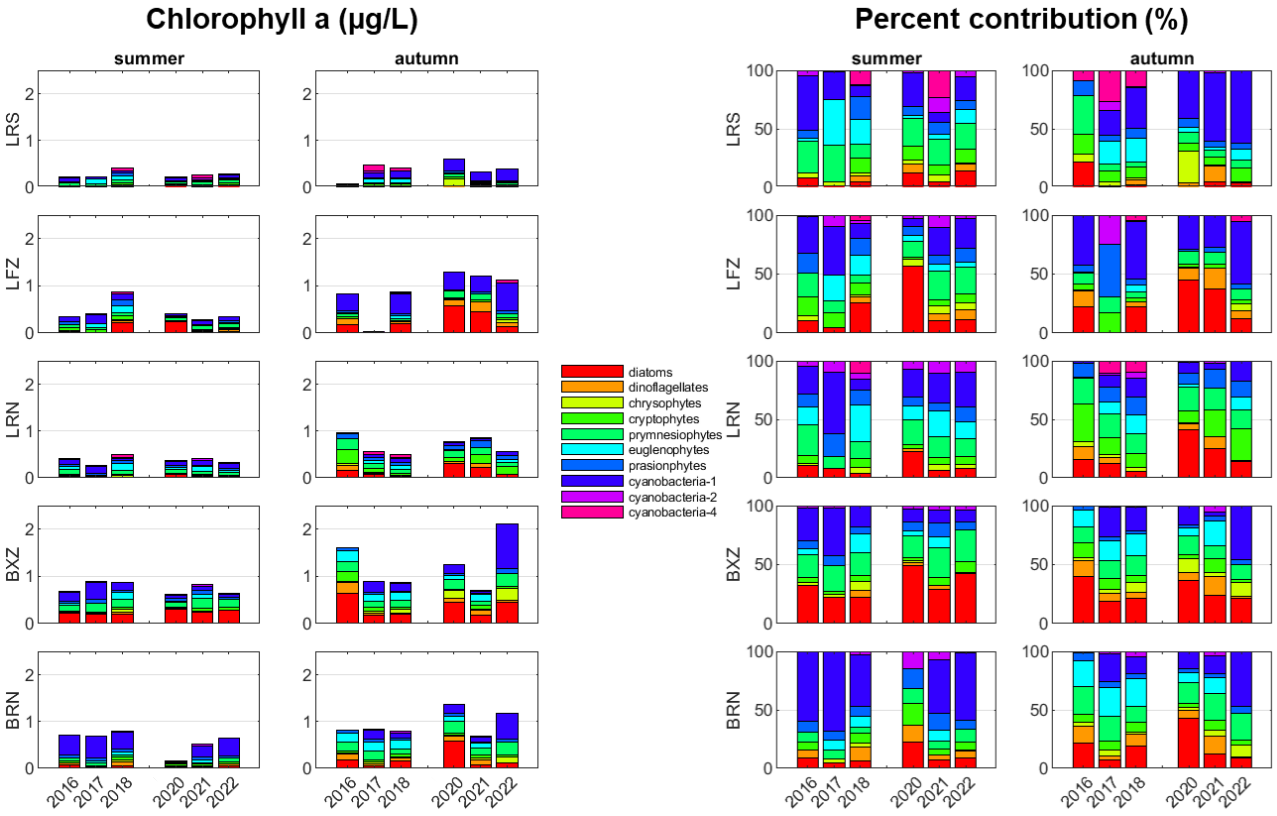

Figure 2-21: Contribution of CHEMTAX derived phytoplankton groups at each site to (left) the total chl-*a* concentration (µg/L) and (right) the relative percentage contribution of each group. No data were available for 2019.

The comparison of the CHEMTAX results with the seasonally averaged phytoplankton cell abundances determined by traditional enumeration methods is shown in Figure 2-22. To integrate and normalise the different phytoplankton size classes determined by light microscopy (i.e., nano-

microphytoplankton) and flow cytometry (i.e., picophytoplankton), cell abundances were converted to carbon biomass.

The inclusion of picophytoplankton reduced the relative contribution of microphytoplankton to the overall composition of the phytoplankton community. Importantly, CHEMTAX provided chl-*a* estimates comparable to carbon estimates for diatoms, prasinophytes and prymnesiophytes. The mean contribution of dinoflagellates estimated by CHEMTAX each season (3-7%) was less than the contribution determined by microscopy (19-23%). This is most likely due to the limitations of using peridinin as a unique diagnostic pigment for identifying heterotrophic dinoflagellates (Throndsen, 1997). Picophytoplankton carbon biomass estimated by flow cytometry accounted for approximately 20% of the total phytoplankton community biomass and included contributions from each of the cyanobacterial groups and 'other unidentified' picophytoplankton. Collectively, the cyanobacterial groups contributed between 28-34% of the chl-*a* biomass estimated by CHEMTAX, with a large contribution (25-29%) attributed to the presence of cyanobacteria-1 (*Trichodesmium*) that are not easily identifiable by microscopy or flow cytometry enumeration methods.

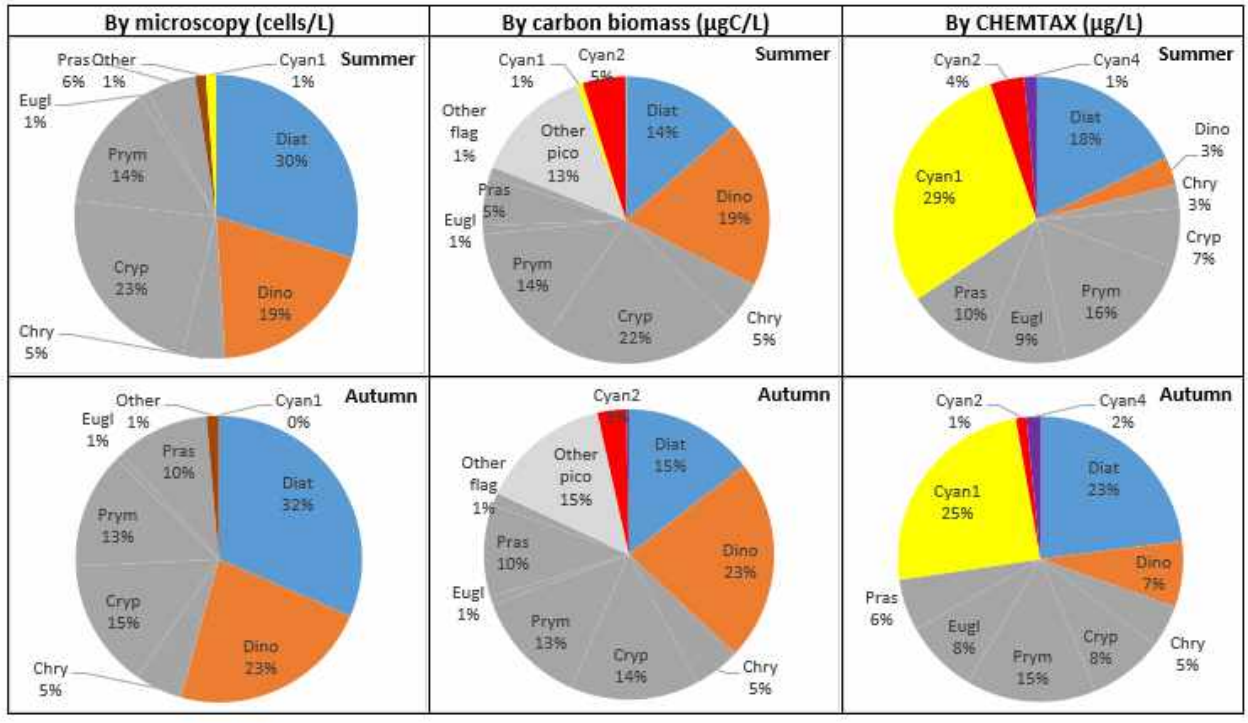

Figure 2-22: Comparison of the composition of the phytoplankton community determined by light microscopy (left) and carbon biomass estimates determined by light microscopy and flow cytometry, which include picophytoplankton, and CHEMTAX estimated phytoplankton composition compared with results of microscopy.

Multivariate analysis of the phytoplankton community composition determined by CHEMTAX indicated a significant interaction between site and season and year and season (Table 2-7). These results indicate that the seasonal influence on phytoplankton composition changes between sites and between years. PCO shows that most of the sites cluster together except during autumn when the composition of the phytoplankton community at BXZ, LFZ and, to a lesser extent, BRN differed from other sites due to the increased abundances of several phytoplankton groups in response to the environmental drivers of the temperature and flushing timescales (Figure 2-23). DistLM analyses (Figure 2-24, Table 2-8) showed a similar distribution of sites with BXZ in autumn both separating out from the offshore sites LRN and LRS. Environmental variables, flushing timescale and temperature, explained 21% of the variation in the phytoplankton community in the community composition. The best overall explanation of the influence of environmental factors came from a six-variable model (flushing timescale, temperature, NH_4^+, PO_4, Si and depth) which explained 29% of the total variability in phytoplankton community structure.

Table 2-7: PERMANOVA analyses for changes in the phytoplankton community composition determined by CHEMTAX.

Multivariate Source	**df**	**SS**	**Pseudo-F**	**P**
Site	4	1.011	7.914	**0.0001**
Year	5	0.624	3.909	**0.0002**
Season	1	0.322	10.092	**0.0003**
Site x Year	20	0.677	1.061	0.4164
Site x Season	4	0.460	3.604	**0.0005**
Year x Season	5	0.601	3.765	**0.0009**
Residual	20	0.638		

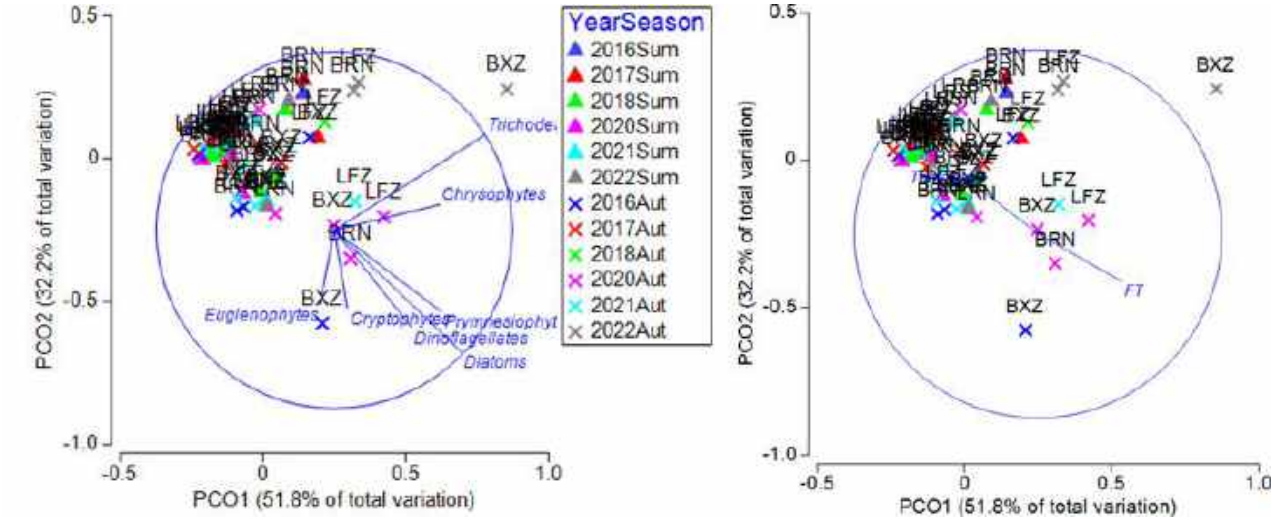

Figure 2-23: Principal Coordinates Analysis (PCO) of the HPLC-derived phytoplankton taxonomic composition. Blue lines show significant groups influencing their composition (left) and significant environmental factors influencing their distribution (right). The length and direction of the vectors represent the strength and direction of the relationship.

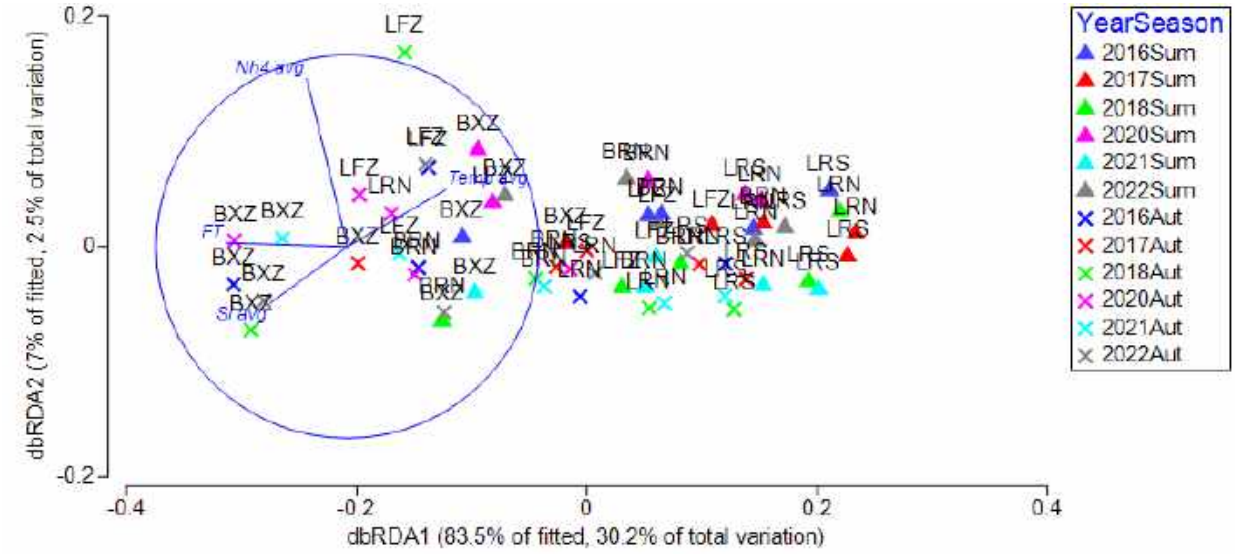

Figure 2-24: Distance-based redundancy analysis (dbRDA) plot of Distance-based linear modelling (DistLM) results in 2-dimensional space for environmental variables and phytoplankton community biomass determined by CHEMTAX. Significant environmental factors influencing their distribution are shown by blue lines. The length and direction of the vectors represent the strength and direction of the relationship.

Table 2-8: Best one to five variable solutions for Distance-based liner modelling (DistLM) analyses of the influence of environmental variables on phytoplankton community structure based on Adjusted R^2 values.

Adj R^2	Variables
0.121	Flushing Timescale
0.212	Flushing Timescale, Temperature
0.249	Flushing Timescale, Temperature, NH_4^+
0.272	Flushing Timescale, Temperature, PO_4, Si
0.285	Flushing Timescale, Temperature, NH_4^+, PO_4, Si

Environmental Drivers of the Planktonic Community Structure

Figure 2-25 shows the amount and relative proportion of carbon biomass distributed among the key autotrophic and heterotrophic groups of the planktonic ecosystem. With the exception of autumn 2020, similar patterns of carbon biomass distribution among planktonic size classes were generally observed within sites and across seasons and years. On average, zooplankton biomass ranged between 47-50 µg C/L across the seasons and made the largest relative contribution (30% summer, 42% autumn) to total community biomass, followed by microphytoplankton 31-38 µg C/L (22% summer, 21% autumn) and picophytoplankton 25 µg C/L (22% summer and autumn). Nanophytoplankton biomass ranged between 13-17 µg C/L and contributed to approximately 10% of the community biomass, while the mean bacterial seasonal biomass ranged between 7-40 µg C/L and contributed between 6 and 15% of the community biomass in summer and autumn, respectively. Spatially, an increase in the proportion of biomass in the pico- and nanophytoplankton, and a decrease in the proportion of zooplankton biomass, was observed between inshore sites (BXZ and BRN) relative to offshore sites (LRS, LFZ, LRN) during summer. During autumn the relative proportion of phytoplankton biomass to zooplankton in the region was generally consistent between sites and years, except in 2020 when bacterial biomass in the region ranged between 5 and 305 µg C/L at LFZ and BXZ, respectively, and contributed to >50% of the community at all sites except LFZ.

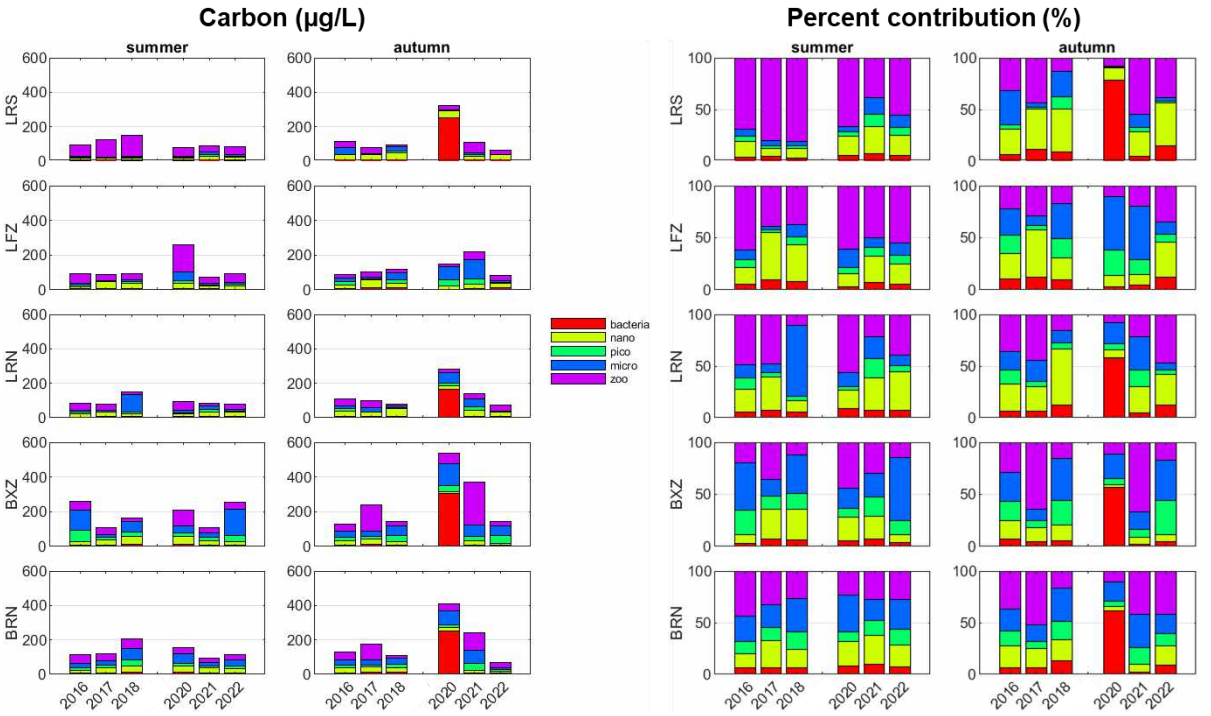

Figure 2-25: Contribution of the key autotrophic and heterotrophic groups within the planktonic ecosystem to (left) the total carbon biomass (µg/L) and (right) the relative percentage contribution of each group. No data were available for 2019.

Multivariate analysis of the plankton community structure based on carbon biomass estimates showed a significant interaction between year and season (Table 2-9). These results indicate that seasonal changes in the structure of the plankton community are different between years. Site was also significant and pairwise tests indicated there were significant differences between LRS and LRN, and between BXZ and BRN. All other pairs of sites were the same.

Table 2-9: PERMANOVA analyses for changes in the plankton community structure.

Multivariate				
Source	**df**	**SS**	**Pseudo-F**	**P**
Site	4	37039	2.995	**0.0038**
Year	5	92159	5.961	**0.0001**
Season	1	17024	5.505	**0.0043**
Site x Year	20	62948	1.018	0.474
Site x Season	4	23271	1.881	0.0529
Year x Season	5	104030	6.729	**0.0001**
Residual	20	61846		

PCO (Figure 2-26) indicated that most sites clustered together except during autumn 2020 when the community structure at BXZ, BRN, LRS and LRN differed from other sites due to increased abundances of bacteria, and to a lesser extent increased micro-and nano-phytoplankton and zooplankton abundances, in response to the environmental drivers temperature and PO_4^+.

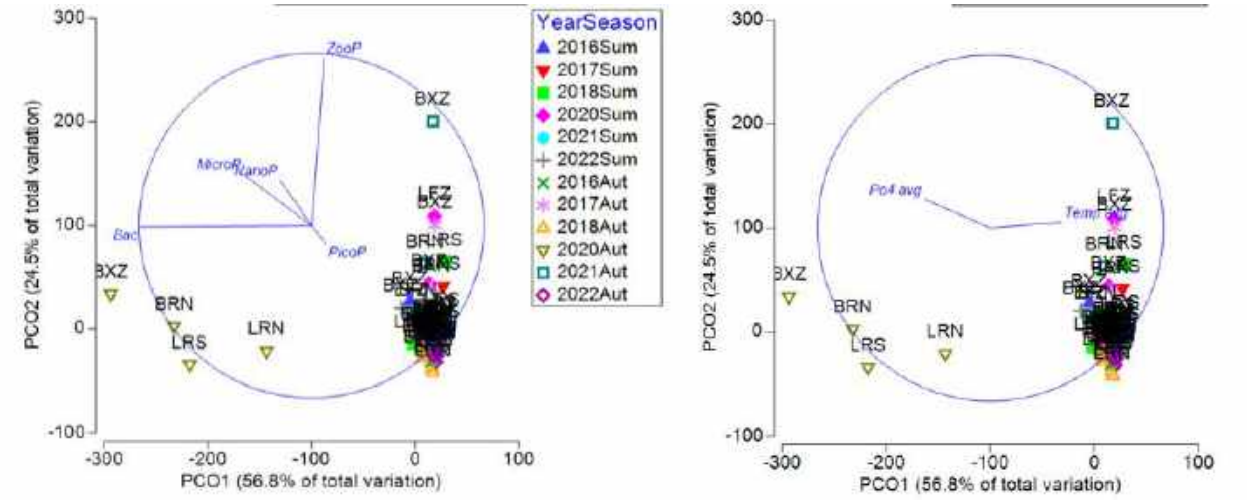

Figure 2-26: Principal Coordinates Analysis (PCO) of plankton community structure. Blue lines show significant groups influencing their structure (left) and significant environmental factors influencing their distribution (right). The length and direction of the vectors represent the strength and direction of the relationship.

DistLM analyses (Figure 2-24, Table 2-10) showed a similar distribution of sites with all sites (BXZ, BRN, LRS, LRN, BXZ and LFZ) in autumn 2002 separating out from other sites. Environmental variables, flushing timescale, temperature and PO_4^+, explained 21% of the variation in the plankton community structure. The best overall explanation of the influence of environmental factors came from a nine-variable model (latitude, flushing timescale, temperature, salinity, depth, TSS, NO_x, PO_4^+, Si) which explained 27% of the total variability in plankton community structure.

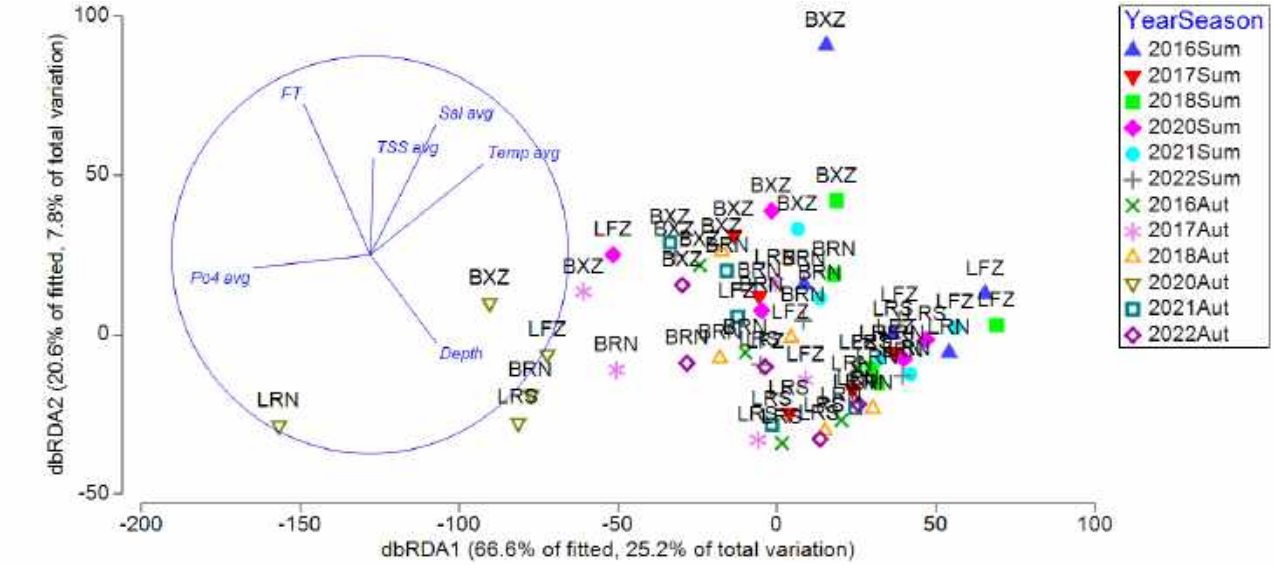

Figure 2-27: Distance-based redundancy analysis (dbRDA) plot of Distance-based linear modeling (DistLM) results in 2-dimensional space for environmental variables and plankton community structure. Significant environmental factors influencing their distribution are shown by blue lines. The length and direction of the vectors represent the strength and direction of the relationship.

Table 2-10: Best one to eight variable solutions for Distance-based liner modelling (DistLM) analyses of the influence of environmental variables on plankton community structure based on Adjusted R^2 values.

Adj R^2	Variables
0.084	Temperature
0.155	Flushing Timescale, PO_4
0.208	Flushing Timescale, Temperature, PO_4
0.230	Depth, Temperature, NO_x, PO_4
0.248	Depth, Temperature, Flushing Timescale, NO_x, PO_4
0.256	Depth, Temperature, Flushing Timescale, NO_x, PO_4, Si
0.258	Depth, Temperature, Salinity, Flushing Timescale, NO_x, PO_4, Si
0.265	Latitude, Depth, Temperature, Salinity, Flushing Timescale, NO_x, PO_4, Si

2.4. Discussion

The results of the monitoring program showed significant spatial and temporal variation in the physical, chemical, and biological parameters examined throughout the region. This is not surprising, considering observations are limited to a snapshot (i.e., one water sample event) taken in summer and autumn of each year.

The estimated maximum annual and monthly loads of NH_4^+ into the LEPZ derived from tuna and finish aquaculture remained relatively constant during the monitoring period (Figure 2-4) and were approximately 10% less than those estimated in 2006 from tuna alone (Tanner and Volkman 2009). NOx, NH_4^+ and PO_4^{3-} concentrations were significantly higher during autumn compared to summer with the highest concentrations of NH_4^+ and PO_4^{3-} consistently measured at LFZ in the tuna aquaculture zone (Figure 2-9, Figure 2-10). The observed concentrations of NO_x and NH_4^+ remained below the ANZECC/ARMCANZ (2000) water quality guideline trigger value concentrations of 50 µg/L for marine waters in the south-central ecoregion legislated under the current *Environment Protection (Water Quality) Policy 2015* which were developed to provide an early warning to 'trigger' further investigation or management action. NH_4^+ concentrations at times exceeded the significantly reduced 2018 revised water quality DGV's (5 µg/L) recommended at the regional scale (ANZG 2018). However, given that 5 out of 12 seasonal means for NH_4^+ at LRS, which measures ambient values in oceanic waters coming into Spencer Gulf, exceeded this lower value, it is likely too stringent to be applied as an indicator guideline value for assessing the potential for adverse ecological effects in this region of Spencer Gulf. Continued monitoring of key water quality parameters (e.g., nutrients, chl-a) and assessment of their ecological impacts is required to develop location-specific guideline values that protect the environmental value of this region. Elevated Si concentrations were consistently observed at inshore sites relative to sites located offshore to the east of Boston Island. Seasonal mean NO_x and Si concentrations typically exceeded the more recent 80th percentile IMCRA default guideline values (Table 2-5) for slightly to moderately disturbed systems recommended for Spencer Gulf. Seasonal mean PO_4^{3-} concentrations were below the IMCRA guideline values. Increased concentrations of NO_x and PO_4^{3-} observed in summer 2020 demonstrate the variability associated with measuring the concentrations of dissolved inorganic nutrients and their likely association with remote processes such as coastal upwelling in the adjacent shelf region.

Consistent with previous studies in the region (Tanner and Volkman 2009, Middleton et al. 2013, Tanner et al. 2020), examination of the observed nutrient concentrations and ratios showed nutrient limitation is likely to be key in limiting phytoplankton growth. Overall, the observed

dissolved inorganic nitrogen concentrations and distributions are consistent with the supply of nutrients associated with seasonal changes in the region's circulation, which influences the connectivity and exchange of nutrients with shelf waters (Petrusevics 1993, Middleton et al. 2013) and the transport and dilution of aquaculture derived NH_4^+ predicted by the ocean model (Figure 2-7). The source of intermittent elevated PO_4^{3-} and Si concentrations is uncertain.

Since elevated concentrations of chl-*a* can reflect increases in nutrient loads (e.g., Hinga et al. 1995), chl-*a* provides an essential indicator of eutrophication (ANZECC/ARMCANZ 2000). Subsequently, chl-*a* concentrations can be used to classify the trophic status of the pelagic environment (Beiras 2018) as oligotrophic (chl-*a* ≤ 0.1), mesotrophic (0.1 < chl-*a* ≤1) or eutrophic (chl-*a* >1). Observed summer chl-*a* concentrations were below the historical ANZECC/ARMCANZ (2000) trigger value of 1 µg/L and the revised IMCRA summertime guideline values of 0.8 µg/L and indicated a mesotrophic system (Figure 2-12). During autumn, chl-*a* concentrations at LFZ, BXZ and BRN increasingly exceeded the recommended ANZECC/ARMCANZ and IMCRA guideline values during the second phase of the sampling program (2019-2022). This indicates a possible change in the trophic state from mesotrophic to slightly eutrophic during autumn at the inshore sites (BXZ and BRN) and in the tuna farming zone (LFZ). This trend is supported by a corresponding increase in the F_p ratio during the autumn at the BXZ and BRN inshore sites (Figure 2-13) and is consistent with the oceanographic modelling that shows nutrients from supplementary fed aquaculture are transported into the inshore waters during autumn. However, other indicators, such as changes in the diatom to dinoflagellate ratio or frequency of occurrence of HAB (Figure 2-20), which previously suggested a change in trophic status (Tanner et al. 2019) did not support the trends identified by changes in the chl-*a* or F_p ratio.

Multivariate analysis of environmental drivers that influence the composition of the phytoplankton community supported the results of the chl-*a* and Fp ratios and showed a clear separation of community assemblages in autumn between the inshore sites (BXZ, BRN) and the offshore sites (Figure 2-24). The environmental drivers responsible for the increased abundances of several phytoplankton groups observed at the inshore sites included temperature and flushing timescales and, to a lesser extent, nutrients. The observed changes in phytoplankton community composition in autumn are consistent with the changes expected under increasing nutrient loads (Howarth 2008, Glibert 2017) and the modelled oceanographic connectivity demonstrated between aquaculture emissions and Boston and Louth Bays (Figure 2-7).

Analysis of plankton community structure showed sites generally maintained similar composition (Figure 2-27). The exception was during autumn 2020 when the community structure at BXZ, BRN, LRS and LRN differed from other sites due to increased abundances of bacteria. Significant environmental drivers that explained the changes in plankton community composition included flushing timescale, temperature and PO_4^+. Possible causes of the elevated bacterial levels and PO_4^+ concentrations are unknown but demonstrate the sensitivity of the system to nutrient inputs, particularly in the inshore waters, which are characterised by reduced flushing.

Collectively, the extended dataset of observations collected by the AEMP program over six summer and autumn periods provided an improved dataset to assess variability and changes in the trophic status of the region. It is recommended that the monitoring of pelagic water quality continue to detect further possible changes and trends in the trophic status of the region. Given that nutrient emissions from aquaculture (and other sources) impact inshore waters with reduced flushing year-round, it is also recommended sampling be extended to cover all four seasons. The additional data will allow for the development of climatologies across the suite of physical, biological, and chemical indicators needed to assess changes in trophic status associated with eutrophication, and natural environmental change from both diffuse (e.g., shelf nutrient supply, run-off) and point sources (e.g., aquaculture). Additional observations will also support the ongoing development of the coupled hydrodynamic-biogeochemical model.

Given the good level of validation demonstrated for the hydrodynamic model against historical physical data collected across the region by this program and other projects (e.g., Doubell and James 2023), it is recommended that the collection of coincident water samples and physical measurements using a CTD are prioritised over future mooring deployments for temperature, salinity, and currents. The addition of sampling for total nitrogen and total phosphorus and 16S sequencing of the bacterial community is recommended to improve our understanding of the role of pathogens in the system and to provide additional indicators to detect and assess shifts in overall ecosystem state. Multivariate analysis showed similarities between inshore and offshore sites and suggests that BRN and LRN could be excluded from future sampling if necessary. Finally, the development of CHEMTAX to quantify phytoplankton community biomass has important implications for future management of the system by providing an additional line of evidence to detect changes in the trophic status of the system and for comparison with other regions (e.g., IMOS sites in Spencer Gulf and Gulf St Vincent) to better assess whether changes in community composition are related to eutrophication or climate change.

3. BENTHIC COMPONENT

3.1. Introduction

Historically, the benthic impacts of aquaculture in South Australia have been assessed by examining infaunal assemblages adjacent to active leases and comparing them to control sites (e.g. Tanner et al. 2020). Infauna are typically good indicators of benthic organic enrichment (e.g. Clarke and Green 1988, Warwick and Clarke 1991, Pearson and Black 2001), which in the context of aquaculture, occurs due to the deposition of waste feed and faeces on the seafloor. Multiple years of monitoring for both lease-scale effects and regional effects have demonstrated no detectable impacts of aquaculture on infauna outside of the aquaculture lease in South Australia (Tanner et al. 2020), although clear impacts have been demonstrated at smaller scales within a lease (Cheshire et al. 1996). To date, the far-field impacts of aquaculture on other components of the benthic ecosystem due to the release of dissolved nutrients has not been assessed.

Seagrasses are an important habitat forming group of plants in shallow marine ecosystems worldwide, with almost 5,000 km^2 occurring in Spencer Gulf (Edyvane 1999, Irving 2014). Seagrasses are known to be sensitive to anthropogenic nutrient inputs, with extensive losses occurring worldwide due to subsequent increased growth of epiphytic algae and phytoplankton, both of which reduce light availability to the seagrass (e.g. Short and Wyllie-Echeverria 1996, Westphalen et al. 2005, Fox et al. 2007, Waycott et al. 2009). Anecdotally, there have been reports of inshore losses of seagrasses around the Boston Bay area, potentially linked to aquaculture, however, no attempt has ever been made to obtain definitive evidence for this. Consequently, here we undertake a first step to determining if seagrasses are being impacted by aquaculture nutrients by assessing cover, structure, biomass and composition of seagrass at sites within the modelled nutrient plume of aquaculture and outside the plume. Unfortunately, no samples are available prior to the commencement of aquaculture, so it is not possible to undertake a gold standard Before After Control Impact study; however, ongoing impacts could be determined by finding changes over time that differ between aquaculture and control sites.

3.2. Methods

Field Sampling

To determine what influence finfish aquaculture around Port Lincoln had on seagrass, cover and composition were assessed at a range of sites in and around the region on two separate

occasions. While ideally a before after control impact design would have been used to unambiguously distinguish aquaculture impacts from other changes, the long history of finfish aquaculture in the region meant that this was not possible. A total of six sites were sampled (Figure 3-1), three of which were predicted to be in the nutrient plume from finfish farming, and three outside the plume, based on modelling results from 2015 and maximum predicted levels of farming (Figure 3-2). It was not possible to choose sites directly adjacent to aquaculture cages, as they were not located directly adjacent to seagrass. All sites were selected to be in 6-8 m depth of water on high density seagrass, to ensure that they were as similar as possible. Where possible, EPA Aquatic Ecosystem Condition Reporting (AECR) sites were used, as these have data on seagrass cover from 2010 and 2016 to provide some historical context. In some cases, the sites had to be moved to meet depth and cover requirements. At each site, a series of eight 50 m long remote video transects were undertaken ~50 m apart, which will provide data directly equivalent to those obtained by the EPA. For each transect, the camera was lowered to within ~1 m of the seafloor at a haphazardly determined point, and then the boat slowly motored for a distance of 50 m, before the camera was retrieved. Vessel co-ordinates were encoded onto the primary footage, which was viewed live on the boat as it was recorded. In addition, secondary high-definition footage was obtained from a GoPro mounted to the primary camera frame.

To assess differences in seagrass morphology and physiology, *in situ* sampling was undertaken. Three subsites ~25 m apart, roughly in the middle of the video transects, were sampled by a diver, who collected 3 core samples and measured chlorophyll fluorescence on ~20 leaves of *Posidonia* seagrass at each subsite. Cores were taken using a 19.5 cm internal diameter stainless steel corer with teeth on the bottom edge to assist in slicing through the seagrass root mat (Figure 3-3). The corer was rotated 20 cm into the sediment, or until refusal if the substrate was rocky, and all above and below-ground seagrass material was removed and placed into a mesh bag. Care was taken to ensure that all leaves that originated within the core were retained in the core and that all leaves originating outside the core were excluded prior to cutting. Core samples were vigorously agitated underwater to remove the majority of sediment, immediately frozen on return to the vessel, and returned to the laboratory for future analysis. Leaves for chlorophyll fluorescence measurements were haphazardly selected, and the effective quantum yield was measured *in situ* using a Walz diving PAM. All measurements were taken 2-3cm from the base of the leaf to ensure consistency, and to avoid epiphyte growth on older portions of the leaves. All sampling was undertaken between June 24-26, 2020, and again between May 2-4, 2022.

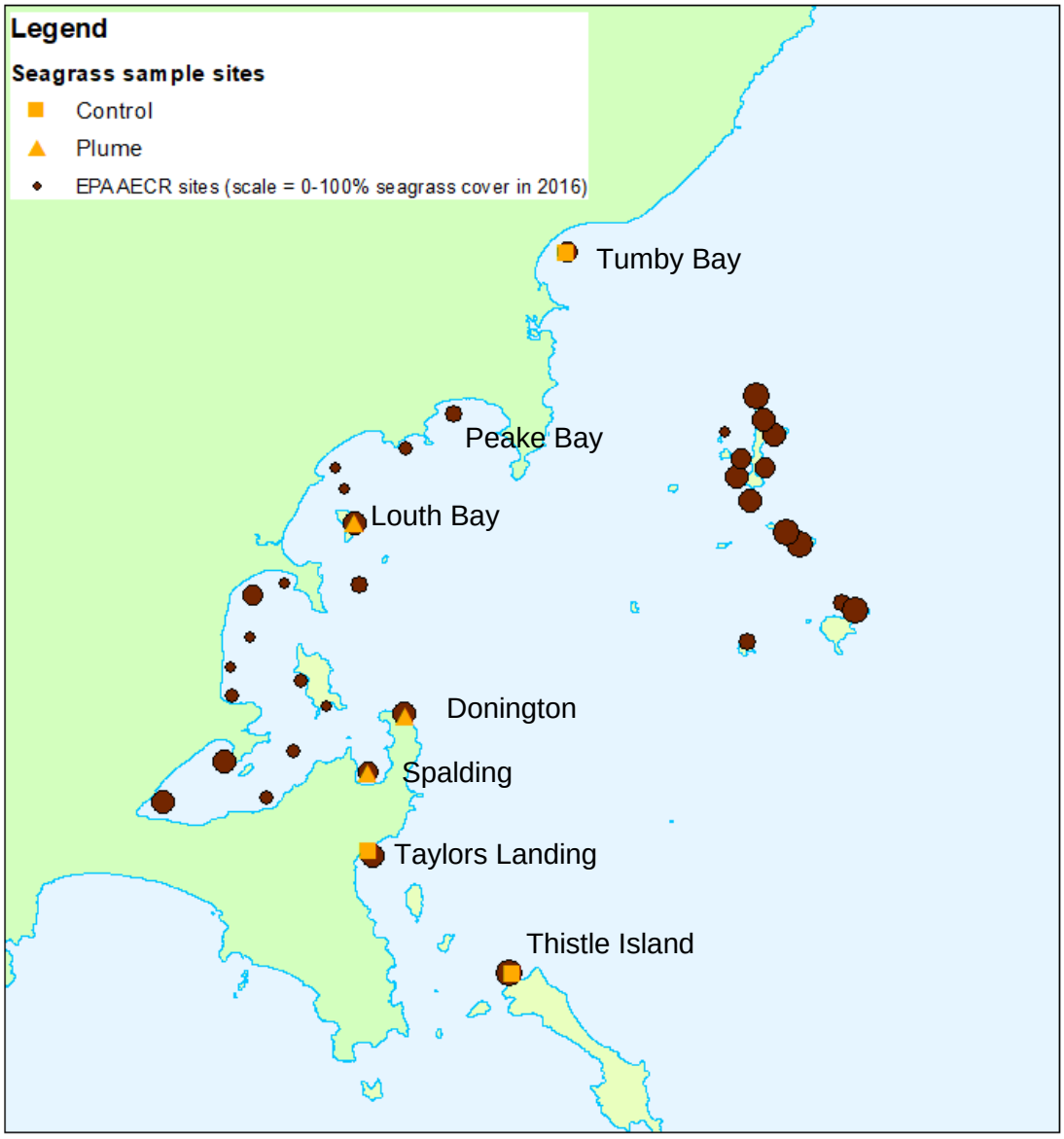

Figure 3-1: Map showing sampling sites (orange) and EPA Aquatic Ecosystem Condition Reporting (AECR) sites (brown, scaled to % cover of seagrass in 2012). The Peake Bay AECR site was surveyed by Clean Seas.

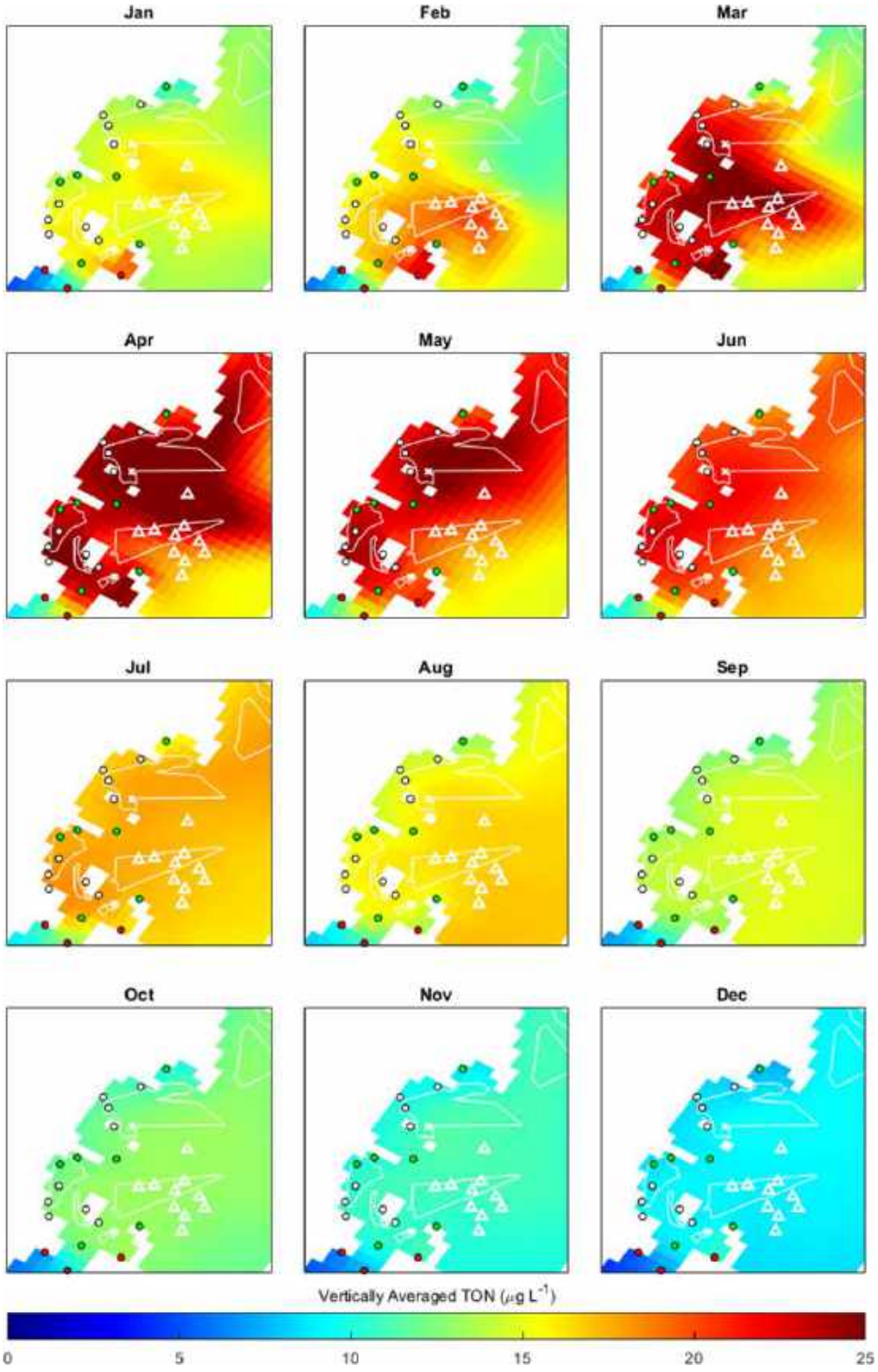

Figure 3-2: Monthly modelled total organic nitrogen (TON) levels in the water column around Port Lincoln at full production. TON represents the sum of modelled phytoplankton and detritus components and was used to demonstrate the potential maximum downstream extent of aquaculture nutrient emissions across the region. Note that this figure was obtained from modelling undertaken in 2015, and is only presented to explain site selection undertaken at that time. It should not be used to interpret changes in seagrass variables, as it has been superseded by the results presented in chapter 2 of this report.

Figure 3-3: Corer used to obtain seagrass samples and shows cutting teeth on the right.

In addition to the data collected by SARDI, Clean Seas collected annual data from 2020-2023 at four sites. Two of these sites were predicted to be in the nutrient plume of aquaculture (Louth Bay and Peake Bay), while two were control sites (Tumby Bay and Taylors Landing). Three of these sites were sampled by SARDI, with Peake Bay (Figure 3-1) being the only site not sampled by SARDI. Similar protocols were used, with ten remote 50 m video transects conducted at each site, although using a downward pointing camera. Unlike the SARDI transects, Clean Seas transects were not specifically selected to be over seagrass habitats, and so could be over reef or sand.

A third set of data was provided by the South Australian EPA, from their Aquatic Ecosystem Condition Reporting (AECR) program. This data set consisted of percent cover of seagrass along 10 random transects at each of 19 sites in and around Boston Bay in 2010, 2016 and 2022. Percent cover of all seagrass species, as well as algae, was recorded at each of multiple stops along each transect. These transects did not specifically target soft sediment, so all stops that were on hard substrate were removed because they were not suitable for seagrass. For this purpose, any frame that was recorded as having 50% or more hard substrate was removed. This left between 3 and 234 frames per transect. The 19 sites retained from a larger number of original sites were selected on the basis that they had data for all three years, whereas other sites only had data for one or two years. The only exception to this was Thistle Island, which was retained

despite only having data for 2010 and 2016, as it was also one of the sites used for the SARDI data collection.

Video Analysis

SARDI data

As an initial estimate of seagrass condition, the data required to calculate the habitat structure index, H′, which ranks the sampled seagrass on a scale of 0-100 (100 being excellent, 0 being poor) were recorded (for further description of the rationale and methods for calculating H' see Murray-Jones et al. (2009), Irving et al. (2013)). Five variables (seagrass area, continuity, proximity, percentage cover, and species identity) were recorded from the video for 50 sequential ~1 m^2 quadrats along each replicate transect, thus covering a whole 50 m transect, and integrated to calculate H'. Information on habitat type (e.g. seagrass, sand, rock, macroalgae) was also collected and the epiphyte load determined.

To obtain the above data, for each transect, the video was paused approximately every 1 m, and a transparent grid of 44 squares overlying the screen was used to facilitate estimation of both percentage of seagrass and percentage of epiphyte cover. Seagrass was scored according to type (note that the difficulty of identification from video meant that seagrass was only identified to genus) and density. The percentage of cover was estimated for all visible seagrass. Other substrate types were scored (e.g. areas of sand) and grouped together for analysis. Epiphyte cover on seagrasses was also estimated in the same way, and re-expressed as a percentage of total seagrass cover.

To determine whether aquaculture had an impact on the measured seagrass variables (H', epiphyte cover and cover of each *Posidonia*, *Amphibolis* and *Zostera*), multivariate analysis was used. A treatment effect (aquaculture vs control) would be evidence of a potential impact of aquaculture on seagrass occurring prior to the commencement of this project, although it would not be conclusive given that no data from before the commencement of aquaculture are available. A Treatment by Year effect would indicate ongoing impacts of aquaculture. Analyses were performed using the PERMANOVA (Anderson 2001) add-on for Primer (v7) (Clarke and Gorley 2015). Year and Treatment were considered fixed effects, with Site nested within Treatment. Before analysis, each variable was standardised by its maximum to account for variables that had different ranges. Euclidean distances were used, with 9999 permutations of residuals under a reduced model. Significant multivariate effects were followed up by individual univariate analyses

using the same procedure. Following PERMANOVA, differences between sites and years were visualised using non-metric multidimensional scaling (nMDS).

Clean Seas data

The Clean Seas video footage was processed in a similar way to SARDI, with the exception that cover classes were used instead of scoring the actual percent cover. The cover classes used were Bare (0%), Sparse (<35%), Moderate (35 - <70%) and Dense (≥ 70%). The cover class data was then provided to SARDI for analysis. These classes were rescored as 0, 1, 2 & 3 respectively, and then analysed using ANOVA following Furman et al. (2018). To further check the validity of this approach, the SARDI data were re-scored and analysed using the same procedure, with this analysis being compared to the original analysis on actual percent cover data.

EPA data

The percent cover for each species of seagrass and group of algae was calculated for each transect, and formed the basis for further analysis. Multivariate analysis of variance was used to determine if there were differences in seagrass cover and composition between sites and over time. Variables retained in the analysis were cover of *Posidonia*, *Amphibolis*, *Zostera*, *Halophila*, Opportunistic algae, Epiphytes, Small green algae and Small red algae. A ninth variable, Sand, was calculated as 100 minus the sum of all others, to ensure that those transects without vegetation were retained in the analysis. As the sites were more broadly distributed than for the other two data sets, no attempt was made to separate them into those in the nutrient plume from aquaculture and those outside the plume. Multivariate data were again visualised using nMDS; however, to reduce noise in the plot, averages were calculated over all ten transects at each site in each year prior to this analysis. Trajectories over time were then overlaid on the plot.

Seagrass morphology and biomass

Seagrass samples were defrosted prior to processing. Leaves were removed from the shoots and the number of leaves and shoots was recorded. Leaf length was measured to the nearest 5 mm, and the width and thickness of five random leaves were measured using digital callipers. Epiphytes were removed from both sides of each leaf using a scalpel, placed into a pre-weighed 20 mL glass scintillation vial, and the total wet weight was recorded. Roots were cut from shoots and combined with other large root material found in the sample. Fine roots tangled among the fibrous seagrass material (sheath) were classified as other below-ground materials. Leaves, shoots, roots and other below-ground material were placed into separate pre-weighed alfoil trays

and total wet weight was recorded. All material was frozen for 24 hrs and then freeze-dried until completely dehydrated (24-72 hrs, depending on moisture content). For larger samples, a sub-sample of known weight was freeze-dried rather than the entire sample. Total dry weight was recorded immediately after freeze-drying and samples were placed into a sealed plastic bag to avoid moisture absorption prior to biomarker analysis.

Analysis followed that for the video data, with the addition that Subsite was nested within Site. The variables included in the analysis were: Epiphyte Weight, Leaf Weight, Shoot Weight, Root Weight, Fibre Weight, Shoot Number, Leaf Number, Average Leaf Length, Average Leaf Width and Average Leaf Thickness. As leaf length, width, and thickness were measured on individual leaves, while the remaining variables were measured on cores, the average of each of these three variables for each core was used in the analysis.

In addition to the above analyses, seagrass shoot density and aboveground biomass were used to calculate a seagrass health index based on the interspecific boundary line (IBL) (Vieira et al. 2022). The IBL is the theoretical maximum biomass for any given density, and the health index used is d_{grass}, which is the distance that any particular seagrass sample is from that boundary line. In this case, we used the IBL for seagrasses calculated by Vieira et al. (2022):

$$\log_{10}B = 4.708 – 0.489 * \log_{10}D$$

where B is aboveground biomass expressed as grams dry weight per square metre, and D is shoot density per square metre. The distance any sample sits away from this line can be calculated as:

$$d_{grass} = (4.708 – 0.489 * \log_{10}D – \log_{10}B) * 0.898$$

High values of d_{grass} indicate poor health, whereas negative values indicate that biomass is exceptionally high.

Biomarkers

Samples of leaf, root and epiphyte material from each individual sample were freeze-dried and analysed for a range of biomarkers to determine if these could provide useful early indicators of impending seagrass decline. Biomarkers analysed were the percentage content of carbon, nitrogen, phosphorus and non-structural carbohydrates, along with stable isotopes of carbon nitrogen and amino acid composition. Total phosphorus concentrations (% DW) were determined

by digesting samples in hot concentrated nitric acid with hydrogen peroxide and analysed using a Perkin Elmer Optima 8000 ICP-OES. Non-structural carbohydrates were determined from the sum of total concentrations of soluble free sugars and the starch content of the plant tissue. The ethanolic extract was quantified for total soluble free sugar adopting the phenol-sulphuric acid assay. Total starch content was determined by hydrolysing the starch to free sugar, which was then quantified by the phenol-sulfuric acid assay. Acid hydrolysed amino acid profiles were determined in samples that were acid hydrolysed and analysed using a Shimadzu LCMS. Results are expressed as mole %.

For stable isotopes, approximately 5 mg of each sample were accurately weighed into tin capsules and sealed ready for analysis. The samples were then analysed for $\delta^{13}C$ & $\delta^{15}N$ using a continuous flow isotope ratio mass spectrometer (Nu Horizon, Wrexham, UK) equipped with an elemental analyser (EA3000, EuroVector, Pavia, Italy) to determine total C and N, respectively. Stable isotope ratios were expressed in δ notation as deviations from a standard in parts per mil (‰):

$$\delta^{13}C = [(R_{sample}/R_{standard})-1] \times 1000.$$

$$\delta^{15}N = [(R_{sample}/R_{standard})-1] \times 1000.$$

Where R_{sample} is the ratio of abundance of ^{13}C /^{12}C or ^{15}N /^{14}N in the sample, and $R_{standard}$ is this ratio in the standard. $\delta^{13}C$ was reported relative to the standard Vienna Pee Dee Belemnite (VPDB) and $\delta^{15}N$ was reported relative to the atmospheric abundance. All samples were corrected for instrument drift and normalised according to reference values (Coplen et al. 2006) using in-house standards (n=25); $\delta^{13}C$ = glycine -31.2‰ , glutamic acid -16.72‰ & triphenylamine (TPA) -29.2‰ & $\delta^{15}N$ = glycine 1.32‰ , glutamic acid -6.18‰ & triphenylamine (TPA) -0.54‰ calibrated against certified reference materials from USGS and IAEA (USGS40, USGS 41, IAEA-2).

Although there were a total of 324 samples for biomarker analysis (2 years x 6 sites x 3 subsites x 3 replicates x 3 compartments), there was not always enough sample available for analysis, especially of epiphytes. All 324 samples were analysed for carbon, nitrogen and their stable isotopes, 321 samples were analysed for phosphorus (3 epiphyte samples missing), 310 for non-structural carbohydrates (12 epiphyte and 2 root samples missing) and 298 for amino acids (20 epiphyte and 6 root samples missing). The missing samples were primarily from Spalding and Tumby Bay in both years, especially 2020.

Data analysis followed that for morphology/biomass, with the inclusion of Compartment as a factor orthogonal to Year and Treatment. Sample could not be included as a factor, as only a single analysis was performed on each compartment of each sample, and thus it was not possible to construct a valid F-test for any term including Sample. As biomarkers fell into three separate groups with different analytical approaches and different patterns of missing values due to small sample sizes (elemental composition, non-structural carbohydrates and amino acids), separate analyses were conducted for each.

3.3. Results

Video Analysis

SARDI data

The overall multivariate analysis indicated a significant interaction between Year and Site, but no interaction between Year and Treatment, and no Treatment effect (Table 3-1). These results indicate that there were differences within sites over time, but these differences differed between sites, and could not be related to aquaculture. The nMDS (Figure 3-4) shows that the differences between years were mainly driven by a higher epiphyte cover in 2020, with the exception of Spalding, which had a higher H' and *Posidonia* cover in 2020. The same patterns were present for each of the univariate variables tested – H', epiphyte cover and *Posidonia* cover. *Amphibolis* and *Zostera* were not analysed individually, as they were only present at 1 and 2 sites respectively.

Table 3-1: PERMANOVA analyses for the effects of aquaculture on seagrass cover in and around Boston Bay.

Multivariate Source	**df**	**SS**	**Pseudo-F**	**P**
Year	1	122000	23.994	**0.0044**
Treatment	1	8403.5	1.0694	0.33
Site(Treatment)	4	31561	41.793	**0.0001**
Year x Treatment	1	8487.6	1.6626	0.2722
Year x Site(Treatment)	4	20501	27.148	**0.0001**
Residual	77	14537		
H'				
Year	1	2714.3	13.248	**0.0263**
Treatment	1	562.93	0.63903	0.3635
Site(Treatment)	4	3533.4	21.165	**0.0001**
Year x Treatment	1	326.17	1.592	0.2702
Year x Site(Treatment)	4	821.44	4.9205	**0.0009**
Residual	78	3255.4		
Epiphyte Cover				
Year	1	108000	26.576	**0.0087**
Treatment	1	4938.3	1.1369	0.2328
Site(Treatment)	4	17446	673.31	**0.0001**
Year x Treatment	1	5909.5	1.4575	0.332
Year x Site(Treatment)	4	16286	628.51	**0.0001**
Residual	77	498.79		
Posidonia				
Year	1	11260	13.581	**0.025**
Treatment	1	2489	0.94406	0.3698
Site(Treatment)	4	10575	17.332	**0.0001**
Year x Treatment	1	1893	2.2832	0.2066
Year x Site(Treatment)	4	3324.3	5.4483	**0.0006**
Residual	78	11898		

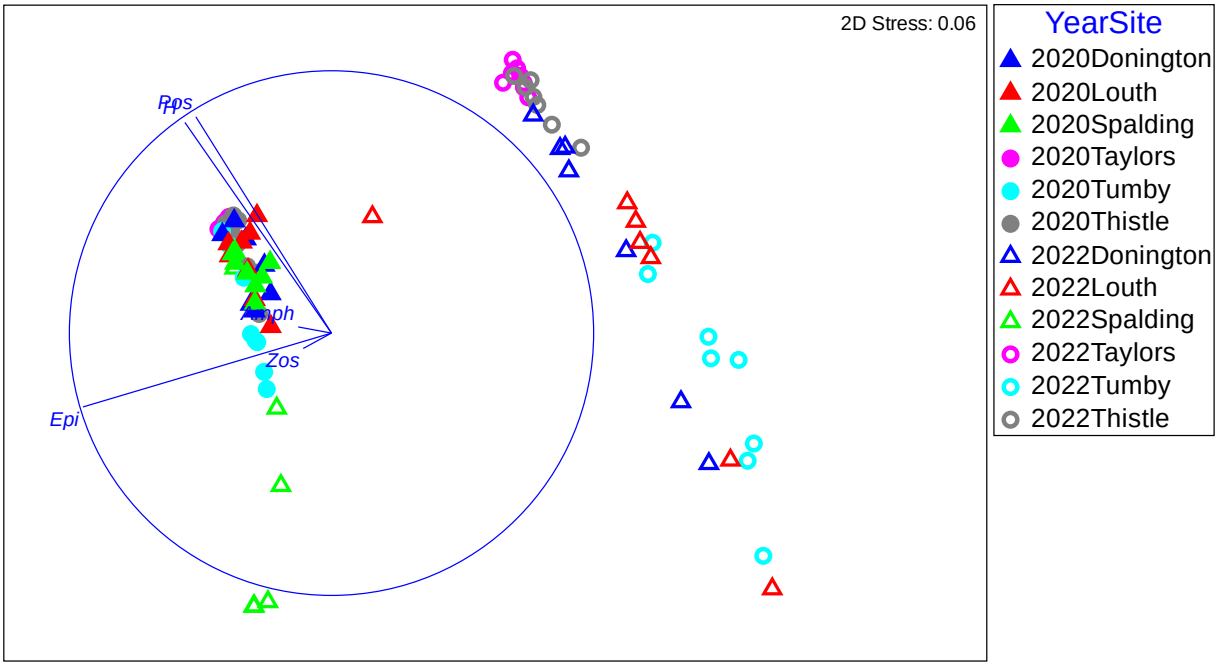

Figure 3-4: Non-metric multidimensional scaling (nMDS) analysis of seagrass cover in and around Boston Bay. Triangles indicate sites within the modelled nutrient plume from aquaculture, while circles indicate control sites outside the plume. Filled shapes represent 2020 samples, while hollow shapes represent 2022. The biplot (straight lines) shows the extent of correlation of each variable in the analysis with the plot, with the circle representing a correlation of 1.

Seagrass condition index decreased at all sites between 2020 and 2022, although the decline was only minor at the two southern control sites (Figure 3-5). Epiphyte cover was consistently high at all sites in 2020, but only at Spalding in 2022. *Posidonia* was overwhelmingly the dominant genus of seagrass at all sites and therefore shows the same pattern as total seagrass, with declines at all sites, although, as with the condition index, these declines were only minor at the two southern control sites. A very low cover of *Amphibolis* and *Zostera* was only present at 1 and 2 sites respectively in 2020, with neither genus being detected in 2022.

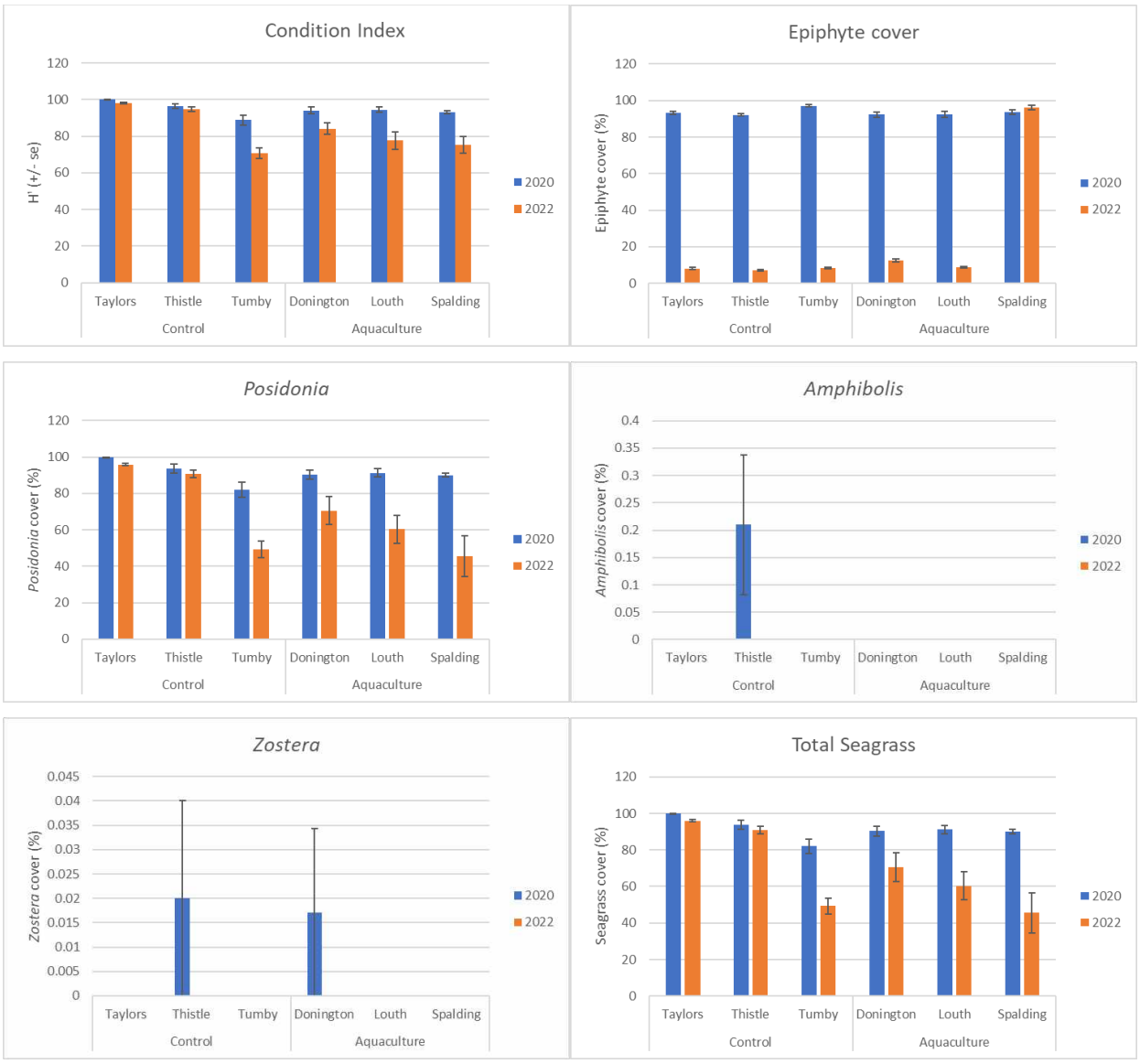

Figure 3-5: Effects of aquaculture on individual seagrass variables from video. All error bars are SE.

Clean Seas data

Re-analysis of SARDI data using the Clean Seas cover classes showed a similar pattern to the full cover data both between sites and over time (Table 3-2, Figure 3-6). The main difference is that Year was significant when the full percent cover data were analysed, whereas it fell just short of being significant when the data were re-coded as cover classes, indicating that the class data are less sensitive than the full data. This lends confidence to the approach to analysing cover score data.

Table 3-2: PERMANOVA analyses comparing the analysis of full seagrass percent cover data, versus cover class data, for the effects of aquaculture on seagrass cover in and around Boston Bay using the SARDI data.

Percent cover	**df**	**SS**	**Pseudo-F**	**P**
Year	1	11301	13.712	**0.0277**
Treatment	1	2505.8	0.94809	0.3661
Site(Treatment)	4	10601	17.382	**0.0001**
Year x Treatment	1	1878.5	2.2791	0.2092
Year x Site(Treatment)	4	3304.7	5.4186	**0.0007**
Residual	78	11893		
Cover classes				
Year	1	8.1195	8.0297	0.0506
Treatment	1	1.1619	0.84145	0.2616
Site(Treatment)	4	5.538	11.185	**0.0001**
Year x Treatment	1	1.625	1.607	0.2701
Year x Site(Treatment)	4	4.055	8.19	**0.0001**
Residual	78	9.6548		

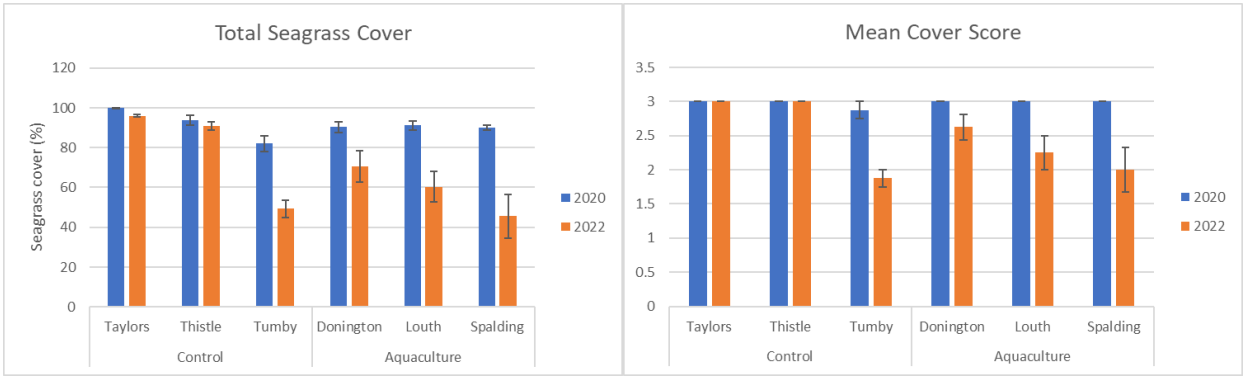

Figure 3-6: Comparison of the effects of aquaculture on seagrass cover when using full percent cover data versus cover classes using the SARDI data. All error bars are SE.

For the Clean Seas data, there were no differences between aquaculture and control sites, years, or their interaction (Table 3-3). There were differences between sites within each treatment, and these changed over time. In particular, Tumby Bay showed substantial temporal variability, while the other three sites showed few differences over time (Figure 3-7).

Table 3-3: ANOVA table for the effect of Aquaculture and Year on total seagrass cover (using cover classes) in and around Boston Bay (Clean Seas data).

Source	df	SS	Pseudo-F	P
Treatment	1	35.431	2.146	0.1708
Year	3	7.2995	2.1007	0.1974
Site(Treatment)	2	33.022	41.643	**0.0001**
Year x Treatment	3	1.934	0.55658	0.6559
Year x Site(Treatment)	6	6.9504	2.9216	**0.0099**
Residual	143	56.699		

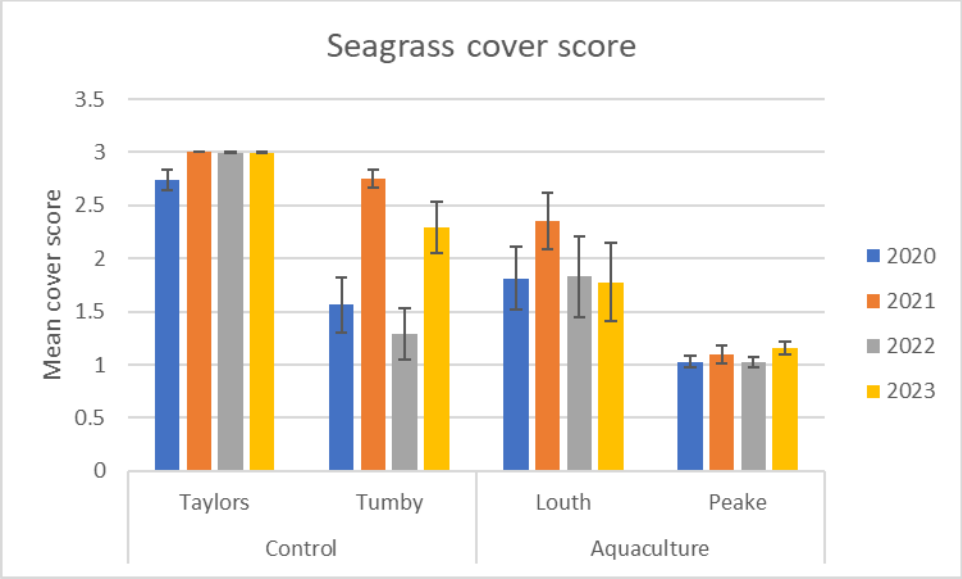

Figure 3-7; Effect of aquaculture and year on seagrass cover (using cover classes) in and around Boston Bay (Clean Seas data). All error bars are SE.

EPA data

There was a significant Site by Year interaction in the EPA data set (Table 3-4), indicating that different sites showed different trends over time in seagrass cover and composition. There was a lot of variability in total seagrass cover between sites, ranging between 0 and almost 80% (Figure 3-8). Some sites consistently increased over time, such as Taylors (m0124), some consistently decreased, such as Spalding and Donington (m0118 and m0122) and others were variable such as Tumby and Louth (m0125 and m0111). The trends are not consistent between the SARDI (and Clean Seas) sites inside and outside the aquaculture nutrient plume (Figure 3-9). The main differences between the sites were driven by the cover of *Posidonia*, the dominant genus, which

was almost perfectly negatively correlated with the cover of bare sand (i.e., they are directly opposite each other on the biplot, Figure 3-10). Epiphytes were the main determinant of the differences on the second axis of the plot. No geographic pattern was obvious at the AECR sites not monitored by SARDI or Clean Seas (Figure 3-11).

Comparison between data sets

It should be noted that while the SARDI, Clean Seas and EPA data sets all involve data collected in similar ways, there are some important differences that preclude direct comparisons. In particular, the SARDI data set is explicitly targeted to seagrass, and the sites were constrained so that all transects were conducted over seagrass in 2020. The EPA data set is from a program that does not explicitly target seagrass, and so the sites were not constrained to only be over seagrass at the start of the study. The Clean Seas transects were similarly not constrained to be over seagrass. Consequently, the higher levels of seagrass seen in the SARDI data are expected.

Table 3-4: PERMANOVA table examining spatial and temporal variation in seagrass cover in and around Boston Bay from the EPA data set.

Source	df	SS	Pseudo-F	P
SIte	18	333750	50.551	**0.0001**
Year	2	11591	15.8	**0.0001**
Site x Year	35	69562	5.4186	**0.0001**
Residual	496	181930		

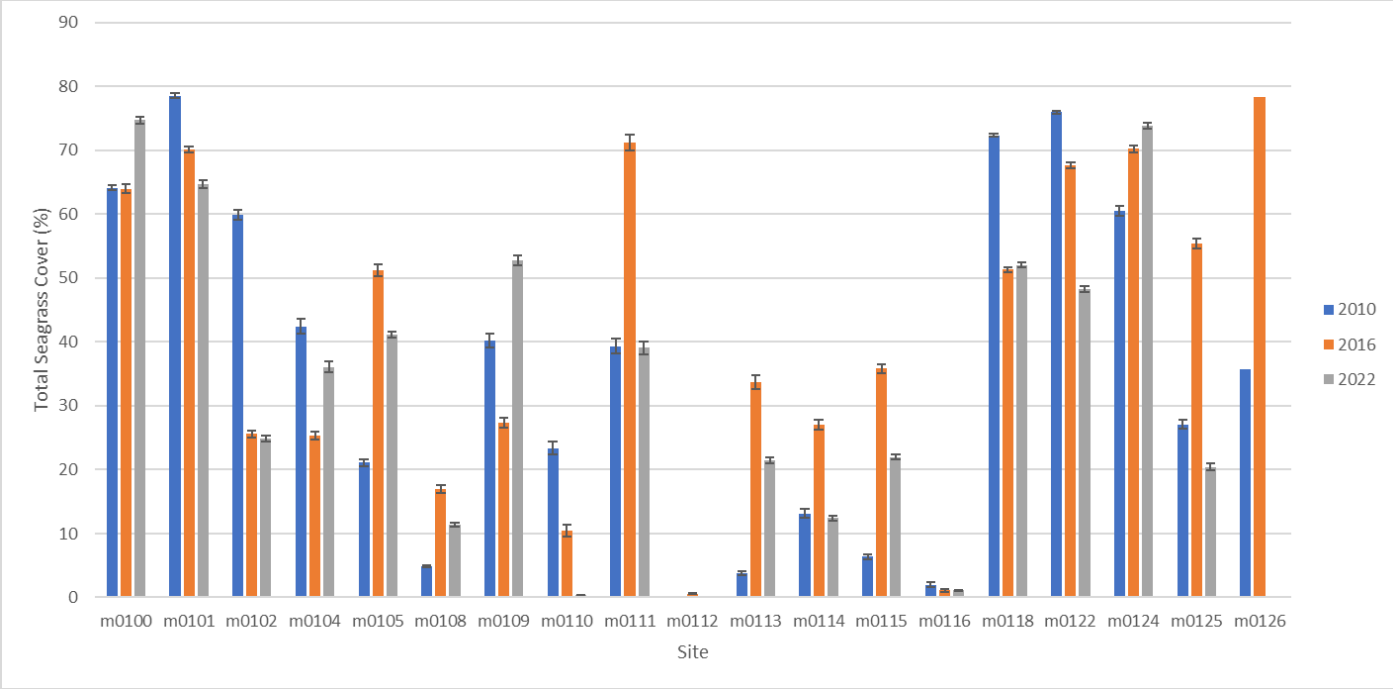

Figure 3-8: Total percent cover of seagrass at the EPA AECR sites over time (error bars are SE).

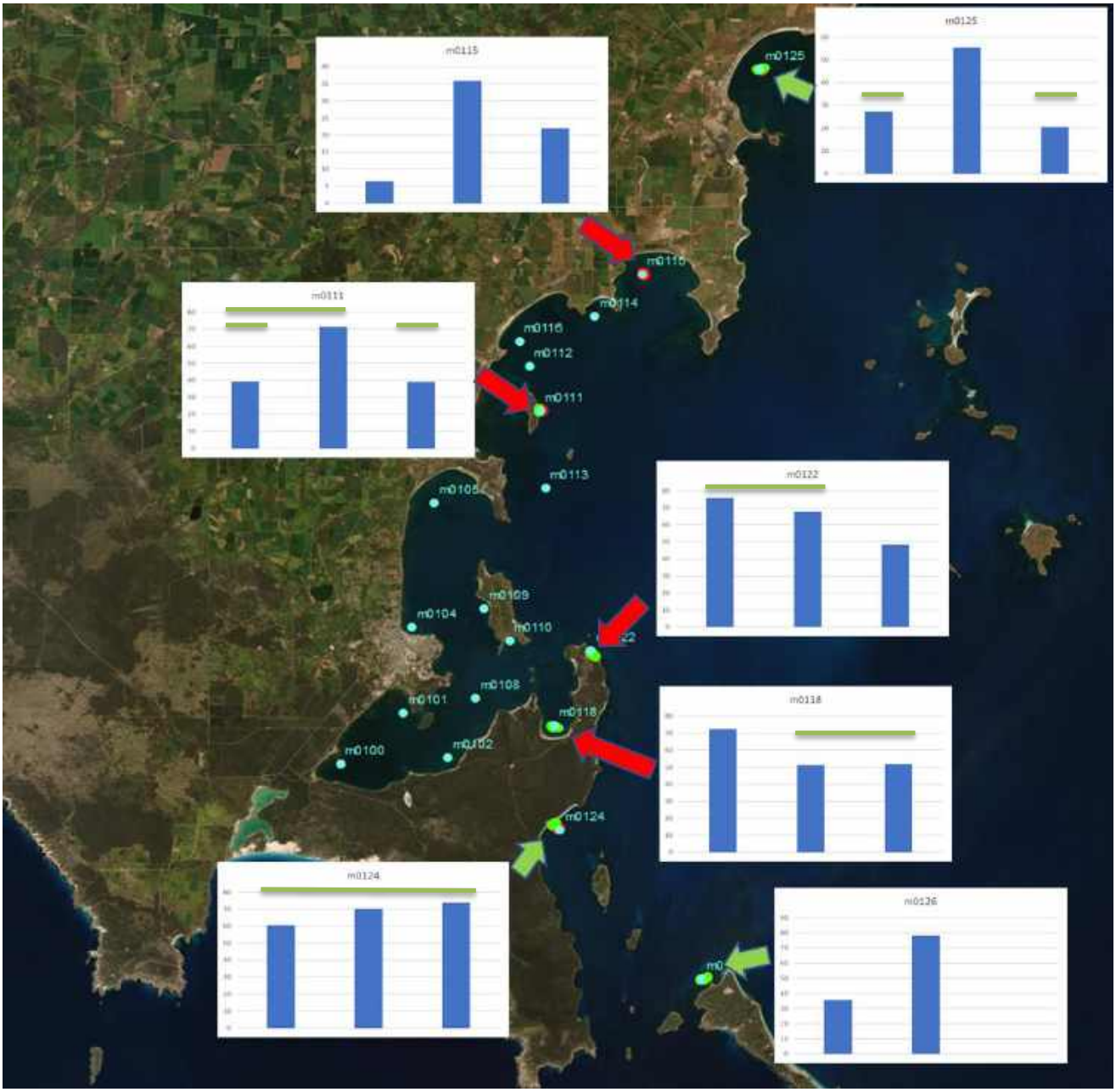

Figure 3-9: Trends in EPA AECR data at the six SARDI sites, as well as the additional site monitored by Clean Seas. Blue bars indicate the total cover of seagrass cover in 2010, 2016 and 2022 respectively. Green lines indicate years that are not significantly different (α=0.05). Note different scales on each panel for clarity.

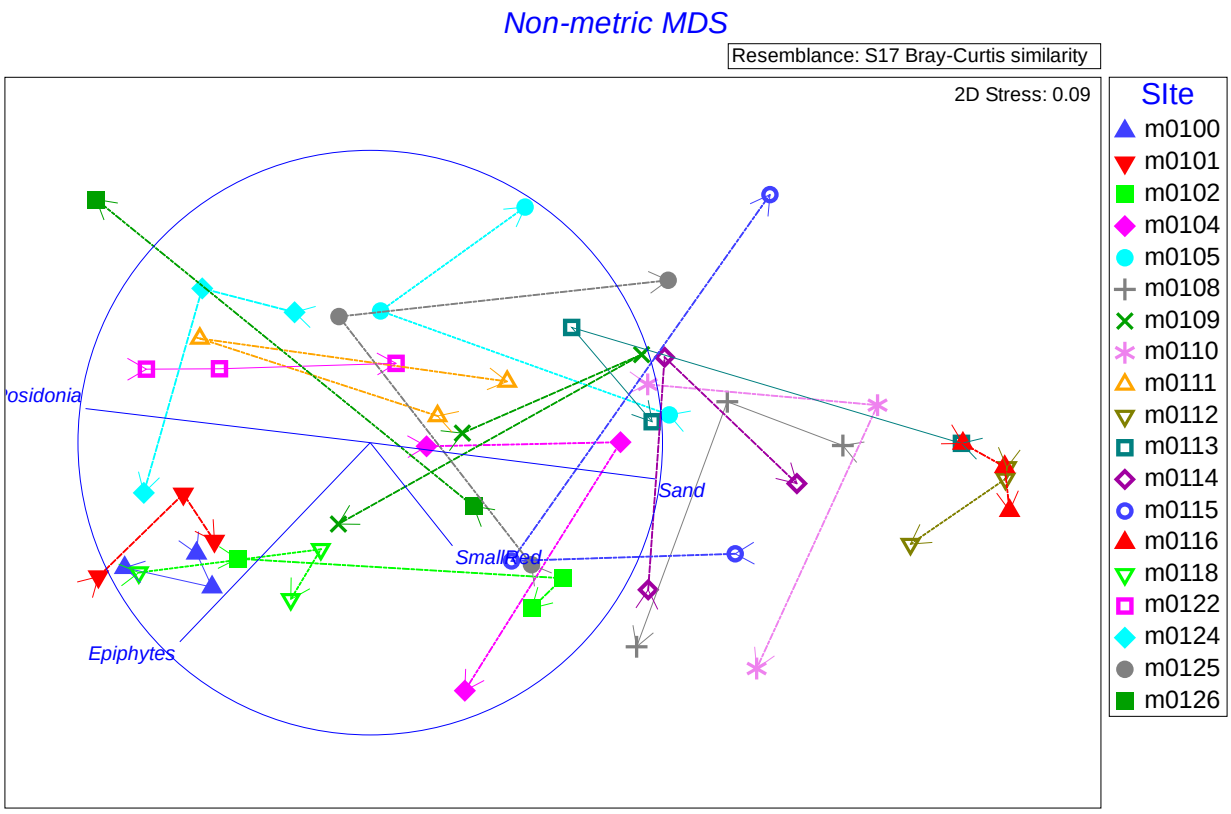

Figure 3-10: Non-metric multidimensional scaling (nMDS) plot of seagrass and algal composition at the EPA AECR sites over time. Lines show the trajectory from 2010 to 2016 to 2022. The biplot (straight lines) show the extent of correlation of each variable in the analysis with the plot, with the circle representing a correlation of 1.

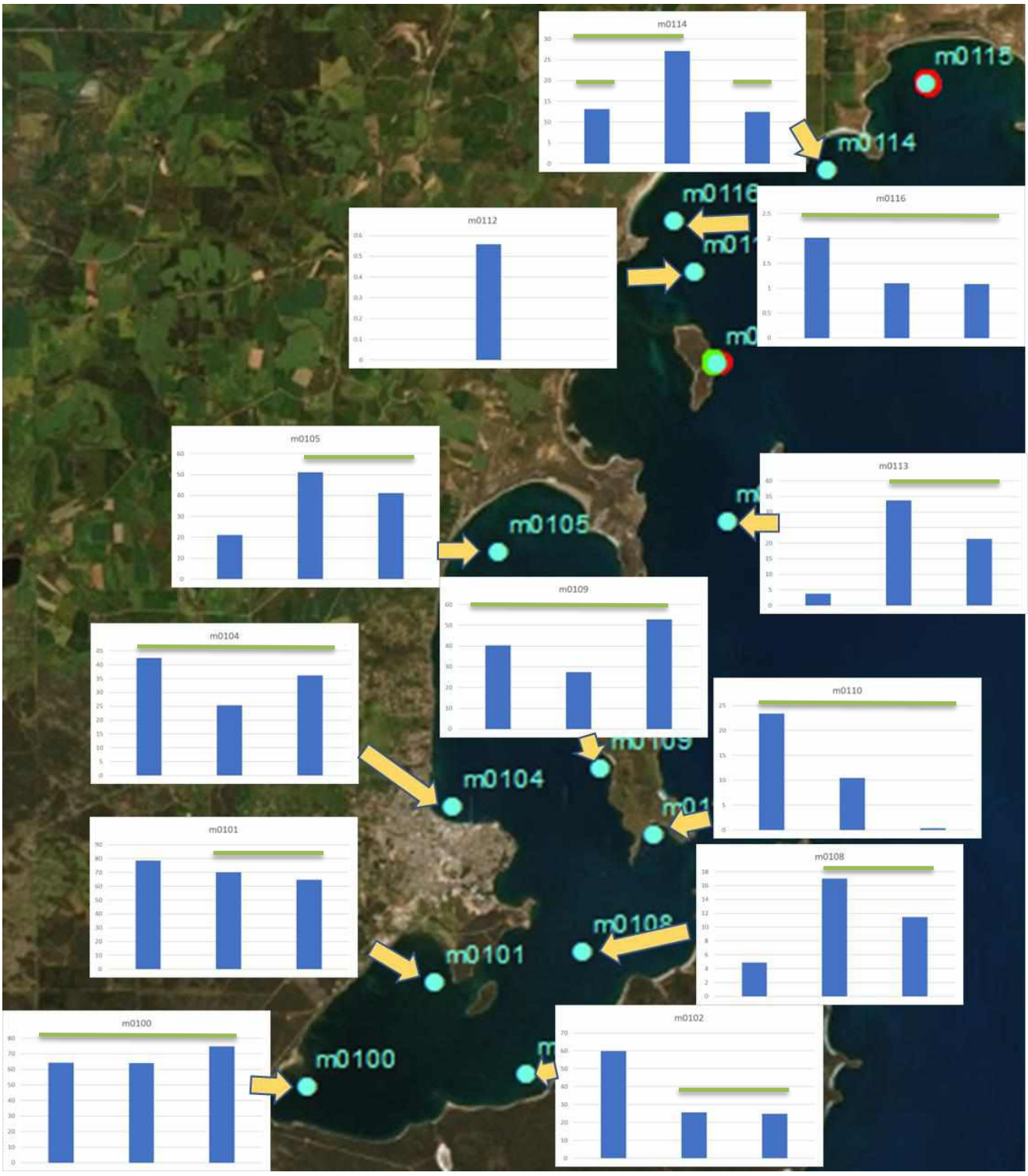

Figure 3-11: Trends in EPA AECR data at sites not monitored by SARDI or Clean Seas. Blue bars indicate the total cover of seagrass in 2010, 2016 and 2022 respectively. Green lines indicate years that are not significantly different (a=0.05). Note different scales on each panel for clarity.

Seagrass Morphology and Biomass

The multivariate analysis again indicated significant spatial variability, which changed between years, but with no effect of aquaculture. There were significant interactions between Year and both Site and SubSite, while neither the Treatment nor the Treatment by Year effects were significant (Table 3-5). The nMDS analysis (Figure 3-12) shows that Spalding (aquaculture) and Tumby (control) had very little variation within or between years. Louth and Donington (both aquaculture) showed slightly greater variation within years, and substantial differences between years. Taylors and Thistle (the two southern control sites) showed the greatest variation within years and the greatest differences between years. The differences between years were more closely correlated with fibre and shoot weight (both higher in 2020 at all sites – see Figure 3-13) and leaf thickness (lower in 2020), while the differences between sites were more heavily influenced by the number of shoots and leaves and the weight of leaves, roots, and epiphytes. Leaf length and width had little influence on the patterns seen.

Table 3-5: PERMANOVA analyses of the effects of aquaculture on seagrass morphology and biomass in and around Boston Bay.

Multivariate Source	df	SS	Pseudo-F	P
Year	1	30214	3.861	**0.0478**
Treatment	1	24670	1.1109	0.4055
Site(Treatment)	4	88830	12.552	**0.0001**
Year x Treatment	1	10540	1.3469	0.2904
Year x Site(Treatment)	4	31301	4.423	**0.0001**
SubSite(Year x Site(Treatment))	24	42462	1.4292	**0.0028**
Residual	72	89128		

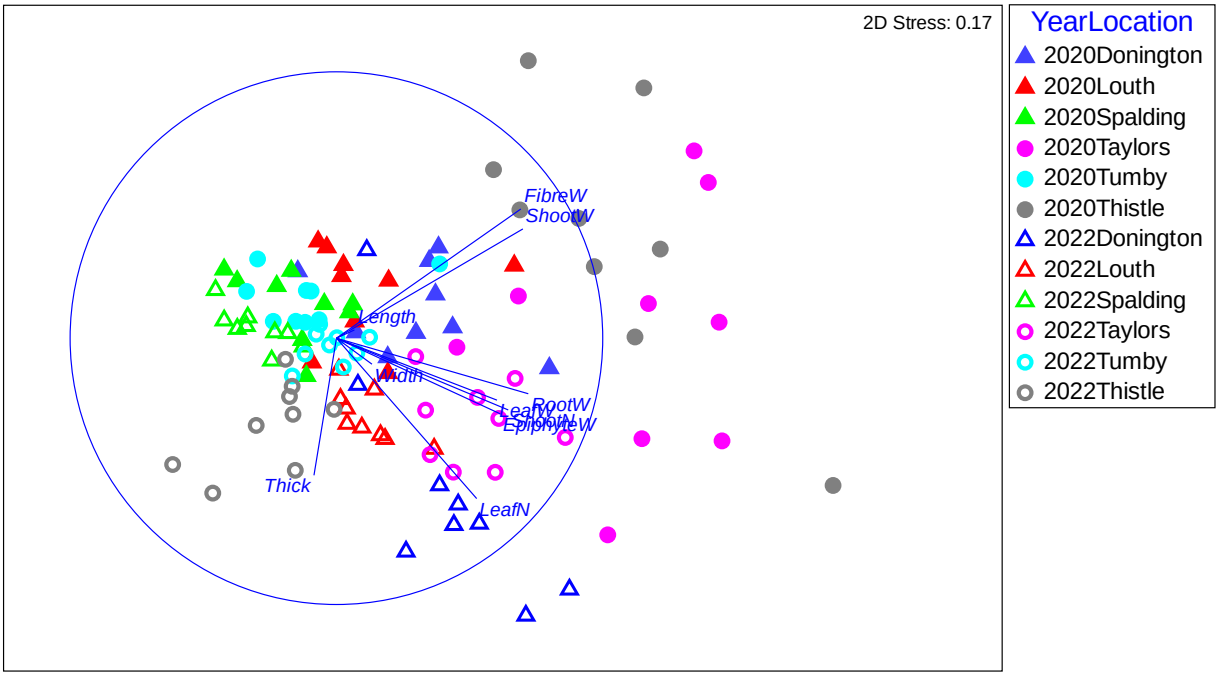

Figure 3-12: Non-metric multidimensional scaling (nMDS) analysis of seagrass morphology and biomass in and around Boston Bay. Triangles indicate sites within the modelled nutrient plume from aquaculture, while circles indicate control sites outside the plume. The filled shapes represent 2020 samples, while the hollow shapes represent 2022. The biplot (straight lines) show the extent of correlation of each variable in the analysis with the plot, with the circle representing a correlation of 1.

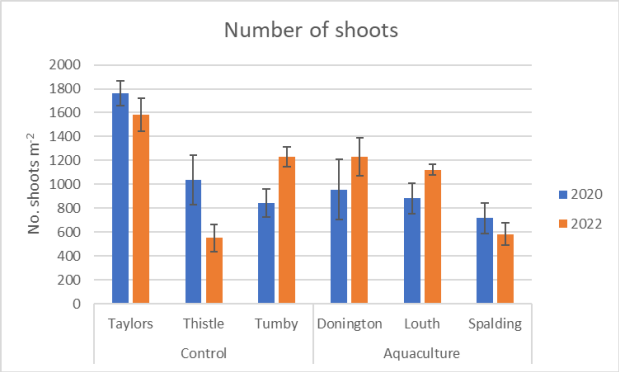
Number of shoots
No. shoots m-2
2000
1800
1600
1400
1200
1000
800
600
400
200
0
Taylors
Thistle
Tumby
Donington
Louth
Spalding
Control
Aquaculture
2020
2022

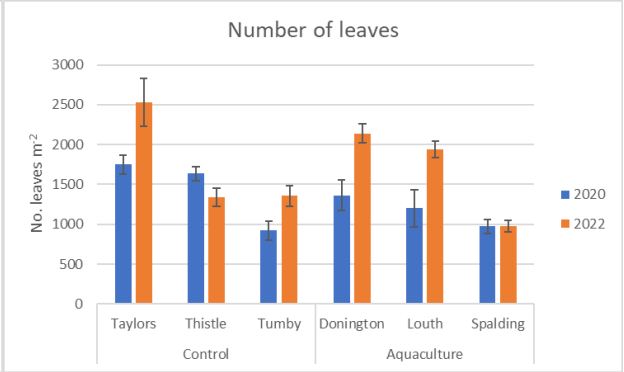
Number of leaves
No. leaves m-2
3000
2500
2000
1500
1000
500
0
Taylors
Thistle
Tumby
Donington
Louth
Spalding
Control
Aquaculture
2020
2022

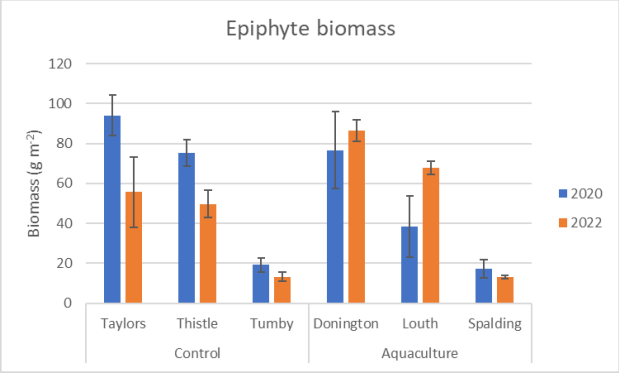
Epiphyte biomass
Biomass (g m-2)
120
100
80
60
40
20
0
Taylors
Thistle
Tumby
Donington
Louth
Spalding
Control
Aquaculture
2020
2022

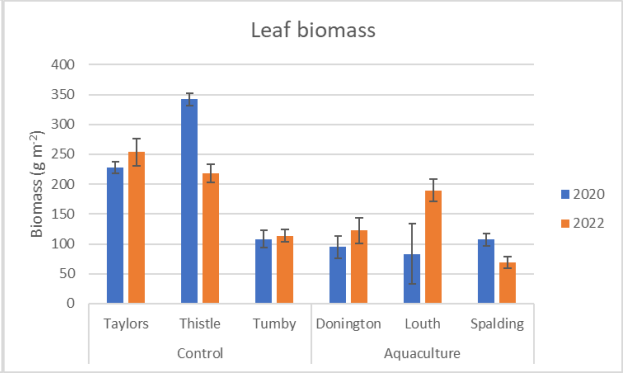
Leaf biomass
Biomass (g m-2)
400
350
300
250
200
150
100
50
0
Taylors
Thistle
Tumby
Donington
Louth
Spalding
Control
Aquaculture
2020
2022

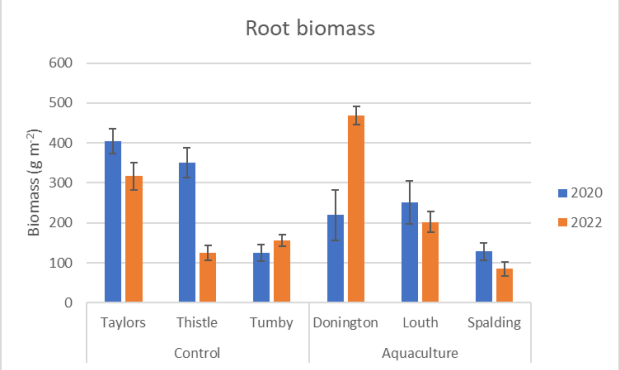
Root biomass
Biomass (g m-2)
600
500
400
300
200
100
0
Taylors
Thistle
Tumby
Donington
Louth
Spalding
Control
Aquaculture
2020
2022

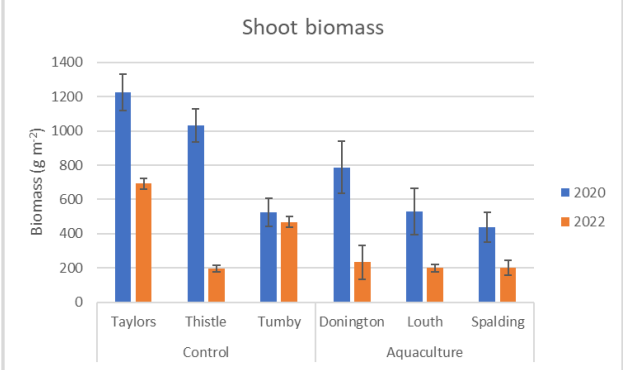
Shoot biomass
Biomass (g m-2)
1400
1200
1000
800
600
400
200
0
Taylors
Thistle
Tumby
Donington
Louth
Spalding
Control
Aquaculture
2020
2022

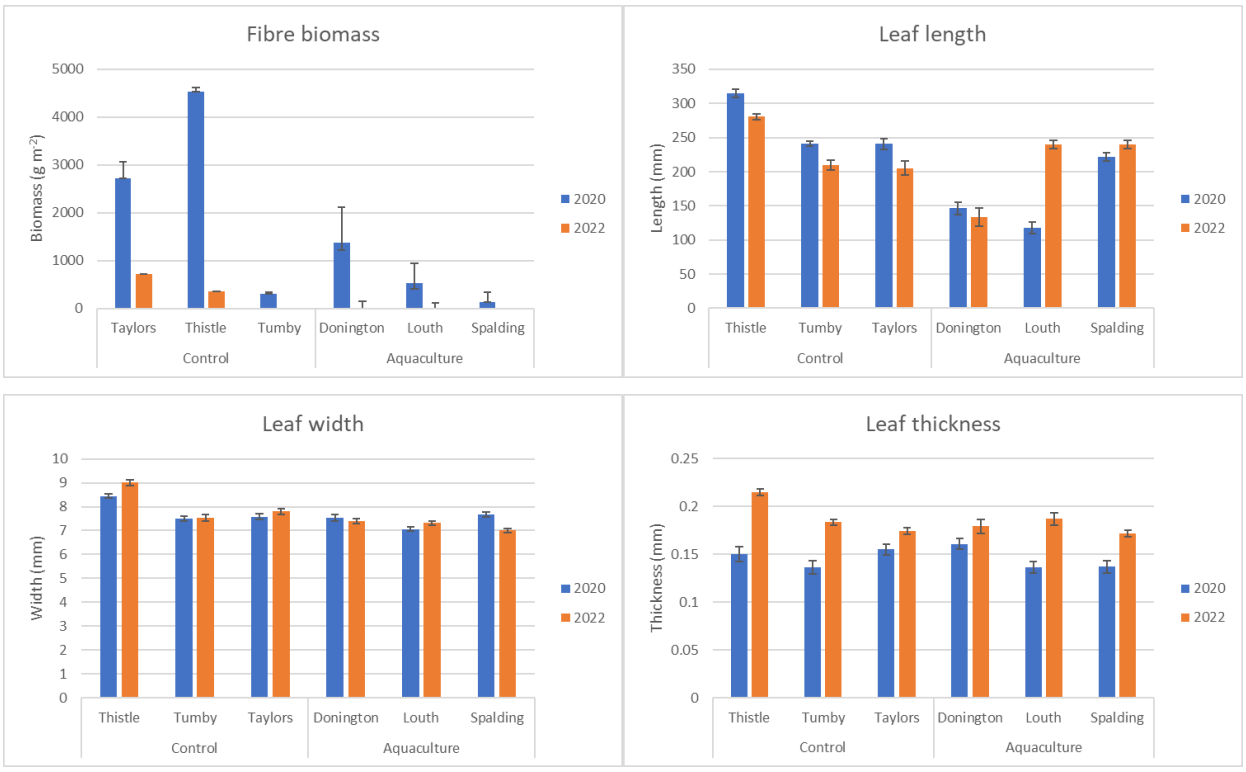

Figure 3-13: Influence of aquaculture and year on seagrass biomass and morphology in and around Boston Bay. All error bars are SE.

The IBL measure of seagrass health (d_{grass}) did not show impacts of aquaculture, with this measure varying between locations within treatments and doing so differently over time (Table 3-6, Figure 3-14). Seagrass health declined at all sites between 2020 and 2022, except for Tumby Bay. The decline is particularly noticeable at the Thistle Island site, which went from second best to second worst in the two years.

Table 3-6: PERMANOVA analyses of the effects of aquaculture on the IBL measure of seagrass health (d_{grass}) in and around Boston Bay.

Source	df	SS	Pseudo-F	P
Year	1	1.4016	5.2729	0.085
Treatment	1	1.9095	3.8134	0.0988
Site(Treatment)	4	2.0029	16.919	**0.0001**
Year x Treatment	1	0.0000884	0.000332	0.9749
Year x Site(Treatment)	4	1.0632	8.9811	**0.0002**
SubSite(Year x Site(Treatment))	24	0.71032	0.92691	0.5665
Residual	72	2.299		

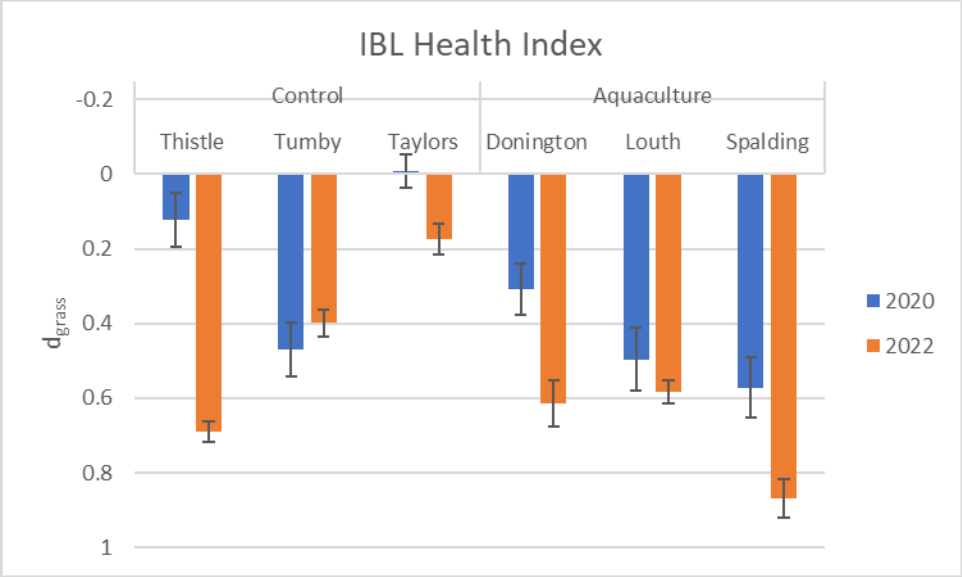

Figure 3-14: Influence of aquaculture and year on the IBL measure of seagrass health (d_{grass}) in and around Boston Bay. Higher values lie further from the theoretical maximum health and, therefore, indicate poorer condition. All error bars are SE.

Chlorophyll Fluorescence

The chlorophyll fluorescence values in 2022 showed a consistent decline over time, suggesting an issue with the instrument, and so only data for 2020 are analysed. There were no differences in the photosynthetic yield associated with Aquaculture or Site, although there were small-scale spatial differences between SubSites (Table 3-7).

Table 3-7: PERMANOVA analyses for the effects of aquaculture on seagrass photosynthetic yield in and around Boston Bay.

Multivariate source	df	SS	Pseudo-F	P
Treatment	1	0.004241	0.049733	0.8986
Site(Tr)	4	0.34162	1.7542	0.2039
SubSite(Si(Tr))	12	0.58616	3.7736	**0.0002**
Residual	353	4.5694		

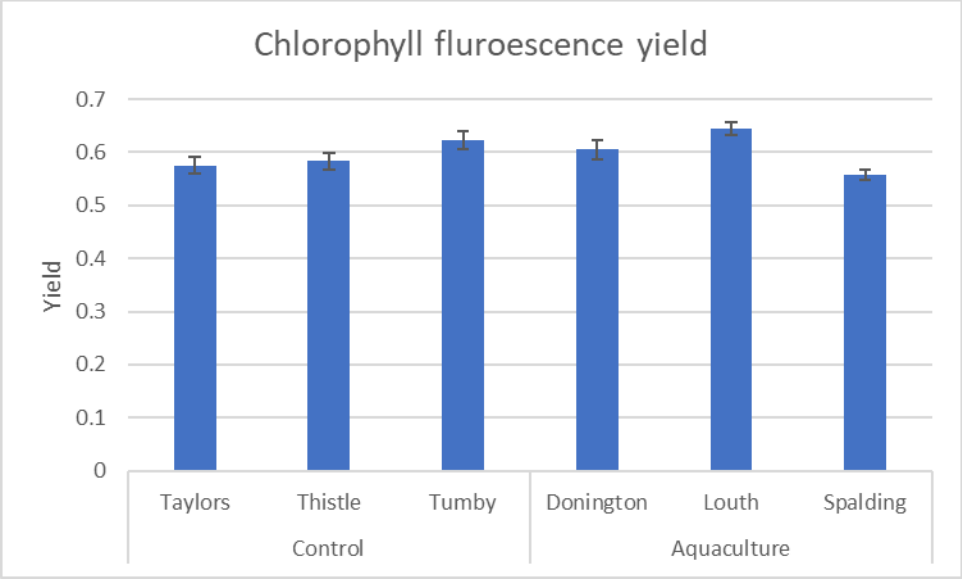

Figure 3-15: Influence of aquaculture and year on seagrass photosynthetic yield in and around Boston Bay. All error bars are SE.

Biomarkers

Elemental composition

Elemental composition (carbon, nitrogen, phosphorus, and isotopes of the first two) did not vary with exposure to the nutrients in the aquaculture plume (there was no Treatment effect, or any significant interaction involving Treatment, in the PERMANOVA; Table 3-8). There was, however, a lot of small-scale spatial variability (significant effects involving Site and SubSite), as well as differences between Years and Compartments. The nMDS indicates that the elemental composition differed between leaves, roots and epiphytes (Figure 3-16). Epiphytes were distinguished from seagrass by high $\delta^{13}C$ and $\delta^{15}N$ and low carbon, while seagrass leaves were distinguished from roots by high nitrogen and phosphorus.

Table 3-8: PERMANOVA results for the effect of aquaculture on the elemental composition of seagrasses and epiphytes in the Boston Bay region. Yr – Year, Tr – Treatment, Co – Compartment, Si – Site, Su – SubSite.

Multivariate source	df	SS	Pseudo-F	P
Year	1	7458	11.447	**0.0048**
Treatment	1	2624.1	0.13424	0.8978
Compartment	2	188000	37.958	**0.0001**
Site(Tr)	4	78189	61.29	**0.0001**
YexTr	1	2381.6	3.6554	0.1013
YexCo	2	2636.2	1.2856	0.2848
TrxCo	2	8824.7	1.7826	0.1371
SubSite(Si(Tr))	12	3827.1	2.2141	**0.0004**
YexSi(Tr)	4	2606.1	1.6957	0.118
CoxSi(Tr)	8	19802	8.3392	**0.0001**
YexTrxCo	2	945.51	0.46109	0.8369
YexSu(Si(Tr))	12	4610.5	2.6673	**0.0001**
CoxSu(Si(Tr))	24	7123.7	2.0606	**0.0002**
YexCoxSi(Tr)	8	8202.4	3.9244	**0.0001**
YexCoxSu(Si(Tr))	24	6270.4	1.8138	**0.0002**
Residual	216	31114		

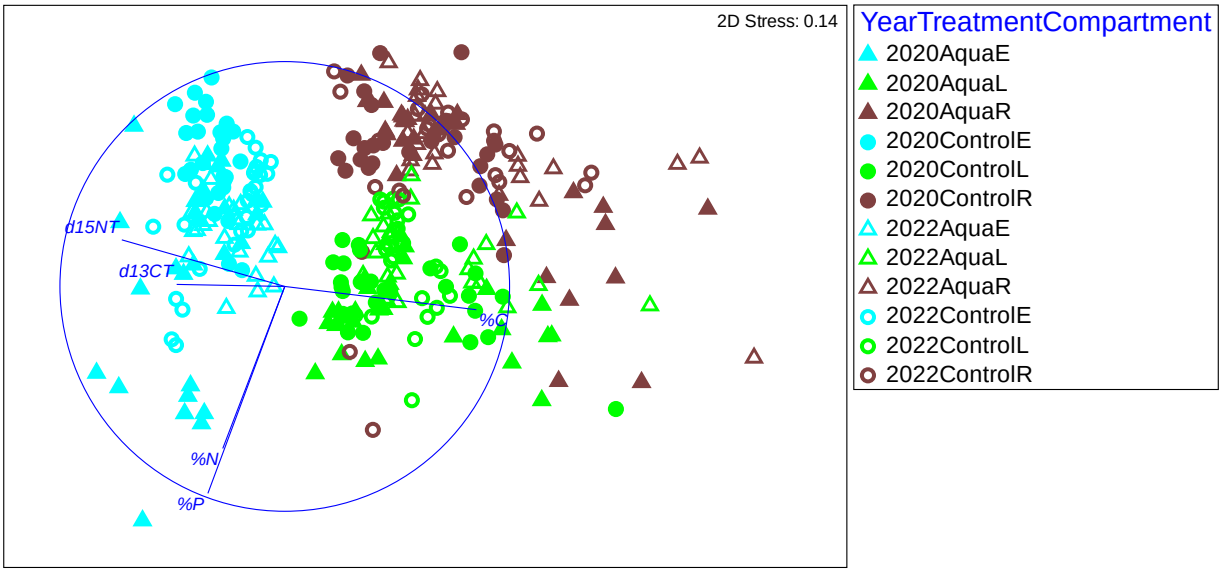

Figure 3-16: Non-metric multidimensional scaling (nMDS) analysis of seagrass elemental composition in and around Boston Bay. Triangles indicate sites within the modelled nutrient plume from aquaculture, while circles indicate control sites outside the plume. The filled shapes represent 2020 samples, while the hollow shapes represent 2022. Blue represents epiphytes, green seagrass leaves and brown seagrass roots. The biplot (straight lines) show the extent of correlation of each variable in the analysis with the plot, with the circle representing a correlation of 1.

Non-structural carbohydrates

Non-structural carbohydrates varied between Compartments, and spatially, but did not vary with any term including Aquaculture (Table 3-9). Seagrass roots had more than twice as much non-structural carbohydrates as did leaves and epiphytes (Figure 3-17). There was also an interaction between Year and Compartment, with roots increasing slightly over time, while epiphytes decreased slightly and leaves remained stable.

Table 3-9: PERMANOVA results for the effect of aquaculture on non-structural carbohydrates in seagrasses and epiphytes in the Boston Bay region. Yr – Year, Tr – Treatment, Co – Compartment, Si – Site, Su – SubSite.

Multivariate source	df	SS	Pseudo-F	P
Year	1	5.257	0.035457	0.8465
Treatment	1	44.981	0.12148	0.7006
Compartment	2	35074	88.781	**0.0003**
Site(Tr)	4	1490	4.0491	**0.0298**
YexTr	1	11.975	0.080765	0.7894
YexCo	2	1446.5	8.8238	**0.0092**
TrxCo	2	225.57	0.57098	0.5676
SubSite(Si(Tr))	12	1110.3	2.8221	**0.0064**
YexSi(Tr)	4	601.29	4.1718	**0.0222**
CoxSi(Tr)	8	1598.5	3.8144	**0.0049**
YexTrxCo	2	183.4	1.1187	0.3781
YexSu(Si(Tr))	12	433.58	1.1021	0.3598
CoxSu(Si(Tr))	24	1261.4	1.6031	0.0509
YexCoxSi(Tr)	8	665.85	2.5523	**0.0379**
YexCoxSu(Si(Tr))	23	749.94	0.99453	0.4686
Residual	203	6655.4		

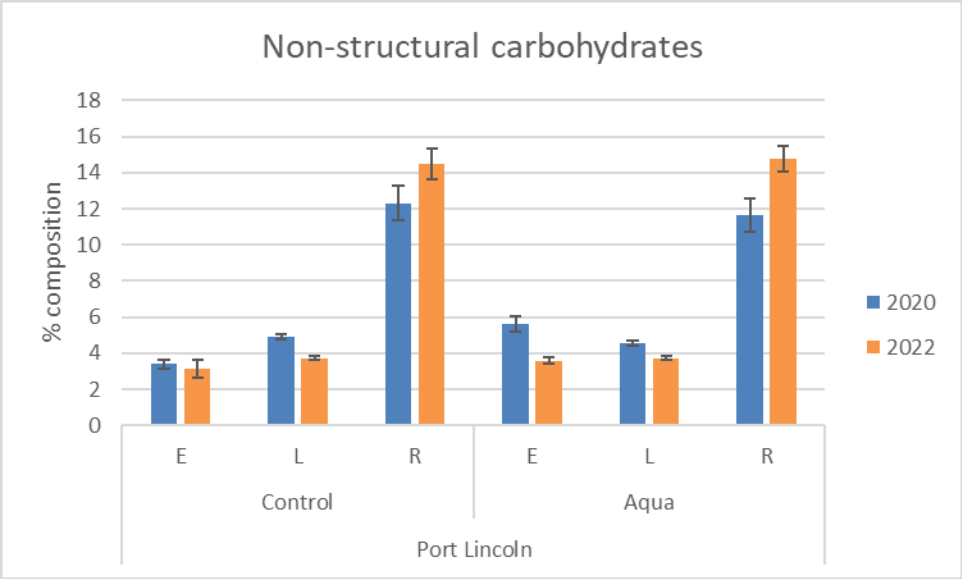

Figure 3-17: Seagrass non-structural carbohydrates in and around Boston Bay. E - epiphytes, L - seagrass leaves, R - seagrass roots. All error bars are SE.

Amino acids

All factors and all interactions had a significant effect on the amino acid composition of the seagrass and epiphyte samples (Table 3-10). The most obvious separation in the nMDS plot was between tissue compartments, with leaves, roots and epiphytes all clustering out separately (Figure 3-18). Roots tended to be high in alanine, lysine and aspartic acid, while the leaves were high in serine, valine, isoleucine, phenylalanine, leucine and proline. Epiphytes were intermediate between the two seagrass compartments. In both years, there was substantial overlap between aquaculture and control samples for both seagrass leaves and roots, whereas the epiphyte samples tended to cluster based on whether or not they were exposed to the nutrient plume from aquaculture, especially in 2022. Based on this, a second PERMANOVA was performed with only the seagrass samples, which showed that the amino acid composition did not change between treatments (Table 3-11). Thus, the impact of aquaculture was confined to the epiphytes only.

Table 3-10: PERMANOVA results for the effect of aquaculture on amino acid composition in seagrasses and epiphytes in the Boston Bay region. Yr – Year, Tr – Treatment, Co – Compartment, Si – Site, Su – SubSite.

Multivariate source	df	SS	Pseudo-F	P
Year	1	64298	20.388	**0.0048**
Treatment	1	12500	3.3444	**0.0209**
Compartment	2	184000	19.336	**0.0001**
Site(Tr)	4	16174	3.1611	**0.0001**
YexTr	1	15182	4.8142	**0.0254**
YexCo	2	68166	7.8707	**0.0001**
TrxCo	2	24442	2.5665	**0.0283**
SubSite(Si(Tr))	12	15785	1.6241	**0.0013**
YexSi(Tr)	4	13614	1.8486	**0.0194**
CoxSi(Tr)	8	41258	3.4445	**0.0001**
YexTrxCo	2	33499	3.868	**0.0042**
YexSu(Si(Tr))	12	24093	2.4788	**0.0001**
CoxSu(Si(Tr))	24	36860	1.8961	**0.0001**
YexCoxSi(Tr)	8	37220	3.3455	**0.0001**
YexCoxSu(Si(Tr))	20	28400	1.7502	**0.0001**
Residual	194	157000		

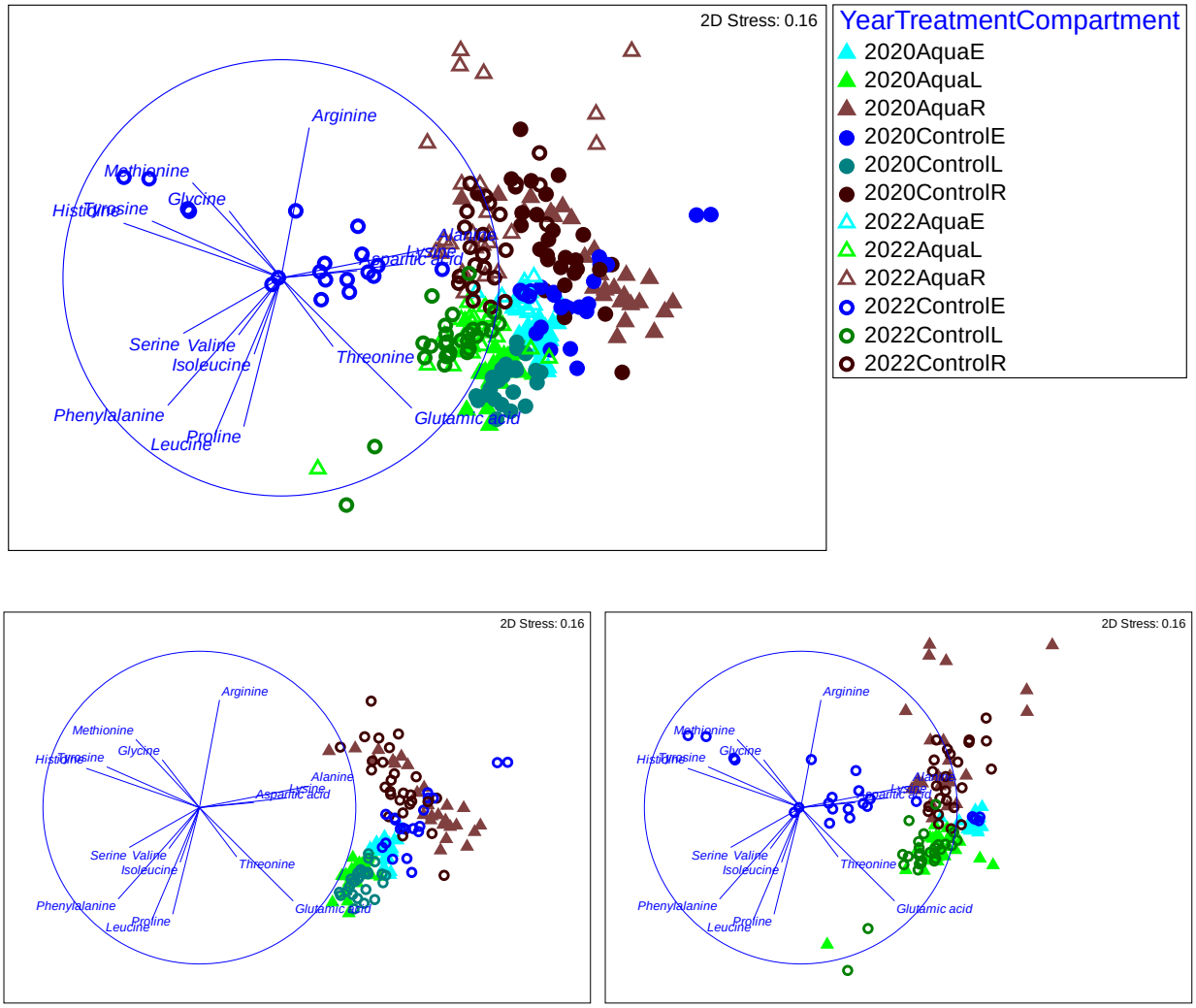

Figure 3-18: Non-metric multidimensional scaling (nMDS) analysis of seagrass and epiphyte amino acid composition in and around Boston Bay. Top – both years combined; Bottom left – 2020 only; Bottom right – 2022 only. Triangles indicate sites within the modelled nutrient plume from aquaculture, while circles indicate control sites outside the plume. The filled shapes represent 2020 samples, while the hollow shapes represent 2022 (top panel only). Blue represents epiphytes, green seagrass leaves and brown seagrass roots. The biplot (straight lines) show the extent of correlation of each variable in the analysis with the plot, with the circle representing a correlation of 1.

Table 3-11: PERMANOVA results for the effect of aquaculture on amino acid composition in seagrasses (no epiphytes) in the Boston Bay region. Yr – Year, Tr – Treatment, Co – Compartment, Si – Site, Su – SubSite.

Multivariate source	df	SS	Pseudo-F	P
Year	1	79572	14.388	**0.0032**
Treatment	1	3.13E+03	0.67508	0.8096
Compartment	1	1.60E+05	25.76	**0.0025**
Site(Tr)	4	18604	2.8901	**0.0001**
YexTr	1	8753.9	1.5828	0.2238
YexCo	1	52346	15.211	**0.0028**
TrxCo	1	5910.4	0.95293	0.4438
SubSite(Si(Tr))	12	19364	2.265	**0.0001**
YexSi(Tr)	4	22181	3.1635	**0.0004**
CoxSi(Tr)	4	24877	3.735	**0.0002**
YexTrxCo	1	9505.2	2.7621	0.0853
YexSu(Si(Tr))	12	21096	2.4676	**0.0001**
CoxSu(Si(Tr))	12	20037	2.3438	**0.0001**
YexCoxSi(Tr)	4	13799	2.2828	**0.0039**
YexCoxSu(Si(Tr))	12	1.82E+04	2.1266	**0.0001**
Residual	138	9.83E+04		

3.4. Discussion

Overall, while there was extensive spatial and temporal variation in the seagrass parameters investigated, the only significant impact of aquaculture was on the amino acid composition of the epiphytes. The SARDI video data showed a general decline in the seagrass condition index over time, probably driven by a concurrent decline in the cover of *Posidonia*. The two southern control sites (Thistle and Taylors) only showed small declines, however, Tumby Bay (northern control) showed a substantial decline which was mirrored by the three aquaculture plume sites. However, the Clean Seas video data showed that cover at Tumby Bay increased in both 2021 and 2023, which were years that SARDI did not sample. The other three Clean Seas sites only showed minor differences over time. If the decline in cover at Tumby Bay in 2022 was anomalous and associated with a local short-term disturbance, or if aquaculture is actually having an impact at this site, then it would potentially have obscured any effects of aquaculture on seagrass cover. Therefore, it is important to continue with this monitoring to confirm if the declines at Tumby Bay are only short-term. It may also help to add additional control sites north and south. The addition of one site north and one site south that require minimal deviation from the existing vessel routes,

and for video only, would be logistically feasible without requiring additional field days. However, new sites would not have existing data available, as there are no suitable EPA aquatic ecosystem condition reporting sites in either area. The addition of new dive sites would require an additional day of field time and potentially substantial increased expense given the decreased likelihood of getting four suitable days of weather in a row compared to three. In addition, it would be desirable to conduct an analysis of seagrass decline in relation to modelled nutrient loadings from aquaculture, rather than the impact versus control analysis undertaken here, to determine if that shows a response to nutrient loading.

The EPA video data cover a longer timescale (commencing in 2010), but are only available every six years. Both the control and the aquaculture plume sites showed variable patterns of cover over time. However, it should be noted that the initial plume modelling was undertaken for 2019, and may not be relevant for other years, especially earlier, when levels of production and the spatial arrangement of leases were different. Plume dispersal modelling is now available for each year that there are seagrass data, but was not available in time to calculate the level of nutrient exposure for each site, and how changes in exposure related to changes in seagrass cover to determine if there is any relationship. Even the longer-term EPA data began well after the beginning of SBT aquaculture in the Port Lincoln region, and thus none of the available data sets give any indication of what the longer-term consequences of nutrient exposure may have been for seagrasses in the region. One possible way to better understand this issue is to examine historical aerial and satellite imagery to assess how the inshore margin of seagrass meadows at selected sites has changed over time. While this would only be correlative, it would show if areas exposed to aquaculture nutrients have experienced a long-term decline in seagrass extent.

In addition to declines in cover across all sites, there were declines in both above- and below-ground biomass at all sites. Although changes in leaf and root biomass were variable, these were dominated by declines at all sites in shoot and fibre biomass during the two-year study. These declines suggest that there are decreases in seagrass density occurring. Interestingly, Tumby Bay experienced the lowest decline in biomass at the control sites, despite having the highest decline in cover, suggesting that at that site, seagrass became patchier, rather than decreasing in density. In fact, the number of shoots and leaves actually increased at this site. Consequently, the IBL seagrass health measure actually improved at this site, whereas it declined at all other sites. This is the first attempt at using this measure in South Australia, and indeed little use has been made of it with *Posidonia* before, and therefore the results should be considered with

caution. However, it has been used successfully to examine seagrass health along nutrient enrichment gradients with other genera, particularly *Zostera* and *Halophila* (Vieira et al. 2022).

The threshold for the loss of *Posidonia* seagrass due to nitrogen loading has been calculated as between 0.8 and 1.1 t N km^{-2} over 6 months off Adelaide (Fernandes et al. 2019). In comparison, the model discussed above shows a loading of roughly 2.2 t N km^{-2} over 6 months across 650 km^2 of the main dissolved inorganic nutrient plume area, although most if not all of this is offshore and does not impinge on seagrasses (Figure 2-7, Figure ***2-8***). For a diverse seagrass assemblage in China, the threshold loading was calculated as 8 μM dissolved inorganic nitrogen (Thomsen et al. 2020) which is equivalent to 112 μg L^{-1}, while both modelled and measured loadings are generally below 50 μg L^{-1}. Although excessive anthropogenic nutrient inputs are almost always detrimental to seagrasses (Burkholder et al. 2007, Lee et al. 2007, Cabaco et al. 2013), in some situations, low levels of input can be beneficial (Vieira et al. 2022)

Epiphyte cover declined greatly at most sites, with the exception of Spalding, where it remained steady. However, biomass was more variable. At sites where a decline was observed, it was much more modest than the decline in cover, and at some sites biomass actually increased. No attempt was made to separate epiphytes into different categories in the biomass samples, and they include encrusting calcareous algae that were not visible in the video footage, as well as the larger (but lighter) fleshy algae that was visible in the video. One of the key pathways through which nutrient enrichment causes declines in seagrass is through increased epiphyte growth, which leads to seagrasses experiencing lower light levels and being smothered (e.g. Bryars et al. 2011, Nelson 2017). However, epiphyte loads can also change with a variety of other environmental factors, including day length and water temperature, so a simple comparison between two time points is insufficient to draw rigorous conclusions about the role of nutrients on epiphytes.

There was no aquaculture biomarker signal detectable in the seagrass compartments, although there were differences in the amino acid composition of the epiphytes between the control samples and the aquaculture plume samples. It is not known whether this difference has ecological consequences. Previous studies that have detected clear biomarker signals from aquaculture and other nutrient inputs are primarily picking up land-based sources, which differ considerably from marine sources (e.g. Roca et al. 2015, Thomsen et al. 2020), although nitrogen enrichment per se has been suggested to lead to increased uptake of nitrogen-rich amino acids as well as to decrease $\delta^{15}N$ in seagrasses from a low nutrient environment (Udy et al. 1999).

However, most of the feed input in the Port Lincoln region are baitfish (primarily sardines), and thus introduce an additional marine signal into a marine system, making them difficult to distinguish. The land-based signal was restricted to the feed used for yellowtail kingfish, which comprised only 17% of all feed inputs. Thus, it was not possible to determine the contribution of aquaculture-derived nutrients to seagrasses. Given this and the high cost of biomarker analysis, it is not considered cost-effective to continue this part of the monitoring program. Epiphytes have a higher turnover rate than seagrasses and may thus be capable of picking up subtler differences (e.g. Vonk et al. 2008). Therefore, they may be useful as an early indicator of nutrient inputs, especially in situations where those inputs have a higher land-based component.

4. CONCLUSION

The pelagic monitoring program and modelling suggest that the nutrient enrichment associated with aquaculture and other unidentified nutrient sources may have a significant impact on the status of the ecosystem in the inshore regions of Boston and Louth Bay during autumn. Evidence for this is based on the results for several phytoplankton indicators (e.g. chl-*a*, F_p ratios and community composition) which suggest the trophic status may be changing from mesotrophic to slightly eutrophic. However, other indicators, such as shifts in the diatom to dinoflagellate ratio or frequency of HAB occurrence which previously suggested a change in trophic status consistent with eutrophication (Tanner et al. 2019) did not support the trends identified by chl-*a* or the F_p ratio. Temperature, reduced flushing, and to a lesser extent nutrients, were identified as the main environmental drivers explaining the biological differences observed at the inshore sites during the autumn.

Collectively, the additional samples collected, and new indicators (e.g., CHEMTAX) developed during this second term of pelagic monitoring program have provided a broader understanding of the spatial and temporal variability associated with the regions pelagic ecosystem and the trophic status of the system. Continued physical, biological, and chemical monitoring is required to develop an improved baseline to detect future changes and trends in the region's trophic status. Given nutrient emissions from aquaculture (and other sources) impact inshore waters with reduced flushing year-round, it is also recommended that monitoring should be expanded to cover all four seasons and additional key indicators of eutrophication.

The only impact of aquaculture found on the seagrass variables examined was a change in the amino acid composition of seagrass epiphytes, although the consequences of this are unknown. However, it should be noted that we only have two sampling events, both of which occurred several decades after aquaculture commenced, and a limited number of sampling sites. Consequently, it is recommended that seagrass monitoring continue for at least another 4 years. Removing the biomarker component of the monitoring should be considered, as it is expensive and did not prove to be particularly useful, although it did show that the sampling design was capable of detecting aquaculture impacts if they exist. It would also be useful to add additional sampling sites to reduce the potential for anomalous results at one site to compromise the potential to detect impacts at others. Adding in additional control video sites between Tumby and Louth, and between Donington and Thistle/Taylors would require little additional work although adding dive sites would be more problematic. Subsuming the current Clean Seas seagrass

monitoring into this program would also make sense from a scientific perspective and would avoid the current duplication of effort from SARDI and Clean Seas sampling the same sites in the same years, albeit with slightly different techniques. The resources saved could then be applied to undertaking video monitoring of all sites (SARDI plus the additional Clean Seas sites) on an annual basis, rather than every two years. If this does not occur, then the Clean Seas video should at least be analysed to provide actual percent cover, rather than cover classes, which could be done with little extra effort. To provide some context around the short-term changes in seagrasses documented here that occurred well after the commencement of aquaculture, it would be useful to undertake an analysis of historical aerial and satellite imagery to assess changes in the inshore margin of seagrasses over time. Finally, future analyses should more directly assess nutrient loadings at each of the seagrass sites and determine if any relationship exists between these loadings and change over time. This nutrient loading data should be able to be extracted from the biogeochemical models presented here, but those results were not available in time for this analysis to be performed. Previously, many years of sampling infauna failed to detect any consistent impacts of aquaculture on this component of the ecosystem (Tanner et al. 2020).

REFERENCES

Anderson, M. J. 2001. A new method for non-parametric multivariate analysis of variance. Austral Ecology **26**:32-46.

ANZECC/ARMCANZ. 2000. Australian and New Zealand guidelines for fresh and marine water quality. Australian and New Zealand Environment and Conservation Council and Agriculture and Resource Management Council of Australia and New Zealand, Canberra:1-103.ANZG. 2018. Australian and New Zealand Guidelines for Fresh and Marine Water Quality 2018. https://www.waterquality.gov.au/guidelines/anz-fresh-marine.

ANZG 2018. https://www.waterquality.gov.au/anz-guidelines/your-location/australia-marine-regions

APHA-AWWA-WPCF. 1998. Standard methods for the examination of water. Sewage and Industrial Waste. American Public Health Association, Washington, DC.

Azam, F., and F. Malfatti. 2007. Microbial structuring of marine ecosystems. Nature Reviews Microbiology **5**:782.

BDO EconSearch. 2023. The economic contribution of aquaculture in the South Australian state and regional economies, 2021/22 A Report for PIRSA Fisheries and Aquaculture Adelaide.

Bode, A., M. T. Alvarez-Ossorio, and N. Gonzalez. 1998. Estimations of meso-zooplankton biomass in a coastal upwelling area off NW Spain. Journal of Plankton Research **20**:1005-1014.

Bryars, S., G. Collings, and D. Miller. 2011. Nutrient exposure causes epiphytic changes and coincident declines in two temperate Australian seagrasses. Marine Ecology Progress Series **441**:89-103.

Burkholder, J. M., D. A. Tomasko, and B. W. Touchette. 2007. Seagrasses and eutrophication. Journal of Experimental Marine Biology and Ecology **350**:46-72.

Cabaco, S., E. T. Apostolaki, P. Garcia-Marin, R. Gruber, I. Hernandez, B. Martinez-Crego, O. Mascaro, M. Perez, A. Prathep, C. Robinson, J. Romero, A. L. Schmidt, F. T. Short, B. I. van Tussenbroek, and R. Santos. 2013. Effects of nutrient enrichment on seagrass population dynamics: evidence and synthesis from the biomass-density relationships. Journal of Ecology **101**:1552-1562.

Cheshire, A., G. Westphalen, A. Smart, and S. Clarke. 1996. Investigating the environmental effects of sea-cage tuna farming. II. The effects of sea-cages. University of Adelaide, Adelaide.

Clarke, K. R., and R. N. Gorley. 2015. PRIMER v7: User manual/tutorial. PRIMER-E, Plymouth.

Clarke, K. R., and R. H. Green. 1988. Statistical design and analysis for a biological effects study. Marine Ecology Progress Series **46**:213-226.

Claustre, H. 1994. The trophic status of various oceanic provinces as revealed by phytoplankton pigment signatures. Limnology and Oceanography **39**:1206-1210.

Cloern, J. E. 2001. Our evolving conceptual model of the coastal eutrophication problem. Marine Ecology-Progress Series **210**:223-253.

Coplen, T. B., W. A. Brand, M. Gehre, M. Gröning, H. A. J. Meijer, B. Toman, and R. M. Verkouteren. 2006. New Guidelines for $\delta^{13}C$ Measurements. Analytical Chemistry **78**:2439-2441.

Doubell, M. J., C. E. James, and J. F. Middleton. 2015. Modelling of oceanographic variables for the development of finfish aquaculture in Spencer Gulf. SARDI Publication No. F2014/000740-1. SARDI Research Report Series No. 830. , South Australian Research and Development Institute (Aquatic Sciences), Adelaide. .

Edyvane, K. 1999. Conserving marine Biodiversity in South Australia. Part 2 - Identification of areas of high conservation value in South Australia. SARDI, Adelaide.

Fennel, K., J. Wilkin, J. Levin, J. Moisan, J. O'Reilly, and D. Haidvogel. 2006. Nitrogen cycling in the Middle Atlantic Bight: Results from a three-dimensional model and implications for the North Atlantic nitrogen budget. Global Biogeochemical Cycles **20**.

Fernandes, M., M. Angove, T. Sedawie, and A. Cheshire. 2007. Dissolved nutrient release from solid wastes of southern bluefin tuna (*Thunnus maccoyii*, Castelnau) aquaculture. Aquaculture Research **38**:388-397.

Fernandes, M., and J. Tanner. 2008. Modelling of nitrogen loads from the farming of yellowtail kingfish Seriola lalandi (Valenciennes, 1833). Aquaculture Research **39**:1328-1338.

Fernandes, M. B., J. van Gils, P. L. A. Erftemeijer, R. Daly, D. Gonzalez, and K. Rouse. 2019. A novel approach to determining dynamic nitrogen thresholds for seagrass conservation. Journal of Applied Ecology **56**:253-261.

Fox, D. R., G. E. Batley, D. Blackburn, Y. Bone, S. Bryars, A. Cheshire, G. Collings, D. Ellis, P. Fairweather, H. Fallowfield, G. Harris, B. Henderson, J. Kampf, S. Nayar, C. Pattiaratchi, P. Petrusevics, M. Townsend, G. Westphalen, and J. Wilkinson. 2007. Adelaide Coastal Waters Study, Final Report, Volume 1, Summary of Study Findings, November 2007. CSIRO, Adelaide.

Fukuda, R., H. Ogawa, T. Nagata, and I. Koike. 1998. Direct determination of carbon and nitrogen contents of natural bacterial assemblages in marine environments. Applied Environmental Microbiology. **64**:3352-3358.

Furman, B. T., E. H. Leone, S. S. Bell, M. J. Durako, and M. O. Hall. 2018. Braun-Blanquet data in ANOVA designs: comparisons with percent cover and transformations using simulated data. Marine Ecology Progress Series **597**:13-22.

Gaylard, S. 2014. Marine pollution within Spencer Gulf. Natural History of Spencer Gulf, Royal Society of South Australia Inc, Adelaide:378-391.

Glibert, P. M. 2017. Eutrophication, harmful algae and biodiversity—Challenging paradigms in a world of complex nutrient changes. Marine pollution bulletin **124**:591-606.

Howarth, R. W. 2008. Coastal nitrogen pollution: a review of sources and trends globally and regionally. Harmful algae **8**:14-20.

Howarth, R. W., and R. Marino. 2006. Nitrogen as the limiting nutrient for eutrophication in coastal marine ecosystems: evolving views over three decades. Limnology and Oceanography **51**:364-376.

Irving, A. D. 2014. Seagrasses of Spencer Gulf. Pages 121-135 *in* S. A. Shepherd, S. M. Madigan, B. M. Gillanders, S. Murray-Jones, and D. J. Wiltshire, editors. Natural history of Spencer Gulf. Royal Society of South Australia Inc., Adelaide.

Irving, A. D., J. E. Tanner, and S. G. Gaylard. 2013. An integrative method for the evaluation, monitoring, and comparison of seagrass habitat structure. Marine Pollution Bulletin **66**:176-184.

Lee, K. S., S. R. Park, and Y. K. Kim. 2007. Effects of irradiance, temperature, and nutrients on growth dynamics of seagrasses: A review. Journal of Experimental Marine Biology and Ecology **350**:144-175.

Lennon, G., D. Bowers, R. Nunes, B. Scott, M. Ali, J. Boyle, C. Wenju, M. Herzfeld, G. Johansson, and S. Nield. 1987. Gravity currents and the release of salt from an inverse estuary. Nature **327**:695.

Loo, M. G. K., and D. Giblot-Ducray. 2014. Yellowtail Kingfish (*Seriola lalandi*) Aquaculture Environmental Monitoring Program 2012/13 Report for Cleanseas Aquaculture Growout Pty Ltd, Boston Bay, South Australia: Licence Numbers AQ00015, AQ00139, AQ00235, FF00085 and FF00090. South Australian Research and Development Institute (Aquatic Sciences). Adelaide. SARDI Publication No. F2010/000207-5. SARDI Research Report Series No. 787.

Loo, M. G. K., and D. Giblot-Ducray. 2015. Southern Bluefin Tuna (*Thunnus maccoyii*) Aquaculture Environmental Monitoring Program 2014 Report: KIS Tuna Pty Ltd, Australian

Fishing Enterprises Pty Ltd and SAMS Sea Farm Pty Ltd, Licence Number AQ00030. Report prepared for the Australian Southern Bluefin Tuna Industry Association Inc. South Australian Research and Development Institute (Aquatic Sciences). Adelaide. SARDI Publication No. F2009/000585-7. SARDI Research Report Series No. 822.

Loo, M. G. K., K. M. Ophel-Keller, and A. C. Cheshire. 2006. Final Report - Development of Novel Methodologies for Cost Effective Assessment of the Environmental Impact of Aquaculture. Aquafin CRC, Fisheries Research and Development Corporation and South Australian Research and Development Institute (Aquatic Sciences). Adelaide. SARDI Publication No. RD03/0036-4.

Loo, M. G. K., K. M. Ophel-Keller, A. C. McKay, Herdina, D. M. Hartley, S. Clarke, and A. Cheshire. 2010. Final Report - Development of rapid environmental assessment and monitoring techniques for application to finfish aquaculture in South Australia. Aquafin CRC, Fisheries Research and Development Corporation and South Australian Research and Development Institute (Aquatic Sciences). Adelaide. SARDI Publication Number F2010/000392-1, SARDI Research Report Series No. 477.

Marquis, E., N. Niquil, and C. Dupuy. 2011. Does the study of microzooplankton community size structure effectively define their dynamics? Investigation in the Bay of Biscay (France). Journal of Plankton Research **33**:1104-1118.

Menden-Deuer, S., and E. J. Lessard. 2000. Carbon to volume relationships for dinoflagellates, diatoms, and other protist plankton. Limnology and Oceanography **45**:569-579.

Middleton, J., M. Doubell, C. James, J. Luick, and P. Van Ruth. 2013. PIRSA Initiative II: Carrying Capacity of Spencer Gulf: Hydrodynamic and Biogeochemical Measurement Modelling and Performance Monitoring. Final report for the Fisheries Research and Development corporation. South Australian Research and Development Institute (Aquatic Sciences), Adelaide. SARDI Publication No. F2013/000311-1. SARDI Research Report Series No. 705.

Murray-Jones, S., A. Irving, and J. Dupavillon. 2009. Seagrass Condition Monitoring: A report to the Adelaide and Mount Lofty Ranges Natural Resources Management Board. Department for Environment and Heritage, Coastal Management Branch. .

Nelson, W. G. 2017. Development of an epiphyte indicator of nutrient enrichment: Threshold values for seagrass epiphyte load. Ecological Indicators **74**:343-356.

Nixon, S. W. 1995. Coastal marine eutrophication: a definition, social causes, and future concerns. Ophelia **41**:199-219.

Nunes Vaz, R. A., G. W. Lennon, and D. G. Bowers. 1990. Physical behaviour of a large, negative or inverse estuary. Continental Shelf Research **10**:277-304.

Paerl, H. W., L. M. Valdes, J. L. Pinckney, M. F. Piehler, J. Dyble, and P. H. Moisander. 2003. Phytoplankton photopigments as indicators of estuarine and coastal eutrophication. BioScience **53**:953-964.

Patten, N. L., P. D. van Ruth, and A. R. Rodriguez. 2018. Spatial variability in picophytoplankton, bacteria and viruses in waters of the Great Australian Bight (southern Australia). Deep Sea Research Part II: Topical Studies in Oceanography **157**:46-57.

Pearson, T. H., and K. D. Black. 2001. The environmental impacts of marine fish cage culture. Pages 1-31 *in* K. D. Black, editor. Environmental Impacts of Aquaculture. Sheffield Academic Press, Sheffield, England.

Petrusevics, P. 1993. SST fronts in inverse estuaries, South Australia-indicators of reduced gulf-shlef exchange. Marine and Freshwater Research **44**:305-323.

Roca, G., T. Alcoverro, M. de Torres, M. Manzanera, B. Martinez-Crego, S. Bennett, S. Farina, M. Perez, and J. Romero. 2015. Detecting water quality improvement along the Catalan coast (Spain) using stress-specific biochemical seagrass indicators. Ecological Indicators **54**:161-170.

Short, F. T., and S. Wyllie-Echeverria. 1996. Natural and human-induced disturbance of seagrasses. Environmental Conservation **23**:17-27.

Shute, A., J. Kämpf, M. Doubell, A. Redondo Roriguez, L. Möller, R. Baring and M. Newman. 2022. Variability of surface and subsurface phytoplankton blooms in a seasonal coastal upwelling system, Continental Shelf Research, **246**: 104832.

Suthers, I., D. Rissik, and A. Richardson. 2019. Plankton: A guide to their ecology and monitoring for water quality. CSIRO publishing.

Tanner, J. E., M. Doubell, P. Van Ruth, C. James, and J. Middleton. 2020. Aquaculture Environmental Monitoring Program: 2015-2019. South Australian Research and Development Institute (Aquatic Sciences), Adelaide. SARDI Publication No. F2019/000334-1. SARDI Research Report Series No. 1053. 67pp.

Tanner, J. E., and J. K. Volkman. 2009. Aquafin CRC-FRDC Southern Bluefin Tuna Aquaculture Subprogram: risk and response: understanding the tuna farming environment. [West Beach, SA], Aquafin CRC; SARDI; FRDC.

Thomsen, E., L. S. Herbeck, and T. C. Jennerjahn. 2020. The end of resilience: Surpassed nitrogen thresholds in coastal waters led to severe seagrass loss after decades of exposure to aquaculture effluents. Marine Environmental Research **160**.

Tuynman, H., A. Cao, M. Dylewski, and R. Curtotti. 2023. Australian fisheries and aquaculture statistics 2022, Fisheries Research and Development Corporation, ABARES, Canberra.

Udy, J. W., W. C. Dennison, W. J. L. Long, and L. J. McKenzie. 1999. Responses of seagrass to nutrients in the Great Barrier Reef, Australia. Marine Ecology Progress Series **185**:257-271.

Van Heukelem, L., and C. S. Thomas. 2001. Computer-assisted high-performance liquid chromatography method development with applications to the isolation and analysis of phytoplankton pigments. Journal of Chromatography **910**:31-49.

Van Meerssche, E., and J. L. Pinckney. 2019. Nutrient Loading Impacts on Estuarine Phytoplankton Size and Community Composition: Community-Based Indicators of Eutrophication. Estuaries and Coasts **42**:504-512.

Vieira, V. M. N. C. S., J. Lobo-Arteaga, R. Santos, D. Leitão-Silva, A. Veronez, J. M. Neves, M. Nogueira, J. C. Creed, C. M. Bertelli, J. Samper-Villarreal, and M. R. S. Pettersen. 2022. Seagrasses benefit from mild anthropogenic nutrient additions. Frontiers in Marine Science **9**.

Vonk, J., J. Middelburg, J. Stapel, and T. Bouma. 2008. Dissolved organic nitrogen uptake by seagrasses. Limnology and Oceanography **53**:542-548.

Warwick, R. M., and K. R. Clarke. 1991. A comparison of some methods for analyzing changes in benthic community structure. Journal of the Marine Biological Association of the United Kingdom **71**:225-244.

Waycott, M., C. M. Duarte, T. J. B. Carruthers, R. J. Orth, W. C. Dennison, S. Olyarnik, A. Calladine, J. W. Fourqurean, K. L. Heck, A. R. Hughes, G. A. Kendrick, W. J. Kenworthy, F. T. Short, and S. L. Williams. 2009. Accelerating loss of seagrasses across the globe threatens coastal ecosystems. Proceedings of the National Academy of Sciences of the United States of America **106**:12377-12381.

Westphalen, G., G. Collings, R. Wear, M. Fernandes, S. Bryars, and A. Cheshire. 2005. A review of seagrass loss on the Adelaide metropolitan coastline. South Australian Research and Development Institute (Aquatic Sciences) Publication No. RD04/0073, Adelaide.

Wiebe, P. H. 1988. Functional regression equations for zooplankton displacement volume, wet weight, dry weight, and carbon. A correction. Fisheries Bulletin **86**:833-835.

Wiebe, P. H., S. Boyd, and J. L. Cox. 1975. Relationship between zooplankton displacement volume, wet weight, dry weight and carbon. Fisheries Bulletin **73**:777-786.

5. APPENDIX

Pelagic and Oceanography Analytical Methods

Dissolved Inorganic Nutrients

Three replicate 100 mL subsamples of seawater were filtered through a 0.45 µm filter, frozen and stored analysis in the environmental chemistry laboratory at SARDI Aquatic Sciences following standard methods (APHA-AWWA-WPCF 1998). Dissolved ammonium (NH_4^+, detection limit 1 µg/L), oxides of nitrogen (NO_x, detection limit 1 µg/L), phosphate (PO_4^{3-}, detection limit 1 µg/L) and silicate (SiO_2, detection limit 20 µg/L were determined by flow injection analysis with a QuickChem 8500 Automated Ion Analyser. Results below the detection limit are assumed to be half the detection limit.

Particulate Matter

Three replicate 1 L subsamples were obtained for the gravimetric determination of the total suspended solid concentration (TSS). Samples were filtered through pre-combusted Whatman GF/F filters (nominal pore size 0.4 µm) using a vacuum pump. Filters were rinsed with 60 mL of milliQ water and folded in half, wrapped in foil and stored at -20 °C prior to further analysis. In the laboratory samples were oven dried at 60 °C for 48 hours before combustion in a muffle furnace at 500 °C for 1 hour in the environmental chemistry laboratory at SARDI Aquatic Sciences.

Bacteria and Picophytoplankton

Following (Patten et al. 2018), three replicate 1 mL subsamples of seawater were obtained for the flow cytometric enumeration of bacteria and picophytoplankton abundances. Bacteria and picophytoplankton samples were fixed in glutaraldehyde with a 0.5% and 0.25% final concentration, respectively. Following fixation all sample were placed in the dark for 15 minutes, then quick frozen in liquid nitrogen and stored at -80 °C until analysis. Bacteria and picophytoplankton samples were thawed at 37 °C. Bacteria samples were diluted 10-fold in Tris EDTA (pH = 8.0, Sigma-Aldrich), stained with SYBR I green (5×10^{-5} final concentration, Molecular Probes) heated at 80 °C for 10 minutes and then cooled to room temperature. Prior to flow cytometric analysis 1 µm fluorescent beads (Polysciences) were added to the bacteria and picophytoplankton samples added as an internal reference.

All samples were analyzed on a FACSVerse (Becton Dickenson) flow cytometer with an acquisition runtime of 2 minutes on low flow rate (~20µL min^{-1}) for bacteria and 3 minutes with a medium flow rate (~50µL min^{-1}) for picophytoplankton. Each sample was weighed before and

after each run to determine the exact volume analyzed for the determination of cell abundances. Different picophytoplankton groups were identified based on the red and orange autofluorescence of chlorophyll, the accessory pigment phycoerythrin, and light scatter properties of side-angle light scatter. Bacteria were identified based on green fluorescence, side-angle light scatter (SSC) and forward-angle light scatter (FSC) using FlowJo® flow cytometry analysis software. Bacteria were separated on plots of side scatter (SSC) and green (SYBR) fluorescence and SSC and red chl-*a* fluorescence. *Prochlorococcus* often coincided with the stained bacterial group. To correct for this, *Prochlorococcus* were included within the bacterial group and bacterial counts were corrected by subtracting total counts of *Prochlorococcus* (obtained from non-stained samples) from the stained bacterial group.

Phytoplankton Abundance and Biomass

A detailed inventory of phytoplankton taxa and their cell abundances was obtained from 1 L seawater samples fixed with acidified Lugol's iodine solution. Enumeration and identification of phytoplankton to genus or species level was carried out by microscopy using the Utermöhl method by Microalgal Services, Victoria, Australia.

Chlorophyll *a* (chl-*a*) biomass and accessory pigments were measured using High Pressure Liquid Chromatography (HPLC). Two-litre water samples were filtered through Whatman GF/F filters (nominal pore size 0.4 µm) using a vacuum pump. Filters were snap-frozen and stored at -80°C prior to analysis via the gradient elution procedure of Van Heukelem and Thomas (2001) on an Algilent 1200 series HPLC system in the environmental chemistry laboratory at SARDI Aquatic Sciences.

Zooplankton Abundance and Biomass

Following the vertical net tows, the external surface of the nets were washed down with seawater, collected in a sample jar and fixed with formalin (5 % final volume). In the laboratory, samples were rinsed through a 35 µm mesh sieve to remove all traces of formalin prior to enumeration. The contents of the sieve were then rinsed into 100 ml measuring cylinders and allowed to settle for 24 hours, after which settling volumes were recorded. Zooplankton were identified to the lowest possible taxonomic level via microscopy, using standard taxonomic methods. Organism numbers were reported as individuals/m^3, according to the volume swept by the net. Volume swept was calculated as the distance travelled by the net (estimated using a General Oceanics flow meter suspended in the mouth of the net) multiplied by the area of the net mouth. Settling volumes were recorded in mL m^{-3} using the volume swept, and were converted to displacement

volumes using a factor for samples without gelatinous zooplankton (0.35) (Wiebe et al. 1975, Wiebe 1988). Displacement volumes were then converted to biomass (mg C m^{-3}) using a factor of 21 for samples with displacement volumes < 1 mL, and a factor of 41 for samples with displacement volumes 1-10 mL (Bode et al. 1998).